SC5345.FR

Copy No. 2

RESEARCH IN HIGH DIELECTRIC PROPERTIES OF FERROELECTRIC MATERIALS

FINAL REPORT FOR THE PERIOD
May 14, 1981 through November 29, 1991

CONTRACT NO. N00014-81-C-0463

Prepared for:

Scientific Officer
Director Metallurgy & Ceramics Program
Materials Sciences Division
Office of Naval Research
800 North Quincy Street
Arlington, VA 22217

R.R. Neurgaonkar
Principal Investigator

Rockwell International Science Center
1049 Camino Dos Rios
Thousand Oaks, CA 91360

JANUARY 1992

Rockwell International
Science Center

UNCLASSIFIED

SECURITY CLASSIFICATION OF THIS PAGE

REPORT DOCUMENTATION PAGE

FORM APPROVED OMB No. 0704-0188

1a. REPORT SECURITY CLASSIFICATION
UNCLASSIFIED

1b. RESTRICTIVE MARKINGS

2a. SECURITY CLASSIFICATION AUTHORITY

3. DISTRIBUTION/AVAILABILITY OF REPORT

2b. CLASSIFICATION/DOWNGRADING SCHEDULE

4. PERFORMING ORGANIZATION REPORT NUMBER(S)
SC5345.FR

5. MONITORING ORGANIZATION REPORT NUMBER(S)

6a. NAME OF PERFORMING ORGANIZATION
ROCKWELL INTERNATIONAL
Science Center

6b. OFFICE SYMBOL *(If Applicable)*

7a. NAME OF MONITORING ORGANIZATION

6c. ADDRESS *(City, State and ZIP Code)*
1049 Camino Dos Rios
Thousand Oaks , CA 91360

7b. ADDRESS *(City, State and ZIP Code)*

8a. NAME OF FUNDING/SPONSORING ORGANIZATION
Office of Naval Research

8b. OFFICE SYMBOL *(If Applicable)*

9. PROCUREMENT INSTRUMENT IDENTIFICATION NUMBER

8C. ADDRESS *(City, State and ZIP Code)*
800 North Quincy Street
Arlington, VA 22217

10. SOURCE OF FUNDING NOS.

PROGRAM ELEMENT NO.	PROJECT NO.	TASK NO.	WORK UNIT ACCESSION NO.

11. TITLE *(Include Security Classification)*
RESEARCH IN HIGH DIELECTRIC PROPERTIES OF FERROELECTRIC MATERIALS

12. PERSONAL AUTHOR(S)
Neurgaonkar, R.R.

13a. TYPE OF REPORT	13b. TIME COVERED	14. DATE OF REPORT *(Year, Month, Day)*	15. PAGE COUNT
Final Report	FROM 05/14/81 TO 11/29/91	1992, JANUARY	

16. SUPPLEMENTARY NOTATION

17. COSATI CODES			18. SUBJECT TERMS *(Continue on reverse if necessary and identify by block number)*
FIELD	GROUP	SUB-GROUP	

19. ABSTRACT *(Continue on reverse if necessary and identify by block number)*

The magnetron sputtering technique has been used to grow morphotropic phase boundary ferroelectric thin films of tungsten bronze PBKNN and perovskite $BaTiO_3$, KTN and PZT. Film crystallinity was found to be strongly influenced by substrate temperature, with temperatures of 500-600°C usually required. Single crystal PSKNN films were grown on SBN:60 substrates, whereas grain-oriented films were achieved on (100)-oriented Si substrates. PLZT films are grain-oriented for (001)-oriented SBN and have excellent surface quality for guided wave applications. This is the first time such films have been grown on tungsten bronze substrates. Both PSKNN and PZT films present a great promise for SLM and electronic memory applications.

20. DISTRIBUTION/AVAILABILITY OF ABSTRACT
UNCLASSIFIED/UNLIMITED ☐ SAME AS RPT. ☒ DTIC USERS ☐

21. ABSTRACT SECURITY CLASSIFICATION
UNCLASSIFIED

22a. NAME OF RESPONSIBLE INDIVIDUAL
W.A. Smith

22b. TELEPHONE NUMBER *(INCLUDE AREA CODE)*

22c. OFFICE SYMBOL

DD FORM 1473 Previous editions are obsolete.

UNCLASSIFIED

SECURITY CLASSIFICATION OF THIS PAGE

TABLE OF CONTENTS

Statement A per telecon Dr. Wallace Smith
ONR/Code 1131
Arlington, VA 22217-5000

NWW 3/2/92

Accesion For	
NTIS CRA&I	☑
DTIC TAB	☐
Unannounced	☐
Justification	
By	
Distribution /	
Availability Codes	
Dist	Avail and / or Special
A-1	

LIST OF FIGURES

LIST OF TABLES

ABSTRACT

This is the final report covering our research on ferroelectric thin films for optoelectronic applications. Over this period, we have explored various techniques and systems for achieving technologically useful thin films and we have succeeded in many instances in producing high quality single crystal or grain-oriented thin films. The following are some of the major accomplishments of this program:

1. The growth of highly grain-oriented $BaTiO_3$, PZT, KTN and PLZT thin films on SBN substrates using the sol-gel and sputtering techniques. This is the first time that such films have been grown on tungsten bronze substrates.

2. The growth of single crystal PSKNN thin films on SBN substrates by the sputtering technique. The selected PSKNN composition has exceptional electro-optic properties and has not as yet been successfully grown as a bulk single crystal. In addition, we have successfully grown doped-PSKNN thin films for photorefractive applications.

3. The growth of grain-oriented PSKNN thin films on semiconducting Si and GaAs substrates. These films were optimized for electronic memory applications.

4. The potential of PSKNN and PLZT films on SBN for electro-optic modulators was established through measurements in our laboratory.

The combinations of properties available in ferroelectric thin films are unique and should lead to many different applications. Our work has demonstrated that several important material combinations can be successfully grown as high quality thin films. In some cases, these materials have never been successfully grown as bulk single crystals of useful size and quality. We propose the following recommendations:

1. Initiate device studies using single crystal PSKNN films for guided wave optics and photorefractive applications.

2. Fe^{3+}- and Ce^{3+}-doped $BaTiO_3$ thin films grown on SBN show a great potential for photorefractive applications.

3. Grain-oriented PSKNN films grown on Si and GaAs are highly suitable for electronic memory applications because they possess high polarization.

1.0 PROGRESS SUMMARY

This report covers work on the growth of ferroelectric thin films carried out in the Ferroelectric Materials Department of the Rockwell International Science Center under this ONR contract. During this period, significant progress has been made in the growth of perovskite PZT, KTN, $BaTiO_3$ and PLZT, and tungsten bronze PSKNN thin films.

The advantages of ferroelectric thin films for optical applications have not been fully exploited due to the difficulties in achieving single crystal films of adequate quality and properties. Isolated examples of successful growth have been reported on such materials as $LiNbO_3$, KLN and most recently on PZT, PLZT and $BaTiO_3$ for optical waveguides, surface acoustic wave (SAW) and electronic memory applications. Based on work reported in the literature, LPE growth is only suitable for lattice-matched substrate materials, and in some instances, the film quality is a severe problem due to the inclusion of solvents. For this reason, rf sputtering and sol-gel techniques have been used extensively in our work to explore simple as well as complex, ferroelectrics based on Pb^{2+}-containing solid solutions.

Selection of Materials

The goal of this work was to identify and grow materials with high optical figures-of-merit and tailor their properties according to device requirements. The basic figures-of-merit for optical applications are considered to be $n^3 r_{ij}/\varepsilon$ and r_{ij}/ε, where n is the refractive index, r_{ij} is the electro-optic coefficient, and ε is the dielectric constant. These constants can be related to the fundamental crystal properties to determine any necessary changes in the crystal composition to optimize the material for a given device application. For example:

$$r_{33} = 2g_{33}P_3\varepsilon_3\varepsilon_0 \qquad \text{or} \qquad r_{33}/\varepsilon_3 = 2g_{33}P_3\varepsilon_0$$

$$r_{51} = 2g_{44}P_3\varepsilon_{11}\varepsilon_0 \qquad \text{or} \qquad r_{51}/\varepsilon_{11} = 2g_{44}P_3\varepsilon_0$$

where g is the quadratic electro-optic coefficient whose value is largely invariant within a given system. However, other properties such as the polarization, and dielectric constant vary widely with composition and temperature. These relations indicate that crystals should possess large polarization to achieve better performance. Most of Pb^{2+}-containing ferroelectrics such as tungsten bronze PSKNN, PBN and perovskite PZT, PLZT and KTN

have significantly higher optical figures-of-merit than currently used materials. For this reason, we have selected tungsten bronze PSKNN and perovskite PZT and KTN compositions for this work. We have also selected doped $BaTiO_3$ films for some photo-refractive switching applications.

During this program, two complementary techniques were used to deposit ferroelectric thin films; namely, rf sputtering and sol-gel. The sputtering technique is well suited for applications where thicker films and high rates of deposition are required. Sol-gel deposition is an inherently slower process but allows the user to have careful control of film thickness down to the angstrom level. As part of the work performed under this contract, PSKNN, $BaTiO_3$ and PZT films were grown using rf sputtering, while the sol-gel technique was used to deposit PZT and KTN thin films. Using lattice matched SBN substrates, high quality single crystal films were obtained in both the sputtered and sol-gel grown materials. Grain-oriented films were observed on other substrates such as Si, GaAs and Al_2O_3.

The growth of tungsten bronze PSKNN thin films using the sputtering technique has been highly successful on various substrates such as Si, GaAs, SBN and Al_2O_3. At present, PSKNN has been grown with great success on three different orientations of SBN, namely (001), (100) and (110), and it is the first time such films are available for device studies. The PSKNN thin films grown on Si and Al_2O_3 are essentially (001)-oriented films and their degree of orientation appears to be very sensitive to the film thickness.

Of the substrates mentioned above, films grown on Si substrates have been studied in the greatest detail and their dielectric constant was found to be close to 1000. The most interesting aspect of these films is that they can be switched from one structural form to another by the application of an external electric field. This also switches the polar axis from (001) to (010). Similar behavior has also been demonstrated for another tungsten bronze composition, PBN:60, near the morophotropic phase boundary (MPB) region. This effect can be used for various applications such as laser hardening and optical switching.

Both PLZT and $BaTiO_3$ thin films have been successfully grown on (001)-oriented SBN substrates. The perovskite films have an excellent lattice match with bronze SBN substrates in the (001) direction and we have already demonstrated the growth of grain-oriented films in this orientation. The PLZT films have been grown for possible use in

electro-optic applications whereas $BaTiO_3$ films have been developed for photorefractive applications.

We anticipate a great future for these films in various applications such as electronic memory, optical modulators, spatial light modulators (SLM), pyroelectric, photorefractive, SAW and piezoelectric devices. However, under this ONR sponsorship, we have only focused on electronic memory, electro-optic modulators and holographically controlled optical switches. The material requirements for each device application are summarized in Fig. 1. We have already demonstrated that tungsten bronze films are useful for electro-optic applications. Once optimized, these films will have a greater impact than the current best $LiNbO_3$.

PHOTOREFRACTIVE	ELECTRO-OPTIC	ELECTRONIC MEMORY
• LARGE n^3r_{ij}/ε	• LARGE r_{ij}/ε	• SQUARE HYSTERISIS LOOP - HIGH POLARIZATION
• HIGH COUPLING COEFFICIENT	• $\Delta n_i > \Delta n_e$	• FAST SWITCHING RESPONSE
• HIGH DIFFRACTION EFFICIENCY	• LOW OPERATING VOLTAGE	• HIGH RETENTION AND RESISTANCE
• FAST RESPONSE TIME	• LOW SPACE CHARGE FIELD	• LOW REVERSIBLE DIELECTRIC CONSTANT
• QUALITY AND CRYSTALLINITY	• QUALITY AND CRYSTALLINITY	• THICKNESS < 2000Å
• T_c ~ 150°C	• T_c ~ 150°c	• T_c ~ 150°C
PSKNN	PSKNN	PSKNN
$BaTiO_3$	PZT AND PLZT	

Fig. 1 Material requirements for various device applications.

As a result of the work performed under this program, several technical papers have been prepared, with three already published. This report includes drafts of some of these papers, published manuscripts and also preliminary results on the sputtering growth and characterization of tungsten bronze PSKNN and perovskite $BaTiO_3$ thin films as well as the sol-gel deposition of PZT and KTN thin films.

To assess the performance of these films in various optical devices applications, we have formed a team with groups at Rockwell (J. Hong), Caltech, University of California,

San Diego, Texas A&M, and Penn State. The results of their studies will be instrumental to our attempts to enhance the films' optical figures-of-merit and thus their device performance. The characteristics of the films developed under this ONR program are excellent in terms of quality, ferroelectric and optical properties. Furthermore, we have achieved control over our growth technique to the extent that films can be reproducibly grown in thickness varying from 5000Å to 10 μm. The properties of these films appear to be ideal for most device evaluations. With appropriate feedback from device community, we expect that suitably optimized thin films will come out of our work within the next one to two years. Figure 2 shows our future research direction for the development of these films in photorefractive, electro-optic and electronic memory applications.

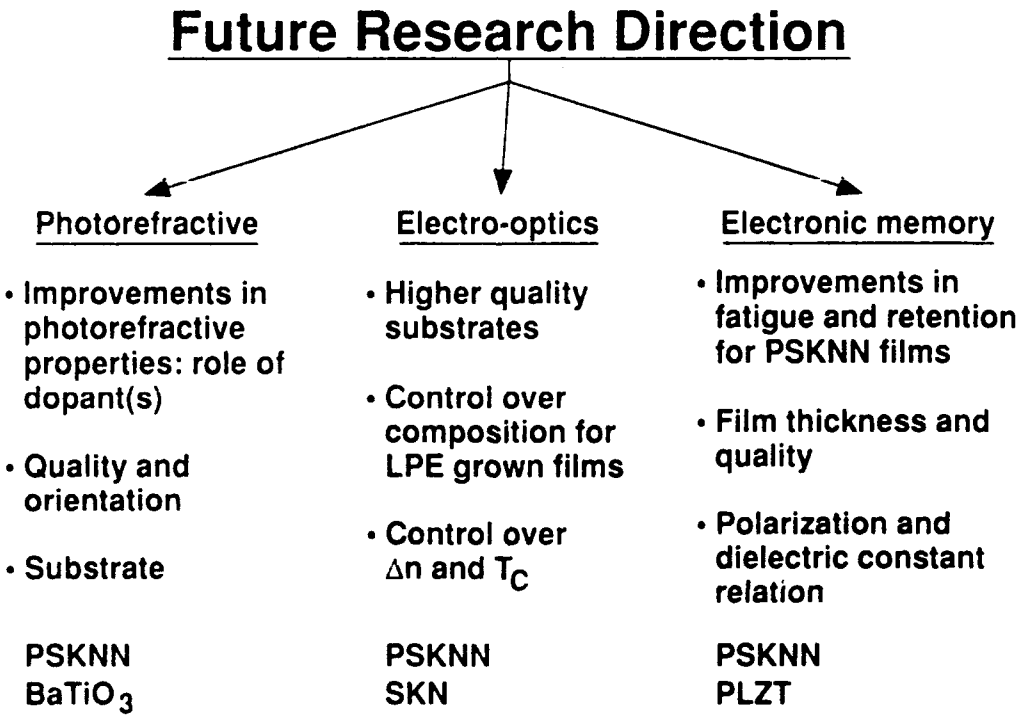

Fig. 2 Future research direction.

2.0 DEVELOPMENT OF PSKNN AND $BaTiO_3$ THIN FILMS

This section describes the growth and characterization of tungsten bronze PSKNN and perovskite $BaTiO_3$ films, which are not given in the attached papers. Both of these ferroelectrics are exceptionally attractive for electro-optic, photorefractive and other applications, and their growth in suitable quality with desired properties will make a significant impact on selected device studies.

2.1 Tungsten Bronze PSKNN Thin Films

Figure 3 shows the ferroelectric tungsten bronze $Pb_{2-x}Sr_xK_{1-y}Na_yNb_5O_{15}$ (PSKNN) system in which the morphotropic phase boundary region is located at x = 0.75. In this region, the electro-optic pyroelectric, piezoelectric and dielectric properties are exceptionally large and are nearly temperature independent. As shown in Fig. 3, on a binary phase diagram, an MPB appears as a nearly vertical line separating two ferroelectric, (mm2) and (mm2), phases, i.e., the boundary occurs at a nearly constant composition over a wide temperature range up to the Curie-temperature. Poled samples near such a boundary show unique and enhanced electro-optic properties because of the proximity in free energy of an alternate ferroelectric structure.

In this system, one can choose the electro-optic r33 or r_{51} coefficient according to device requirements. The transverse (r_{33}) electro-optic coefficient is large at the SNN side of MPB region while the longitudinal (r_{51}) electro-optic coefficient is large on PKN side. Furthermore, it is important to note that the spontaneous polarization (> 60 $\mu coul/cm^2$) is large on both sides of the MPB. The polar direction is different in these two forms: in the SNN side, the polar axis is along the (001) direction, while in the PKN side the polar axis is along the (100) or (010) directions. As illustrated in Fig. 3, one can grow films with either coefficient (r_{33} or r_{51}) by selecting (001) or (100)-oriented SBN substrates. In this work, we have selected a composition close to the MPB region having the polar axis along the (001) direction (SNN side) and have grown thin films on various substrates (Table 1) with excellent success.

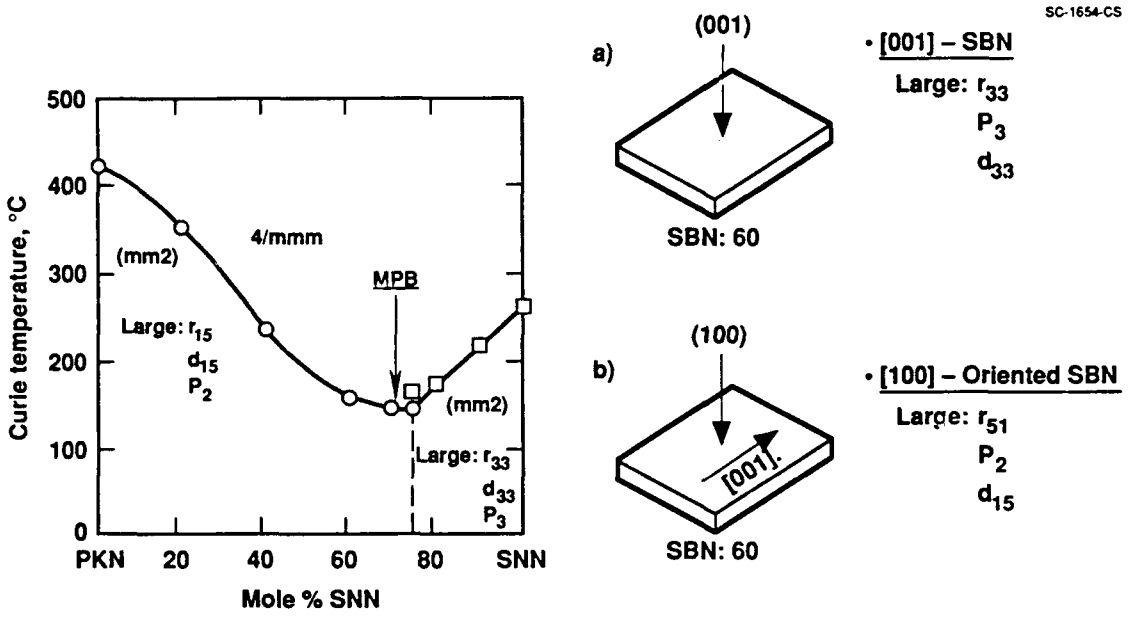

Fig. 3 Morphotropic phase boundary in the PSKNN system.

Table 1
Growth Conditions for Tungsten Bronze PSKNN Thin Films

Substrate Temp. Substrate	Annealing Temp. (°C)	(°C)	Dielectric Crystallinity	Constant
SBN:60 - Substrate				
(001)-oriented	300	650	S.C. Film*	---
(100)-oriented	300	650	S.C. Film*	---
Al_2O_3 - Substrate				
(100)-oriented	400	750 Oriented	Partially-	
Si - Substrate				
(100)-oriented	300	500-650	Grain-oriented	500-900
(100)-oriented	200	500-650	Polycrystalline	400-600

*Single crystal thin films.

The $Pb_{0.4}Sr_{1.6}K_{0.2}Na_{0.8}Nb_5O_{15}$ (PSKNN) thin films were deposited with an rf magnetron sputtering system. (100)-oriented Si and (001) and (100)-oriented SBN:60 substrates were used and the films were annealed at 550-600°C in an argon atmosphere. The sputtering conditions were as follows:

Target-Substrate Distance:	4-7 cm
Input Power Density:	1.9 to 2.4 W/cm^2
Gas Mixture:	Ar:O_2 (50:50)
Substrate Temperature:	100-400°C
Deposition Rate:	50 to 100Å/hr
Annealing Temperature:	550-600°C

Figure 4 shows an x-ray diffraction pattern for a PSKNN thin film deposited on (100)-oriented Si with Pt-electrodes as an intermediate layer. The growth and annealing conditions seem to be favorable to induce complete grain-orientation in ferroelectric PSKNN thin films. For growth below a 300°C substrate temperature, the films, as shown in Fig. 4, are essentially polycrystalline and require annealing around 600°C. As-grown films deposited above 300°C show a few x-ray diffraction peaks which were too weak to be identified; however, annealing above 550°C produced completely grain-oriented films. Based on these observations, it is clear that if the films are deposited above 500°C, it may be possible to eliminate the post-growth annealing step. This could be advantageous since annealing often degrades the surface quality.

Figure 5 shows grain-orientation as a function of film thickness for PSKNN films grown on Si. As can be seen from this result, the grain-orientation is sensitive to the film thickness and above 4 μm, other orientations are present, thus reducing the film's polarization and other properties. We believe that approximately 4 μm thick films can be obtained in completely grain-oriented form and above this limit, mixed oriented grains are seen. For applications such as electronic memory or SLMs, one needs much thinner films; hence we do not anticipate any problems in using these films for such applications.

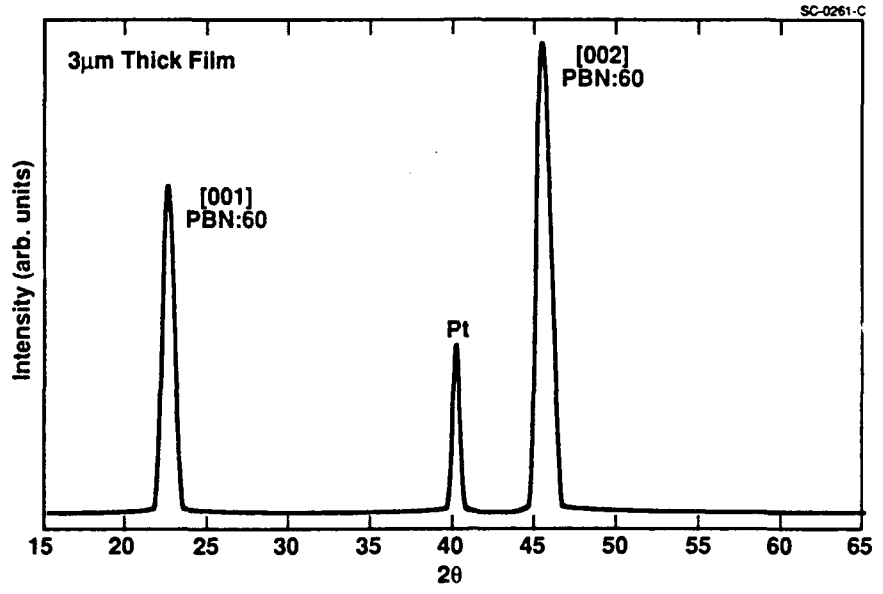

(a)

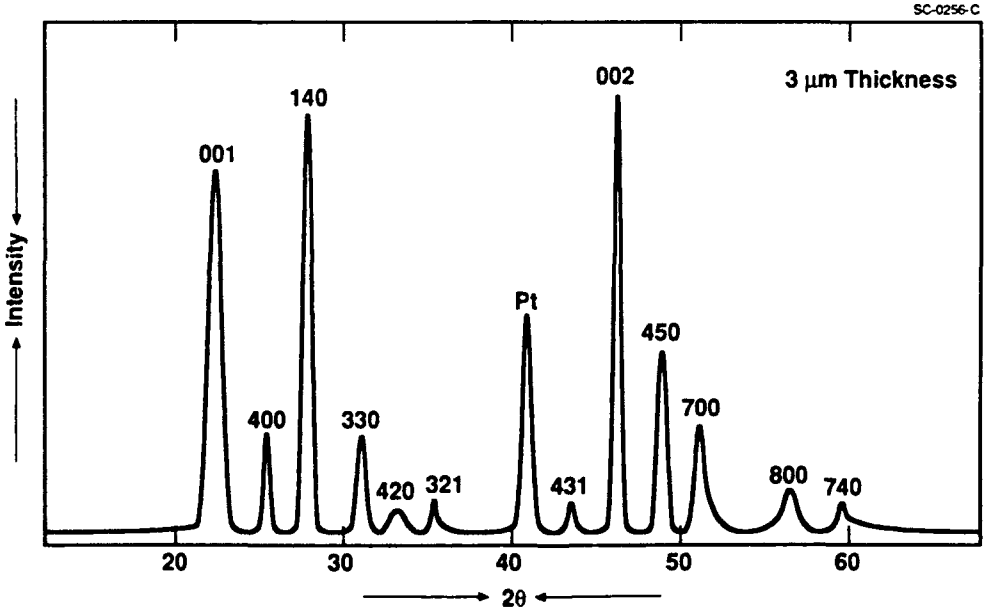

(b)

Fig. 4 X-ray diffraction pattern for PSKNN films deposited on [100]-oriented Si.

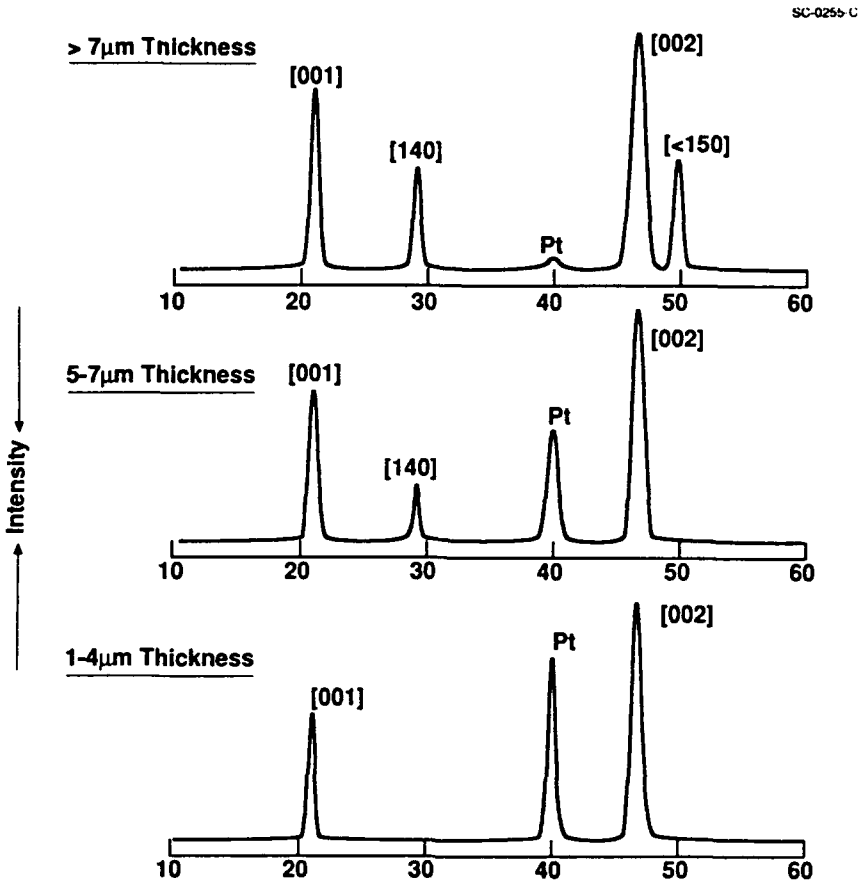

Fig. 5 Grain-orientation as a function of film thickness for PSKNN films on Si.

Figure 6 shows the XRD patterns of PSKNN single crystal thin films grown on (001)-oriented SBN:60 substrates. The films are typically 4 μm or above in thickness and since the lattice match between PSKNN and SBN is very close, the quality of these films is generally good. As can be seen from this figure, the crystallinity on SBN substrates depends on annealing temperature and it improves as the annealing temperature is raised. Currently, we have been successful in reducing the annealing temperature by raising the substrate temperature to over 300°C during the deposition. The films grown on SBN substrates are clear and the film quality depends on substrate quality. For this reason we have been using optical quality substrates for optical modulator and holographically controlled optical switch applications. In the case of holographic applications, one needs films which are highly photorefractive, requiring film doping. Based on our extensive work on photorefractive SBN and BSKNN single crystals, dopants such as Ce^{3+}/Ce^{4+}, Fe^{2+}/Fe^{3+}

and Rh^{3+}/Rh^{4+} are very effective in producing the desired photorefractive speed and coupling. In the present case, PSKNN films are doped with Fe^{2+}/Fe^{3+} and this addition has not required any substantial changes in the growth conditions.

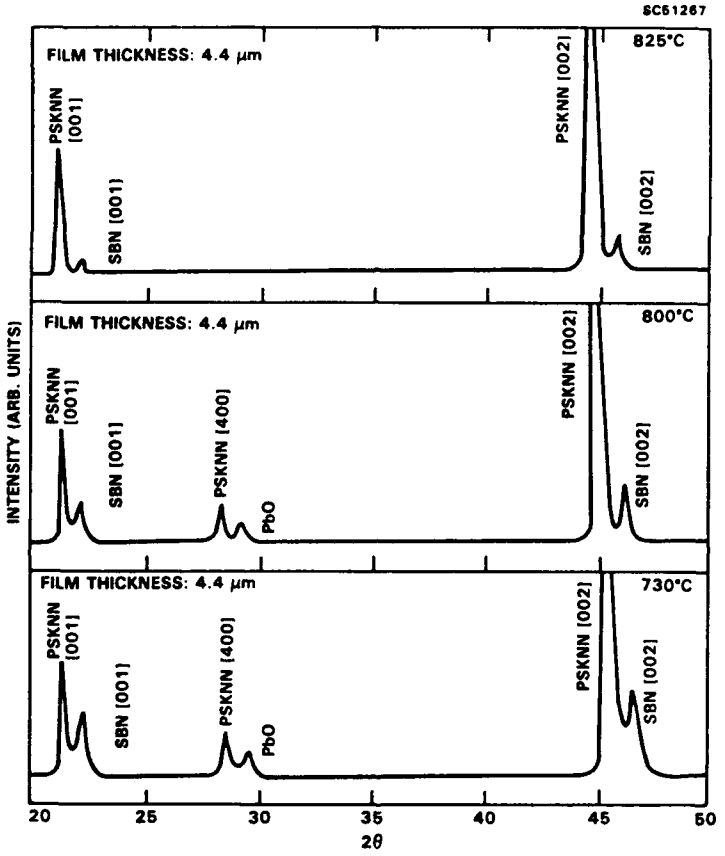

Fig. 6 X-ray diffraction pattern of PSKNN single crystal thin films on [001]-oriented SBN:60.

Ferroelectric and optical properties of PSKNN thin films deposited on Si and SBN are under study and are being evaluated in terms of film thickness and quality. The summary of our measurements is as follows:

1. Major Results on PSKNN Thin Films

* Completely grain-oriented films on Si substrates obtained up to 4 μm. The polarization increases with alignment of grains along the (001) direction.

* Single crystal films on (001) and (100)-oriented SBN:60 obtained with excellent optical quality.

* Switching of polar axis and structural symmetry with an applied external electric field is possible (15 kV/cm).

* Initial measurements indicate the refractive index for these films is higher than SBN:60.

2. Applications for PSKNN Thin Films

* Films grown on Si exhibit a figure-of-merit suitable for electronic memory and SLM applications.

* Optical modulators and holographically controlled optical switches appear to be feasible with our single crystal PSKNN thin films.

* Field induced switching is under study for laser hardening and optical switch applications.

2.2 Perovskite $BaTiO_3$ Thin Films

Under the ONR sponsorship, we have studied a number of perovskite thin films including PZT, PLZT, $Pb_{1-x}Bi_xTi_{1-x}Fe_xO_3$ (PBTF), KTN and $BaTiO_3$. The current status of this work has been briefly summarized in Table 2. The development of grain-oriented PZT and PLZT thin films has been studied in Japan and they have been successful in growing PZT (smaller unit cell compositions) on perovskite $SrTiO_3$ substrates. However, only a small range of perovskite materials can be grown using $SrTiO_3$ because of its small unit cell (a = 3.89Å). On the other hand, we have had considerable success in growing a wide range of perovskites on tungsten bronze substrates (Fig. 7). A detailed summary of work on grain-oriented PLZT is presented in the attached paper (in the present report).

In this section, we describe our progress in developing grain-oriented $BaTiO_3$ thin films on tungsten bronze SBN:60 substrates. For the first time such grain-oriented $BaTiO_3$ films are being successfully grown for photorefractive and electro-optic applications.

Table 2
Current Status of Perovskite Thin Films

Substrate Temp Composition	Annealing Temp (°C)	(°C)	Crystallinity	ε at R.T.	Remarks
PZT & PLZT					
(100)-oriented Al_2O_3	300	650	Polycrystalline	600	Needs to be improved
(100)-oriented Si**	300	600	Partially oriented	800	Good quality
(001)-oriented SBN	400	600	Grain-oriented	----	Excellent quality
(100)-oriented GaAs**	300	550	Poorly crystallized	800	Needs to be improved
PBTF					
(100)-oriented Si	300	650	Polycrystalline	----	
(001)-oriented SBN	300	700	Grain-oriented	----	Excellent quality
KTN*					
Quartz substrate	--	600	Polycrystalline	1000	Quality needs to be improved
(001)-oriented SBN	--	600	Grain-oriented		Excellent quality
$BaTiO_3$					
(100)-oriented Si	300	700	Partially oriented	2300	Good quality
(001)-oriented SBN	400	700	Grain-oriented	3000	Good quality

*Grown by sol-gel technique.
**Observed hysteresis behavior.

$BaTiO_3$ is one of the most promising materials for electro-optic and photorefractive applications because of its extremely large electro-optic coefficient (r_{51} = 1640 x 10^{-12} m/V). Currently many photorefractive device concepts such as phase conjugators, optical computing, image processing and laser hardening are emerging. However, severe crystal growth problems make $BaTiO_3$ single crystals very difficult to grow in decent size

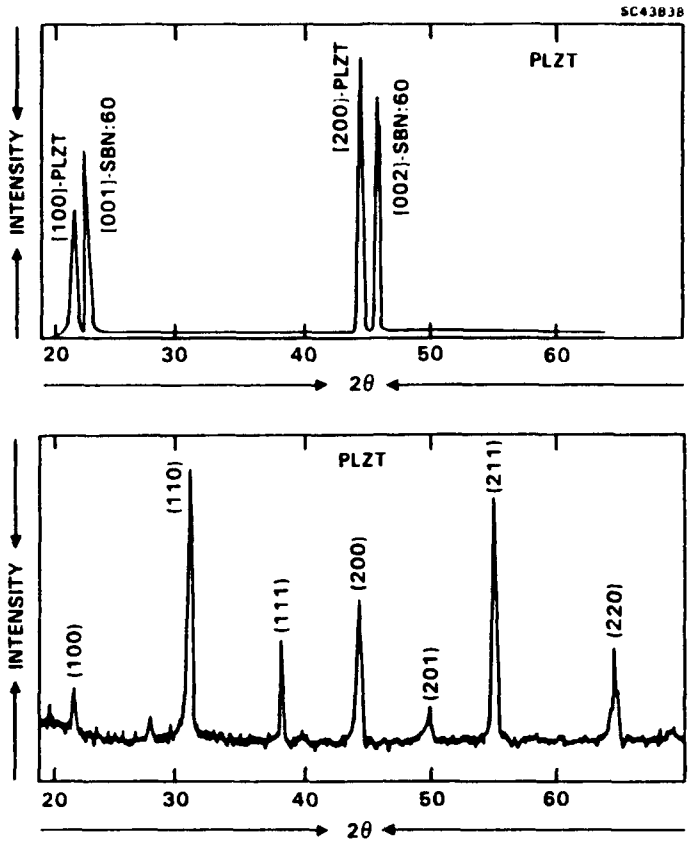

Fig. 7 [100]-oriented PLZT films on SBN:60 substrates.

and quality. As the crystal is pulled from the melt, a nonferroelectric hexagonal structural form of the material tends to form at the growth temperature and persists to room temperature. To help reduce this tendency, crystals are often grown slightly off congruent composition. A second difficulty in growing single crystals is the formation of twins when the material is cooled through the paraelectric: ferroelectric phase transition (m3m to 4mm). This phase transition is accompanied by the formation of 90° and 180° twins which makes the material very difficult to pole. For this reason, currently we are extending our efforts to develop grain-oriented/single crystal $BaTiO_3$ thin films for photorefractive applications.

It is interesting to note that $BaTiO_3$ has an excellent lattice-match with SBN:50, another important ferroelectric material. The lattice constants for $BaTiO_3$ in the ferroelectric form are A = 3.980Å and C = 4.01Å. The lattice constant c for SBN:50 is 3.965Å, making it an excellent candidate for epitaxial growth in the (001) direction. For this reason, SBN:50 substrates were selected for the growth of $BaTiO_3$ films.

$BaTiO_3$ thin films have been grown by the same sputtering technique developed for tungsten bronze PSKNN thin films. For this growth, we use a single target containing $BaTiO_3$ with excess of TiO_2. The target was made in our laboratory and it is approximately 3" in diameter. The growth conditions used for $BaTiO_3$ depositions are as follows:

Target - Substrate Distance:	5-7 cm
Input Power Density:	2.3 to 2.8 W/cm^2
Gas Mixture:	$Ar:O_2$ (80:20)
Substrate Temperature:	200-400°C
Deposition Rate:	50-100Å/hr
Annealing Temperature:	500-700°C

Table 3 summarizes the growth conditions and crystallinity of various $BaTiO_3$ thin films. The degree of grain-orientation obtained in this system depends on the substrate temperature during the film deposition. As shown in Fig. 8(b), when the deposition was made at substrate temperatures below 400°C, the films are essentially polycrystalline. However, when the substrate temperature was kept over 400°C during the deposition, the films are highly crystalline and they are oriented along the (100) direction. This is clearly shown in Fig. 8(a) by the fact that only the (100) and (200)-oriented $BaTiO_3$ peaks are observed when deposited on (001) oriented SBN:50 substrates. In both these cases, the films were post annealed at 700°C after the deposition was terminated.

Our recent study of the growth of tungsten bronze SCNN thin films on SBN:60 substrates indicates that the presence of the tetragonal or orthorhombic form of SCNN depends strongly on annealing conditions and substrate orientation. In the present study, we plan to explore such an approach to achieve (001)-oriented $BaTiO_3$ thin films [different annealing conditions as well as other SBN orientations (3 x 4.01 of $BaTiO_3$ = a-axis of SBN)].

To use these $BaTiO_3$ films for holographically controlled optical switch and other photorefractive applications, one needs fast photorefractive response and high coupling in

Table 3
Growth Conditions for $BaTiO_3$ Thin Films

Composition	Sub Temp (°C)	Anneal Temp (°C)	Crystallinity	Dielectric Constant
$BaTiO_3$	200	700	Polycrystalline	2400
$BaTiO_3$	300	700	Polycrystalline	2400
$BaTiO_3$	400	650	(100)-oriented Thin Films	3000
$BaTiO_3$	400	725	(100)-oriented Thin Films	3000
$BaTiO_3$;Fe	400	700	(100)-oriented Thin Films	3000

the desired spectral range. In both undoped $BaTiO_3$ or SBN crystals, these properties are not adequate but they can be increased by several orders of magnitude by a suitable doping scheme. Based on our current successful photorefractive work on tungsten bronze family and other ferroelectric materials, we have found that Ce^{3+}, Rh^{3+}, Fe^{3+}, Cr^{3+} or Mn^{3+} dopants are excellent choices to improve both speed and coupling.

In the present study, we have been growing $BaTiO_3$ films doped with Fe^{2+}/Fe^{3+} to improve the photorefractive response in these films. Fe-doped $BaTiO_3$ is considered to be very active and for this reason we have selected this dopant as a starting point. As shown in Table 3, the growth conditions of doped $BaTiO_3$ need not be changed because of the addition of Fe^{3+}. The amount of Fe in the target is about 0.015 wt%. Both doped and undoped films are smooth and are of reasonable quality. It must be stated that the film quality also strongly depends on the substrate quality. Once the film growth conditions are well established, we plan to use optical quality SBN substrates.

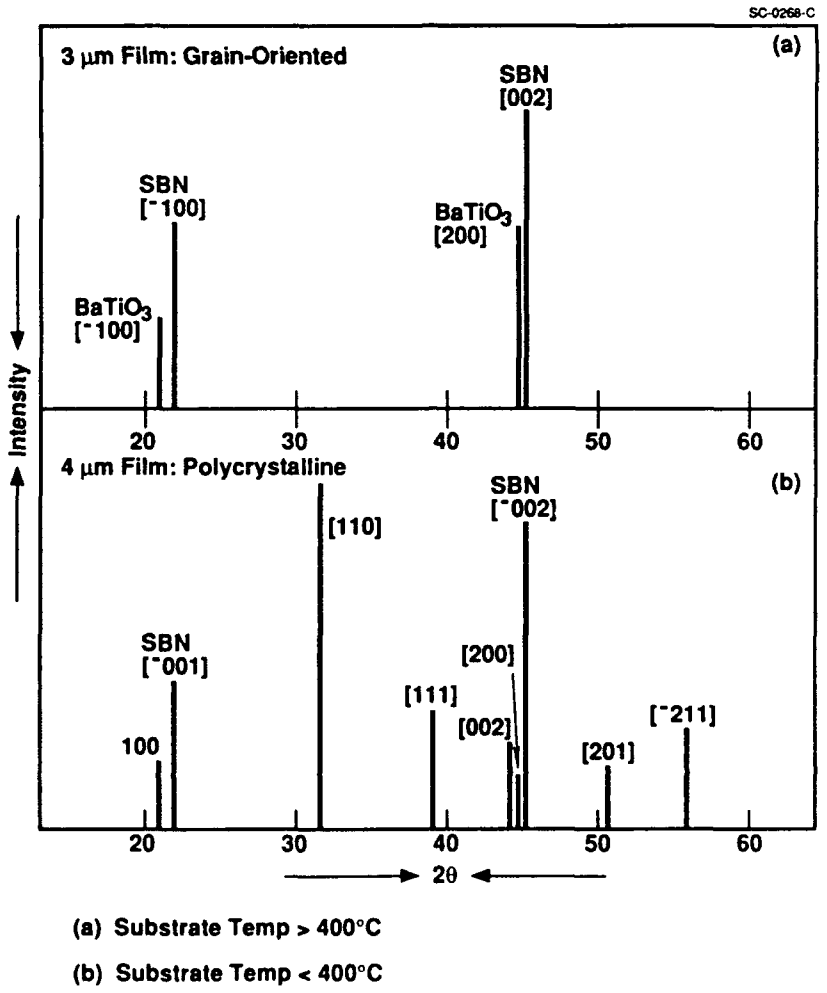

Fig. 8 X-ray diffraction pattern of $BaTiO_3$ thin films on [001]-oriented SBN substrates.

At present, efforts are underway to measure the temperature dependence of the dielectric constant for these films. The dielectric constant at room temperature for $BaTiO_3$ crystals is as follows:

$\varepsilon_{11} = 4100$

$\varepsilon_{33} = 120$

$P_3 = 24\ \mu coul/cm^2$

The measurements of the dielectric constant at room temperature for these films have been given in Table 3. As can be seen from this data, the dielectric constant for grain-oriented films is over 3000 indicating that the films are oriented in the (100) direction. The reduction in dielectric constant suggests that either our annealing temperature is low or the composition of $BaTiO_3$ films is slightly off of its stoichiometric composition. Further experiments are underway to establish the composition of the films by measuring the temperature dependence of the dielectric constant. This measurement will point out the desired changes in either film composition or annealing conditions. Once we optimize the dielectric and polarization properties of these films, we plan to explore their photorefractive properties.

In summary, we have demonstrated for the first time the growth of grain-oriented $BaTiO_3$ thin films on SBN:50 substrates. To capitalize on this success, we are currently improving the quality and photorefractive properties with respect to:

1. Film Quality
   - Grain-Orientation vs film thickness
   - Optical quality of doped films
2. Photorefractive Properties
   - Role of dopants: Fe^{3+}, Ce^{3+} and Rh^{3+}
   - Speed and coupling vs concentration of dopant

3.0 GROWTH OF KTN AND PZT FILMS BY THE SOL-GEL TECHNIQUE

This section briefly describes the sol-gel growth technique followed by the results of the characterization of perovskite KTN and PZT films. Both of these ferroelectrics are exceptionally attractive for electro-optic, photorefractive and other applications, and their growth in suitable quality with desired properties will make a significant impact on selected device studies.

3.1 Perovskite KTN and PZT Thin Films

Currently, many researchers are using the sol-gel technique to fabricate PZT thin films for use in electronic memory applications. Typically, films grown by this technique are polycrystalline. However, because of the excellent homogeneity and small particle size of sol-gel films, the spontaneous polarization of PZT films grown by this technique has been observed as high as 25 $\mu coul/cm^2$. There have been some reports from Japan of the fabrication of grain-oriented $LiNbO_3$ and related thin films by this technique for guided wave optical applications. In our present perovskite work, the single crystal SBN:60 wafers which are used as substrates, provide an excellent lattice match to both PZT and KTN. Consequently, we have been able to deposit highly grain-oriented films of these perovskite compositions.

The precursors used in the KTN growth were potassium ethoxide, tantalum ethoxide and niobium ethoxide, while lead acetate, titanium iso-propoxide and zirconium n-propoxide were used for the PZT films. In both compounds, the appropriate amount of each precursor chemical was added to methoxy ethanol. Once the stoichiometry of the solution was fixed in this manner, the solution could be further diluted with additional solvent to control the film thickness. The solution preparation procedure was performed in an inert atmosphere (N_2) to prevent the hydrolysis of the starting materials. After a solution of the appropriate composition and concentration was made, the solution was dripped onto a clean substrate and them spun on a conventional photoresist spinner. After the deposition step, the sample was hydrolyzed in air at 200°C for several hours. The sample was annealed at between 450 and 650°C to effect the complete hydrolysis of the film and to provide sufficient energy for good crystallization. Using this procedure, thin films of KTN and PZT ranging in thickness from 1000Å to 1.5 μm were grown.

For the KTN film growth, both [001]- and [100]-oriented SBN:60 substrates were used. The large difference in refractive index between KTN and SBN make them an excellent candidate for guided wave optical applications. A summary of the current status of this system is given in Table 4. Although good stoichiometric KTN was observed on both [001]- and [100]-oriented substrates, single crystal films were only obtainable on the [001]-oriented SBN. This is not surprising because the close lattice match in these materials is only in the c axis. Figure 9 shows the x-ray diffraction patterns of two KTN thin films of different thicknesses grown on [001]-oriented SBN:60. The close lattice match is readily apparent by the close proximity of the [001] and [002] peaks of each material. This figure also confirms the highly crystalline nature of the films by the fact that no other KTN reflections are observed. As expected, the relative intensity of the KTN [001] and [002] features increases with film thickness. In the 3500Å film, the KTN peak is smaller than that of the SBN substrate, but after reaching 1.0 μm in thickness, the KTN reflection becomes the dominant peak.

Table 4
Current Status of Sol - Gel Grown Thin Films

Composition	Substrate	Annealing Temp (°C)	Crystallinity	Remarks
PZT	SBN [001]	600	highly grain-oriented film	Δn is large : useful for guided wave optics
PZT	SBN [100]	600	polycrystalline	
PZT	Al_2O_3 [001]	650	grain - oriented	Δn is large : useful for guided wave optics
KTN	SBN [001]	650	highly grain-oriented film	Δn is large : useful for guided wave optics
KTN	SBN [100]	650	polycrystalline	

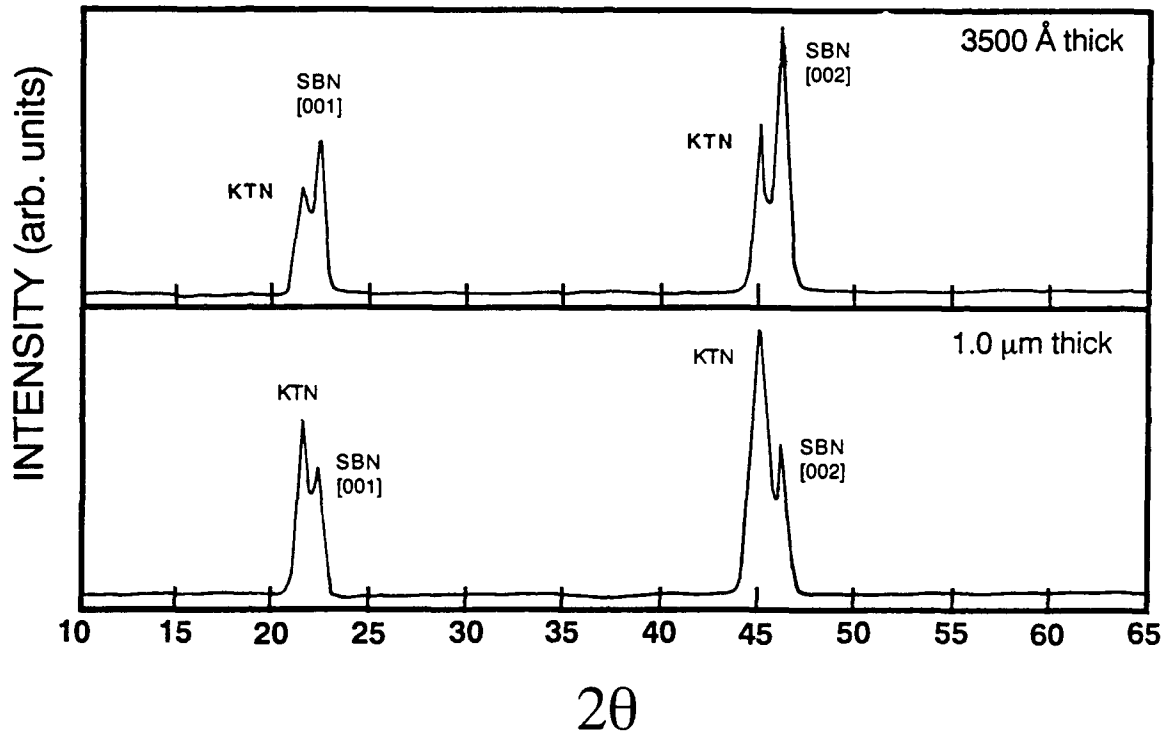

Fig. 9 X-ray diffraction pattern of sol-gel grown KTN thin films on SBN substrates.

Similar experiments were performed in the growth of PZT thin films. For this work, [001]-oriented Al_2O_3 as well as both [100]- and [001]-oriented SBN:60 were used as substrate material. As in the case of KTN, the best crystallinity was observed when PZT was deposited on [001]-oriented SBN. Once again the c axis in this system provides the best lattice match for film growth. Figure 10 shows the x-ray diffraction pattern of a 2500Å thick PZT film grown on [001]-oriented SBN. The extremely close proximity of the [001] and [002] features of the film and substrate once again indicate the excellent lattice match. These films are extremely well oriented as evidenced by the fact that only [00l]-type features are observed. The absence of additional peaks also indicates that no second phases or significant impurities are present.

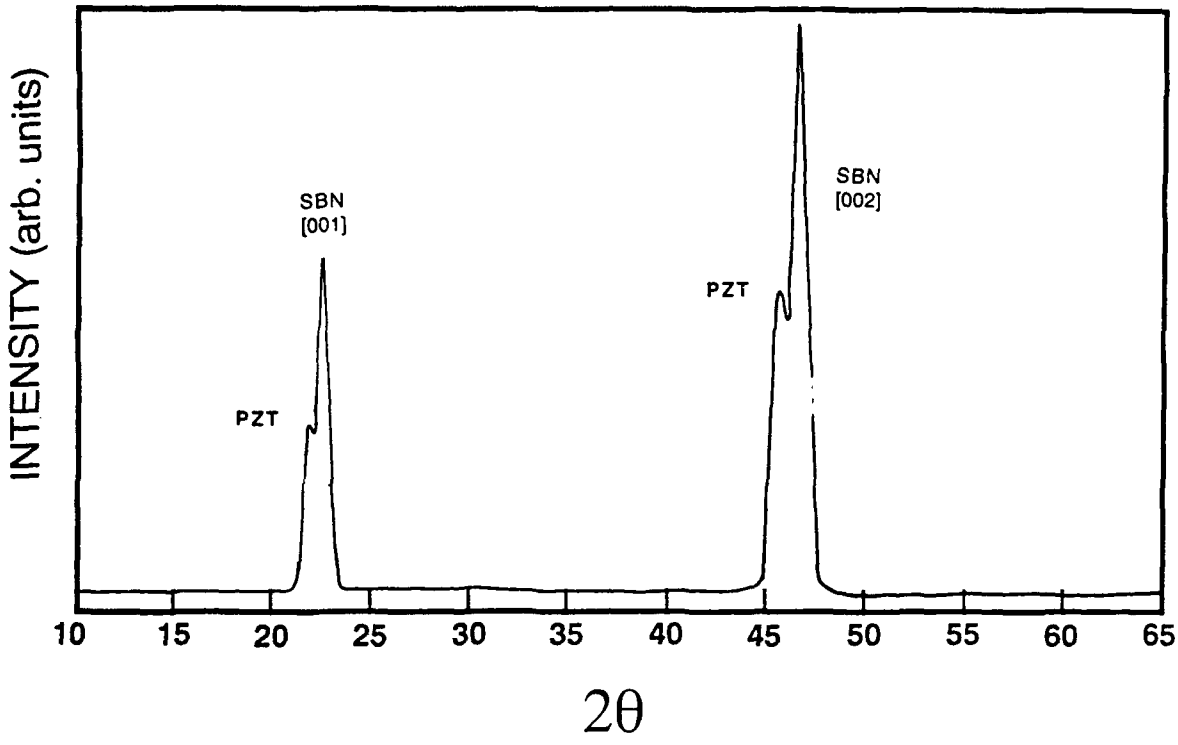

Fig. 10 X-ray diffraction pattern of PZT thin film grown on [001]-oriented SBN substrate using the sol-gel technqiue.

Al_2O_3 substrates were also used for the sol-gel growth of PZT. In this instance, high quality grain-oriented films were observed. Characterization of these films by x-ray diffraction indicates the films are single phase and that no significant impurities are present. Table 4 also gives a summary of the sol-gel growth of PZT thin films on both types of substrates. As is the case with KTN, PZT thin films grown on SBN or Al_2O_3 are also promising candidates for optical wave guide applications.

In summary, we have successfully demonstrated that the sol-gel technique can be used to grow high quality KTN and PZT thin films on SBN or Al_2O_3 substrates. Highly grain-oriented films are observed on [001]-oriented SBN substrates for both compositions. However, even when polycrystalline films are obtained, as in the case of [100]-oriented SBN, the film quality is still excellent. With further work, these systems could make a significant impact on guided wave optics applications.

4.0 EPITAXIAL GROWTH OF PLZT SINGLE CRYSTAL FILMS ON BRONZE SBN SUBSTRATES BY THE SPUTTERING TECHNIQUE

EPITAXIAL GROWTH OF PLZT SINGLE CRYSTAL FILMS ON BRONZE SBN SUBSTRATES BY THE SPUTTERING TECHNIQUE

R.R. Neurgaonkar, I. Santha and J.R. Oliver
Rockwell International Science Center
Thousand Oaks, CA 91360

and

L.E. Cross
The Pennsylvania State University
University Park, PA 16802

ABSTRACT

This paper reports the preliminary results of epitaxial growth of single crystal PLZT thin films on tungsten bronze $Sr_{0.6}Ba_{0.4}Nb_2O_6$ (SBN:60) substrates by the rf sputtering technique. The films were deposited primarily with (100) SBN substrate orientation and temperatures over 500°C. These films exhibit excellent epitaxy with film orientation along the (100) direction. A multilayer approach has been proposed to improve film quality and properties.

INTRODUCTION

A lanthanum-modified lead-zirconate-titanate solid solution system (PLZT) is a well known ferroelectric material. PLZT is transparent in the visible and near-infrared regions, has various electro-optic[1] and photochromic[2] activities, and promises excellent optoelectronic properties. There have been numerous concepts for its application in electronic and optoelectronic devices making use of these interesting properties, e.g., in a nonvolatile FET memory with ferroelectric gates;[3,4] optical switches;[5] image storage;[6] optical modulators;[7] and, optical display devices.[8] Considerable practical interest has been generated on a PLZT thin films for the purpose of reducing the drive voltage, miniaturization and cost reduction of optoelectronic devices.

Quite recently, several attempts to prepare a PLZT thin films have been initiated using rf sputtering and electron beam evaporation,[9-13] and some PLZT thin films possessing good ferroelectric properties have been obtained. However, from the viewpoint of applications in optical waveguide systems, the preparation of better thin films with high transparency in required. The most significant obstacle in obtaining good transparency and electro-optic properties is the difficulty in growing the perovskite structure with large grain size on suitable substrate materials during film deposition and heat treatment, since the grains increase absorption due to light scattering. We have conducted a series of experiments on the epitaxial growth of PLZT thin films on single crystal tungsten bronze $Sr_{0.6}Ba_{0.4}Nb_2O_6$ (SBN:60) substrates and have succeeded in growing these films with good crystallinity. In this paper, the growth of these thin films, their structural properties, and their applicability to electro-optic devices in integrated optics are discussed.

Experimental Procedure

The sputtering targets employed were a mixture of PLZT and PbO. Approximately 5 mole% excess of PbO was added in the targets to control the Pb^{2+} concentration in the films. The targets were prepared using ceramic sintering or hot-pressing; well-mixed powders were cold pressed and then sintered or hot-pressed at 1000°C after ball-milling. The Zr:Ti ratio was 45:55 and the La^{3+} concentration varied between 2 to 5 mole% in these targets. The targets thus prepared showed no extra phases and were fabricated in 3 in. diameters to obtain uniform film deposition.

The PLZT thin films were deposited with an MRC rf sputtering instrument; the sputtering conditions are summarized in Table 1. SBN:60 crystal substrates of dimensions 10 × 10 × 1 mm were cut in the (001) plane. Some of the substrates were polished to optical quality, etched with HF acid after polishing, or mechanochemically polished. The substrate temperature was maintained between 100 to 500°C during these film growths.

RESULTS AND DISCUSSION

The epitaxial growth of PZT and PLZT has been subject of great interest for various applications, with film growth proving successful on various substrates (MgO, Si, SiO_2, Al_2O_3, Pt, glass, etc.). However, the films obtained on these substrates are basically polycrystalline, with frequent occurrences of a pyrochlore phase. Recently, Higuma et al[14,15] grew PLZT films on $SrTiO_3$ substrates and reported that the films were single crystal with excellent epitaxy. $SrTiO_3$ is cubic at room temperature with a lattice constant a = 3.905Å, while PLZT can be either rhombohedral or tetragonal, depending upon the Zr:Ti ratio. The lattice constants for the tetragonal PLZT solid solution are a = 3.904 to 4.05Å

and c = 4.05 to 4.15Å. Thus, one can adjust the film composition such that there is a good lattice match with the substrate. In the present work, we have employed tungsten bronze SBN:60 substrates which are tetragonal at room temperature with lattice constants a = 12.468Å and c = 3.938Å.[16] The PLZT composition selected for epitaxial growth was $Pb_{0.97}La_{0.03}Zr_{0.45}$- $Ti_{0.55}O_3$ (3/45/55) with lattice constants a = 3.955Å and c = 4.125Å. This composition has an excellent lattice match with SBN:60 substrates in the following two orientations:

$$(100)_{film} = (001)_{sub.} \qquad [a_{film} = c_{sub}]$$

$$3 \times (001)_{film} = (100)_{sub.} \qquad [3 \times c_{film} = a_{sub}]$$

As shown in Fig. 1, 3 cm diameter, 7 cm long SBN:60 single crystals of optical quality were used in these growths.[17,18] Two other tungsten bronze crystals having slightly bigger lattice constants, SBN:50 and BSKNN-1, are also available for use as substrates.

PLZT thin films were deposited on (001)-oriented SBN:60 with substrate temperatures varied between 100 and 500°C. As summarized in Table 1, all films were grown in an $Ar:O_2$ atmosphere. The sputtering conditions were as follows:

Target-Substrate Distance:	4-5 cm
Input Power Density:	1.9 to 2.4 W/cm^2
Gas Mixture:	$Ar:O_2$ (50:50)
Substrate Temperature:	100 to 500°C
Deposition Rate:	50-100Å/hr
Annealing Temperature:	600-650°C

Figure 2 shows x-ray diffraction patterns of PLZT thin films deposited on glass and SBN:60 substrates and annealed at 600°C. All of the tetragonal perovskite peaks of PLZT were observed when the film was deposited on glass, with the formation of the pyrochlore phase below 600°C. This result is consistent with work reported by various researchers, including our earlier work.[5-15,19] However, when the film was deposited on the (001)-oriented SBN:60 substrates, only the (100) and (200) diffraction peaks of the film were observed. This clearly shows that the PLZT films deposited on SBN substrates are single crystal with excellent epitaxy. We believe that this is the first time such perovskite films have been grown on tungsten bronze substrates.

The growth of PLZT films was investigated at various substrate temperatures and it was found that the films grown below 400°C were weakly crystallized and needed subsequent annealing above 500°C. However, films grown at substrate temperatures of 500°C or above were well crystallized, single crystal films. Furthermore, the use of SBN substrates completely suppressed the formation of the pyrochlore PLZT phase even at lower temperatures. On the other hand, PLZT films grown on other substrates such as glass, Pt, Al_2O_3 and quartz always exhibited a pyrochlore phase and required high-temperature annealing to convert to the perovskite phase.

The occurrence of a pyrochlore phase is a subject of great interest in Pb^{2+}-containing perovskites and it usually appears when the unit cell c/a ratio is below 1.06, as shown in Fig. 3. Since c/a for $PbTiO_3$-$BiFeO_3$ is 1.17, one does not observe the pyrochlore phase on this system. On the other hand, the pyrochlore phase is found for all compositions in the $PbTiO_3$-$PbZn_{0.33}Nb_{0.66}O_3$ system. The latter is exceptionally important for electro-optic and piezoelectric applications because it exhibits both electro-optic and piezoelectric coefficients very large with a large spontaneous polarization.

The lattice constant a is estimated to be 3.955Å in the PLZT films, in close agreement with the ceramic target value. Electron diffraction patterns need to be studied to ascertain the single crystallinity and polar direction in these films. PLZT deposited on SBN:60 substrates are completely transparent in the visible, cutting off in the IR because of substrate absorption. According to work by Okuyama et al,[15] PLZT films deposited on MgO and $SrTiO_3$ are transparent from the visible to the near-IR. Optical measurements on their films suggest that the optical loss is about 6 db/cm, which is slightly higher than that of $LiTaO_3$ single crystals. However, the half-wave voltage is about one fourtieth of that for $LiNbO_3$, and the reduction of the element size would compensate for the large loss factor. We suspect that this loss can be suppressed further by using well matched substrates such as SBN:60 or other bronze materials.

FUTURE PLANNED WORK: MULTILAYER THIN FILMS

Since the growth of single crystal PLZT thin films on SBN:60 has been successful, it opens up various ways one can improve film quality. If the optical quality or optical loss remains a problem for device applications, a multilayer approach may be appropriate for these films. Since tungsten bronze $Pb_{0.6}Ba_{0.4}Nb_2O_6$ (PBN:60) has a c lattice constant close to the a constant of PLZT, a possibility is to first deposit a PBN:L60 layer on an SBN:60 substrate and then deposit the PLZT film on this layer. Figure 4 summarizes our experimental approach for this concept. As shown in the figure, additional layers of PBN:60 and PLZT may be deposited to improve the film quality of the final film layer. For spatial light modulators and guided wave optics, it is advantageous for the films to have an optical refractive index larger than the substrate, while still maintaining a large optical figure-of-

merit, r_{ij}/ε. As shown in Fig. 4, PLZT possesses a significantly larger index than tungsten bronze materials, with Δn of around 0.10.

ACKNOWLEDGEMENT

This work was supported by the AFOSR (F49620-86-C-0052) and ONR (N00014-81-C-0463). The authors are grateful for discussions on this research with W.F. Hall and W.K. Cory.

REFERENCES

1. G.H. Haertling and C.E. Land, J. Am. Ceram. Soc. 54, 11, (1971).
2. K. Tanaka, Y. Higuma, K. Wakino and M. Murata, J. Am. Ceram. Soc. 59, 465, (1976).
3. Y. Matsui, Y. Higuma, M. Okuyama, T. Nakagawa and Y. Hamakawa, Proc. Ist Meeting of Ferroelectric Mat. and Their Appl. (FMA Office, Kyoto, 1978) p. 37.
4. Y. Hamakawa, Y. Matsui, Y. Higuma, T. Nakagawa, Tech. Digest, IEEE IEDM, Washington DC, 297 (1977)
5. W.E. Perry and B.M. Soltoff, Ferroelectrics, 10, 201, (1976).
6. C.E. Land and W.D. Smith, Appl. Phys. Lett. 23, 57 (1973).
7. S.G. Varnado, W.D. Smith, IEEE J. Quantum Electron. EQ-8, 88, (1972).
8. A. Kuwamada, K. Suzuki and G. Toda, Ferroelectrics, 10, 25, (1976).
9. K. Tanaka, Y. Higuma, K. Yokoyama, T. Nagakawa and Y. Hamakawa, Jpn., J. Appl. Phys. 15, 1381, (1976).

10. M. Ishida, H. Matsunami and T. Tanaka, J. Appl. Phys. 48, 951, (1977).

11. M. Ishida, S. Tsuji, K. Kimura, H. Matsunami and T. Tanaka, J. Cryst. Growth, 45, 393, (1978).

12. A. Okada, J. Appl. Phys. 49, 4495, (1978).

13. t. Nagakawa, J. Yamaguchi, T. Usuki, Y. Matsui, M. Okuyama, and Y. Hamakawa, Jpn., J. Appl. Phys., 18 897 (1979).

14. Y. Higuma, K. Tanaka, T. Nakagawa, T. Kariya and Y. Hamakawa, Jpn. J. Appl. Phys. 16, 1707 (1977).

15. M. Okuyama, T. Usuki and Y. Hamakawa, Appl. Physics, 21, 339, (1980)

16. A.A. Ballman and H. Brown, J. Cryst. Growth.

17. R.R. Neurgaonkar and W.K. Cory, J. Opt. Soc. Am. B3(2), 274 (1986).

18. R.R. Neurgaonkar, W.K Cory, J.R. Oliver, M.D. Ewbank and W.F. Hall, Opt. Eng. 26(5), 392 (1987).

19. R.R. Neurgaonkar, I. Santha, E.T. Wu, J.R. Oliver and L.E. Cross, to appear in J. Mat. Science.

Table 1

Growth of PLZT Thin Films on SBN Substrates

PLZT Film	Lattice-Match	As-Grown	Annealed Above 600°C	Lattice Constant	Remarks
(001)-oriented SBN:60 (substrate)					
≤ 400°C	0.40%	Weakly crystallized	Single crystal film	3.953Å	Excellent quality
≥ 550°C	0.40%	Well crystallized	Single crystal film	3.957Å	Excellent quality
Glass-Substrate					
≤ 400°C	—	Amorphous	<600°C pyrochlore >500°C perovskite	a = 3.961Å	Pyrochlore phase problem
≥ 550°C	—	Weakly crystallized pyrochlore	600°C perovskite (polycrystalline)	c = 4.121Å	
Lattice Constants:	SBN:60	a = 12.458Å,	c = 3.938Å		
	PLZT	a = 3.955Å,	c = 4.125Å		

FIGURE CAPTIONS

Fig. 1 SBN:60 singhle crystals grown along <001>.

Fig. 2 Perovskite PLZT thin films on tungsten bronze SBN:60 substrate.

Fig. 3 The c/a ratio for perovskite materials.

Fig. 4 Advantages of multilayer ferroelectric thin films.

PEROVSKITE PLZT THIN FILMS ON T.B. SBN SUBSTRATES

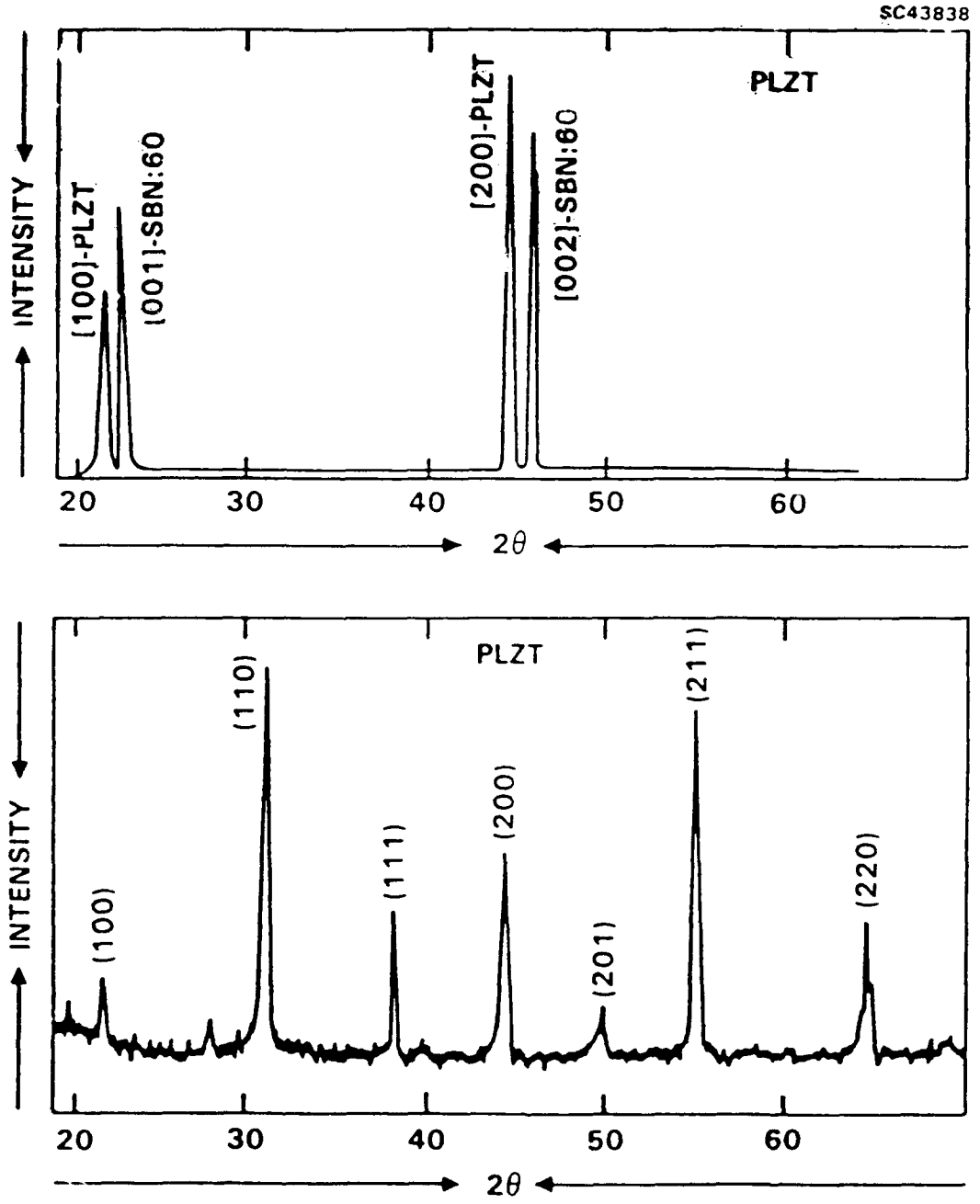

SC5345.FR

LEAD TITANATE-BISMUTH FERRITE

SC44827

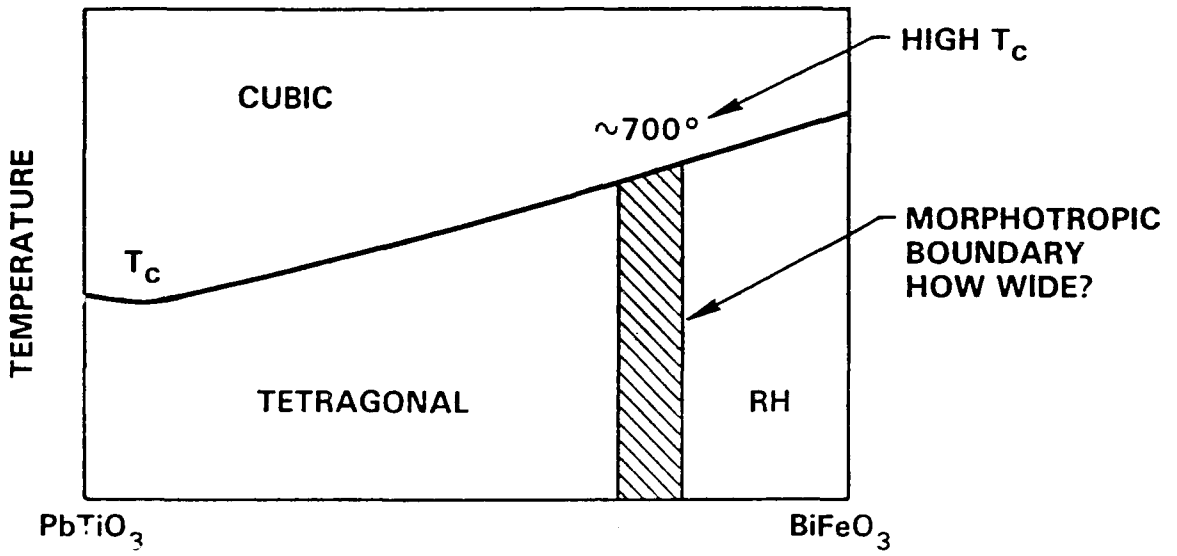

VERY LARGE STRAIN

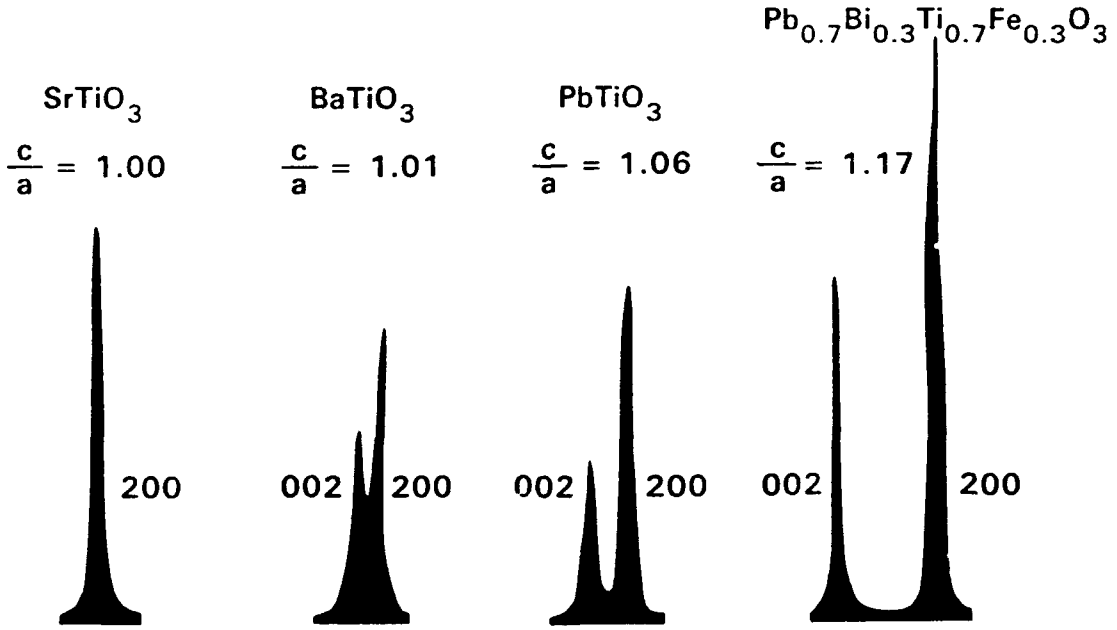

X-RAY (200) PEAKS

Rockwell International
Science Center

ADVANTAGES OF MULTILAYER FERROELECTRIC THIN FILMS

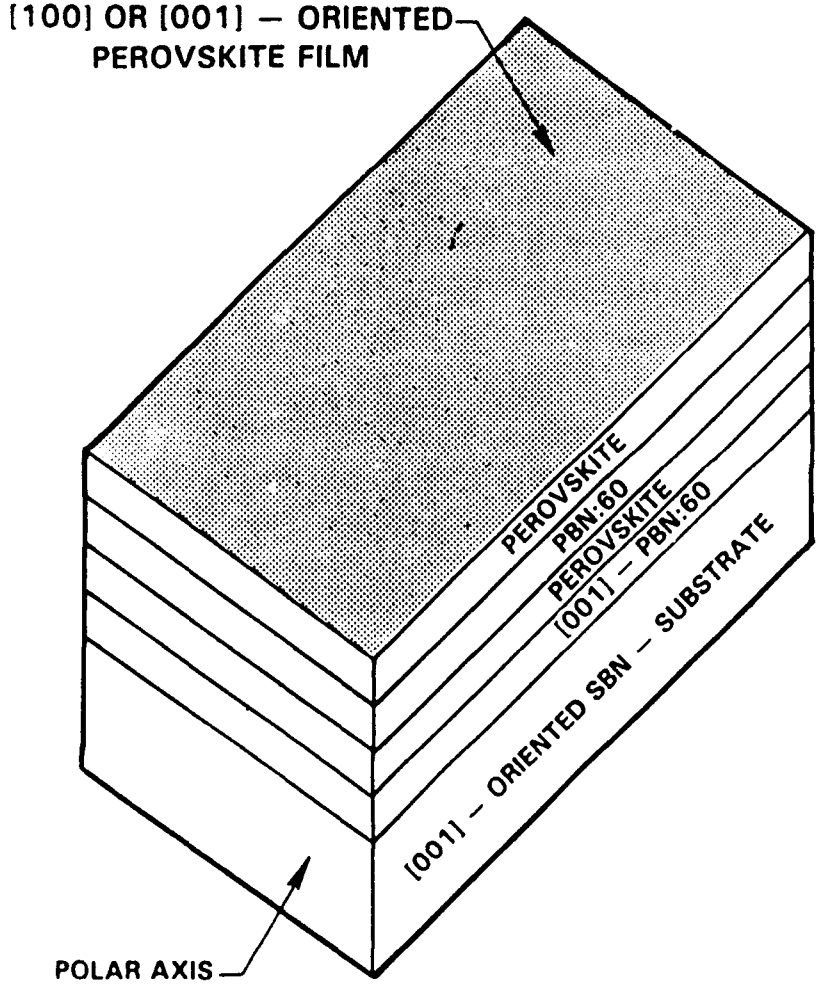

SC42626

SBN:60	PBN:60	PEROVSKITES
[001]	[001]	[100] OR [001]
n = 2·24	n = 2·32	n = 2·4 TO 2·76
LARGE r_{33}, ε_{33}	LARGE r_{51}, ε_{11}	LARGE r_{51}, ε_{33}
T_C = 78°C	T_C ≈ 280°C	T_C = 100 – 300°C

PEROVSKITE FILMS

PZT, PLZT, PZNT, PBFT

APPLICATIONS

- OPTICAL WAVEGUIDES AND SWITCHES
- 3-D STORAGE AND DISPLAY
- PYROELECTRIC AND PIEZOELECTRIC
- MULTILAYER CAPACITORS

Rockwell International
Science Center

Rockwell International
Science Center
SC5345.FR

5.0 GROWTH OF PEROVSKITE PZT AND PLZT THIN FILMS

Rockwell International
Science Center
SC5345.FR

JOURNAL OF MATERIALS SCIENCE 25 (1990) 2053–2055

Growth of perovskite PZT and PLZT thin films

R. R. NEURGAONKAR, I. SANTHA, J. R. OLIVER, E. T. WU
Rockwell International Science Center, Thousand Oaks, California 91360, USA

L. E. CROSS
Pennsylvania State University, University Park, Pennsylvania 16802, USA

This paper reports preliminary results on the fabrication of perovskite PZT and PLZT thin films using a sputtering technique. For glass, quartz and sapphire substrates, it was necessary to raise the substrate temperature above 550° C to achieve perovskite tetragonal structures of interest. Growth at temperatures below 550° C yielded a major pyrochlore structure phase. Excess of PbO in the target was also required to maintain stoichiometry in these films.

1. Introduction

Recently, considerable attention has focused on the development of low-loss ferroelectric thin films for optical waveguides. Several attempts have been made to grow single crystal waveguide films using materials such as $LiNbO_3$ [1–3], PLZT [4–], KLN and SBN [7, 8]. More recently, other ferroelectric materials such as $BaTiO_3$ and PBN have been considered using semiconductor substrates for various optical applications, including waveguides, spatial light modulators, switches and pyroelectric detectors. The top surfaces of as-grown $LiNbO_3$ and SBN films fabricated by liquid phase epitaxial growth, chemical vapour deposition, melting methods and so on, are relatively rough so that they must be optically polished to couple a light beam into the film. On the other hand, polishing is not necessary for sputtered thin films. Therefore, the sputtering technique has been used in the present work to develop perovskite PZT and PLZT films using a variety of substrates such as glass, quartz and sapphire. This paper reports the growth of PZT and PLZT films and their associated growth problems.

2. Experimental procedure

The sputtering targets employed were a mixture of PZT or PLZT and PbO. Approximately 5 mol % excess PbO was added in these targets to control the Pb concentration in the films. The targets were prepared using ceramic sintering or hot pressing; well-mixed powders were cold pressed and then sintered or hot pressed at 1100° C after ball-milling.

Sapphire (Al_2O_3) and quartz (SiO_2) substrates were first etched by sputtering. The substrates were mounted on a heating block with a stainless steel mask of 0.2 mm thickness. Substrate temperature was monitored by a Pt–Pt.Rh 13% thermocouple inserted into the centre of the substrate holder. The sputtering conditions, summarized in Table I for each material, are as follows:

Target–substrate distance	5 cm
Input power density	1.9 to 2.4 W cm^{-2}
Sputtering gas	Ar:O_2 (40:60 or 50:50)
Gas pressure	8 to 12 μm
Substrate temperature	300 to 600° C
Deposition rate	20 to 25 Å h^{-1}
Annealing temperature	700 to 800° C

3. Experimental results and discussion

PZT and PLZT compositions have been of practical interest for the last 25 years and are being exploited for optical applications such as switches, modulators, image storage and optical display devices. PZT occurs on the pseudobinary $PbZrO_3$–$PbTiO_3$ system and exhibits a morphotropic phase boundary at a Zr:Ti ratio of 52:48, as shown in Fig. 1. However, the development of bulk single crystals has been hindered by growth problems associated with Pb^{2+} losses during growth and cracking when cycling through the

TABLE I Growth condition for PZT and PLZT films

Substrate	Substrate temperature		Atmosphere	Power density (W cm^{-2})	Film thickness (μm)	Remarks
	≤ 550° C	~ 600° C				
PZT films						
Glass	Pyrochlore	Perovskite	50% Ar + 50% O_2	2.2–2.4	1–5	
Quartz (SiO_2)	Pyrochlore	Perovskite	50% Ar + 50% O_2	2.2–2.4	3–10	Excellent films
Sapphire (Al_2O_3)	Pyrochlore	Perovskite	50% Ar + 50% O_2	2.2–2.4	3–10	Reasonable quality
PLZT films						
Glass	Pyrochlore	Perovskite	40% Ar + 60% O_2	1.9–2.1	3–10	Reasonable quality
Quartz (SiO_2)	Pyrochlore	Perovskite	40% Ar + 60% O_2	1.9–2.1	2–8	Excellent quality
Sapphire (Al_2O_3)	Pyrochlore	Perovskite	40% Ar + 60% O_2	1.9–2.1	2–5	Reasonable quality

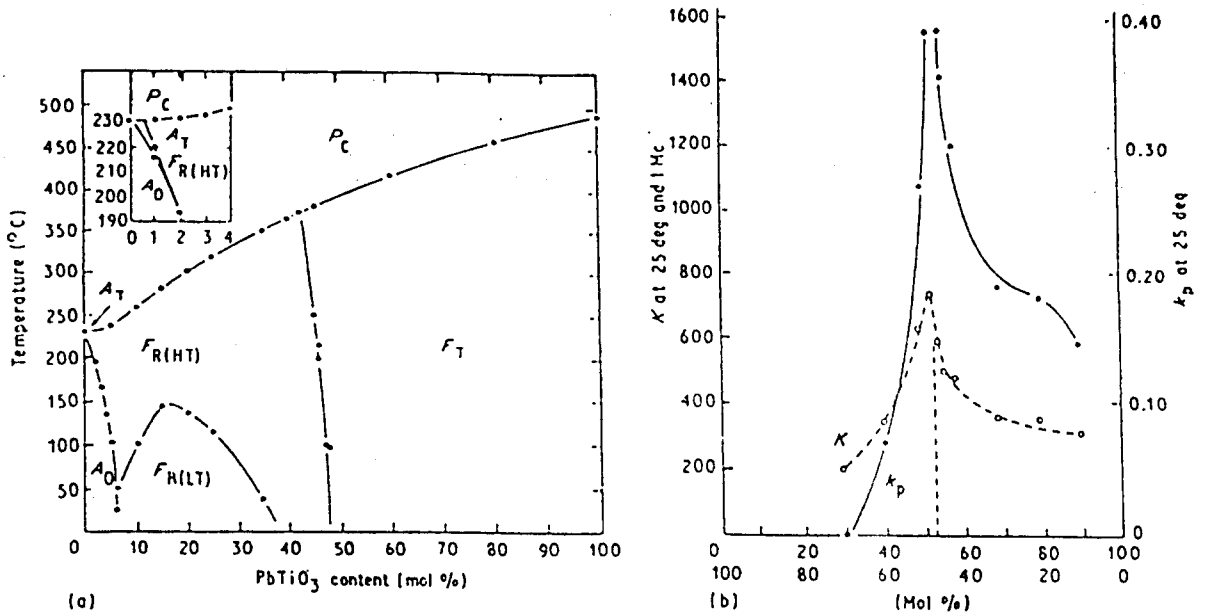

Figure 1 Morphotropic phase boundary in the PZT system.

paraelectric/ferroelectric phase transition. For this reason, thin-film growth of these compositions is now being explored in several countries [9–11].

The deposition of PZT and PLZT films by the sputtering technique has shown that the structure of the film is sensitive to the substrate temperature (Fig. 2). PZT or PLZT thin films having a pyrochlore structure were obtained below 550° C, whereas a perovskite structure was obtained above 600° C. However, traces of $PbTi_3O_7$ were observed with Pb^{2+} deficiencies, and for this reason, an extra 5 mol % PbO was incorporated in the targets to stabilize the film composition.

Fig. 3 shows the X-ray diffraction patterns of PLZT films sputtered on fused quartz and sapphire and for a PLZT(9/65/35) hot-pressed ceramic. In Fig. 3, (a) is for a film (~4 μm thickness) sputtered at a substrate temperature of 550° C with a target containing 5 mol % of PbO excess, (b) is for a film sputtered at 600° C with a target containing 3 mol % PbO excess, and (c) is for the hot-pressed PLZT ceramic target.

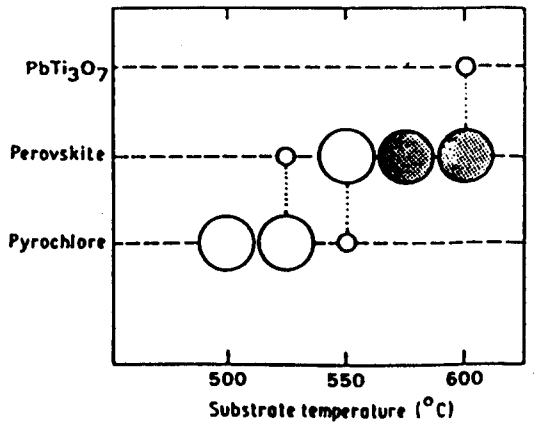

Figure 2 Structural sensitivity of PZT and PLZT compositions.

The good agreement between the thin film and ceramic target patterns shows that the films have maintained the desired perovskite structure, although they are polycrystalline due to the poor lattice match with the substrates. A small split of the (200) peak into (200) and (002) was observed after a post-growth anneal at 700° C/2 h, indicating a tetragonal symmetry. However, this caused some loss of Pb^{2+}, as indicated by the appearance of small second phase peaks associated with ZrO_2. To maintain a perovskite phase during growth, substrates were held at 600–650° C; growth temperatures below 350° C resulted in completely amorphous films which could not be annealed to a crystalline form. Although excess PbO is clearly required to maintain film stoichiometry during growth, based on evidence from this work and the results of others [1], the optimum excess PbO amount still needs to be established.

4. Future planned work: multilayered ferroelectric films

Recent work by Higuma *et al.* [12] has shown that the growth of PLZT single crystal films is possible using

TABLE II Lattice match between PZT/PLZT and tungsten bronze substrates

Film composition	(001)-oriented tungsten bronze substrates			Perovskite $SrTiO_3$
	SBN:60	BSKNN	PBN:60	
PZT (40:60)				
a = 4.042 Å	2.6%	1.99%	1.4%	3.01%
c = 4.082 Å	3.6%	3.00%	3.00%	4.12%
PLZT (8/40/60)				
a = 4.029 Å	2.1%	1.5%	1.1%	2.5%
c = 4.072 Å	3.4%	2.7%	2.1%	4.3%
PBN:60				
a = 12.501 Å	0.38%	0.20%	-	-
c = 3.985 Å	0.65%	0.35%	-	-

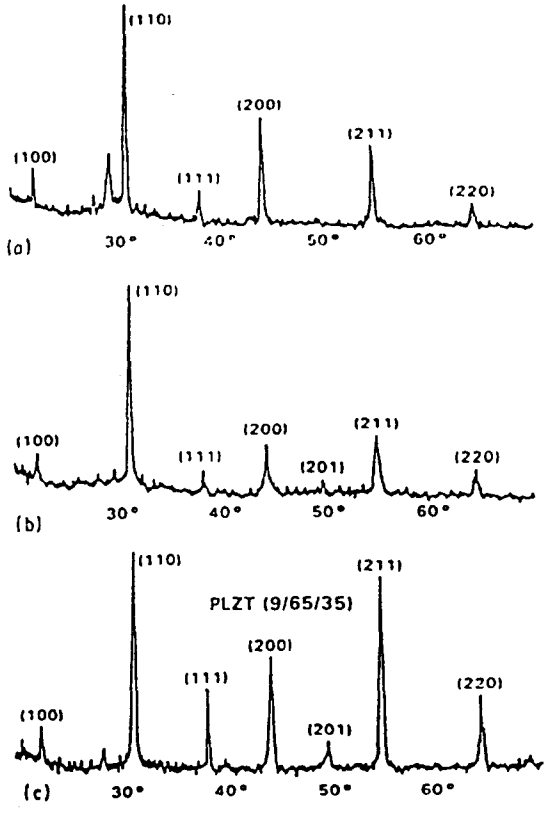

Figure 3 X-ray diffraction patterns of PLZT sputtered films and hot-pressed ceramic. (a) Film sputtered with a target with 5 mol % excess PbO; (b) film sputtered with a target with 3 mol % excess PbO; and (c) hot-pressed ceramic.

perovskite $SrTiO_3$ substrates at temperatures between 500 and 700° C. Although film growth was successful, there was a considerable lattice mismatch between the film and the substrate. Table II summarizes the lattice match of PLZT with $SrTiO_3$ and other ferroelectric crystals, including tungsten bronze SBN and PBN. The lattice match between PLZT and PBN is very good for (0 0 1)-oriented PBN and potentially allows the growth of better quality PLZT films. In future work, we propose to develop PZT and PLZT films as follows.

1. SBN:60 substrate with a 5 μm PBN:60 film for lattice matching to PZT or PLZT.

2. SBN:60 substrate with a 5 μm PBN:60 film and then alternate PLZT and PBN layers to develop a superlattice structure.

Since the lattice mismatch between PLZT and PBN is small, we expect that optical-quality PZT/PLZT films or PLZT-PBN superlattices can be more readily achieved with these film structures. An additional advantage is the ability to improve the lattice match by adjustment of the Pb:Ba ratio in PBN and thereby improve PZT/PLZT film crystallinity.

The previously discussed considerations for the electrical evaluation of PBN:60 thin films also apply here in the case of PZT/PLZT films. Because of the additional complexity of PZT/PLZT thin-film growth, the growth of good quality films on metallized substrates may be vastly more difficult than for PBN:60. A closely spaced surface electrode configuration appears to be a preferable geometry for electrical characterization of PZT/PLZT films, at least in the near term. A high-temperature sample holder to accommodate this type of geometry for d.c. conductivity, pyroelectric and dielectric measurements over a wide temperature range is now being designed and tested for this purpose.

Acknowledgement

This work was supported by the AFOSR (Contract No. F49620-86-C-0052) and ONR (Contract No. N00014-81-C-0463). The authors are grateful for the discussions on this research with W. F. Hall and T. McGill (Caltech).

References

1. A. OKADA, *J. Appl. Phys. Lett.* 48 (1977) 2905.
2. M. ISHIDA, S. TSUJI, K. KIMURA, H. MATSUNAMI and T. TANAKA, *J. Cryst. Growth* 45 (1978) 393.
3. M. ADACHI, T. SHIOSAKA and A. KAWABATA, *Ferroelectrics* 27 (1980) 89.
4. Y. HIGUMA, K. TANAKA, T. NAGAWA, T. KARIYA and Y. HAMAKAWA, *Jpn J. Appl. Phys.* 16 (1977) 1707.
5. M. ISHIDA, T. TSUJI, K. KIMURA, H. MATSUNAMI and T. TANAKA, *J. Cryst. Growth* 45 (1978) 383.
6. H. ADACHI, T. KAWAGUCHI, K. SETSUNE, K. OHJI and K. WASA, *Appl. Phys. Lett.* 42 (1983) 867.
7. T. SHIOSAKI, M. ADACHI and A. KAWABATA, *Thin Solid Films* 96 (1982) 129.
8. R. R. NEURGAONKAR and E. T. WU, *Mat. Res. Bull.* 22(8) (1987) 1095.
9. C. A. T. SALAMA and E. SICIUNAS, *J. Vac. Sci. Technol.* 9 (1971) 91.
10. T. NAGAMOTO, T. KOSAKA, S. OMORI and O. OMOTO, *Ferroelectrics* 37 (1981) 681.
11. S. IIDA and S. KATAOKA, *Appl. Phys. Lett.* 18 (1971) 391.
12. Y. HIGUMA, K. TANAKA, T. NAGAWA, T. KARIYA and Y. HAMAKAWA, *Jpn J. Appl. Phys.* 16 (1977) 1707.

Received 25 November 1987
and accepted 3 March 1988

6.0 FERROELECTRIC PROPERTIES OF LANTHANUM-MODIFIED $Sr_{0.6}Ba_{0.4}Nb_2O_6$ SINGLE CRYSTALS

Journal of Crystal Growth 89 (1988) 463–470
North-Holland, Amsterdam

FERROELECTRIC PROPERTIES OF LANTHANUM-MODIFIED $Sr_{0.6}Ba_{0.4}Nb_2O_6$ SINGLE CRYSTALS

R.R. NEURGAONKAR, J.R. OLIVER and W.K. CORY

Rockwell International Science Center, Thousand Oaks, California 91360, USA

and

L.E. CROSS

Materials Research Laboratory, The Pennsylvania State University, University Park, Pennsylvania 16802, USA

Received 20 October 1987; manuscript received in final form 22 January 1988

The role of La^{3+} in tungsten bronze $Sr_{0.6}Ba_{0.4}Nb_2O_6$ (SBN:60) ferroelectric crystals has been studied with respect to Czochralski crystal growth parameters and fundamental ferroelectric properties. Direct substitution of La^{3+} for Sr^{2+} or Ba^{2+} results in a significant decrease of the ferroelectric phase transition temperature and, consequently, dramatic increases in the room temperature dielectric constant and pyroelectric coefficient along the polar axis. Although La-modified SBN:60 is more difficult to grow, it was possible to grow defect-free crystal boules up to 2 cm diameter with optical quality, striation-free crystals found for lanthanum modifications up to 1.0 mol%.

1. Introduction

Tungsten bronze solid solution crystals such as $Sr_{1-x}Ba_xNb_2O_6$ (SBN), either doped or undoped, have proven to be excellent materials for various applications such as guided wave optics [1], photorefractive [2–7], millimeter wave [8–10] and pyroelectric [11,12] device applications. Tetragonal (4mm) bronze crystals, such as SBN, exhibit excellent transverse ferroelectric and optical properties in contrast to perovskite $BaTiO_3$ crystals which show strong longitudinal optical properties. Fig. 1 shows the classification of the various types of tungsten bronze crystals based on their crystal structure and ferroelectric and optical properties. Included among these are important bronzes such as SBN, BSKNN, KLN, SKN, morphotropic PBN, SNN and SCNN [13,14] all of which have potential utility in millimeter wave and optical applications, although high-quality crystal growth has proven to be difficult in some instances.

The present paper focused on modified versions of the congruently melting [15] $Sr_{0.6}Ba_{0.4}Nb_2O_6$ (SBN:60) crystal composition with La^{3+} substituting for Sr^{2+} or Ba^{2+} in the crystal lattice. Previous work by Liu and Maciolek [11] has shown that rare-earth-modified $Sr_{0.5}Ba_{0.5}Nb_2O_6$ (SBN:50) results in a lowered ferroelectric phase transition temperature and thereby improved pyroelectric properties. However, SBN:50 is an incongruently melting bronze composition which is difficult to grow in bulk single crystal form, particularly with good optical quality. SBN:60, on the other hand, can be grown with excellent optical quality [14] and therefore presents the opportunity to grow modified crystals of comparable high quality for potential millimeter wave, optical and pyroelectric applications.

2. Experimental

2.1. The SBN:60-$M^{3+}NbO_4$ system

Modified forms of SBN were initially studied using sintered ceramic samples. For convenience,

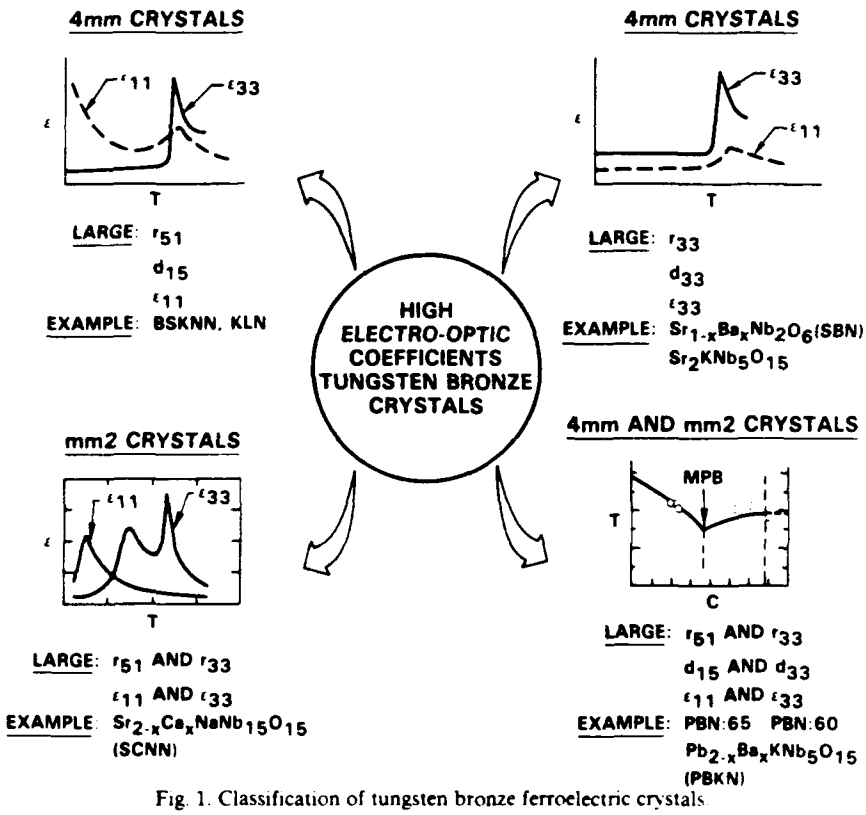

Fig. 1. Classification of tungsten bronze ferroelectric crystals.

modifications of the composition SBN : 50 were examined because of its higher phase transition temperature (− 120 versus 75 °C for SBN : 60). Reagent grade $BaCO_3$, $SrCO_3$, Nb_2O_5 and La_2O_3 or Y_2O_3 oxide powders were used for these ceramics, with the thoroughly mixed materials calcined at 1000 °C, ball-milled in acetone, and then cold-pressed and sintered at 1350 °C for 4 h. Rare earth modifications of $Sr_{0.75}Ba_{0.25}Nb_2O_6$ (SBN : 75) and SBN : 60 ceramic compositions were also checked for solid solubility and structure using X-ray diffraction measurements.

Since lanthanum and yttrium exist in trivalent states, modifications of SBN : 50 were attempted in the following manner:

(1) $Sr_{0.5-x}M^{3+}_xBa_{0.5}Nb_2O_{6+x}$,

(2) $Sr_{0.5-3x}La_{2x}\square_xBa_{0.5}Nb_2O_6$,
M = La or Y,

where □ represents a lattice site vacancy. Equivalent substitutions for Ba^{2+} were also examined. The phase diagram for La-modification is illustrated in fig. 2; X-ray analysis showed that the

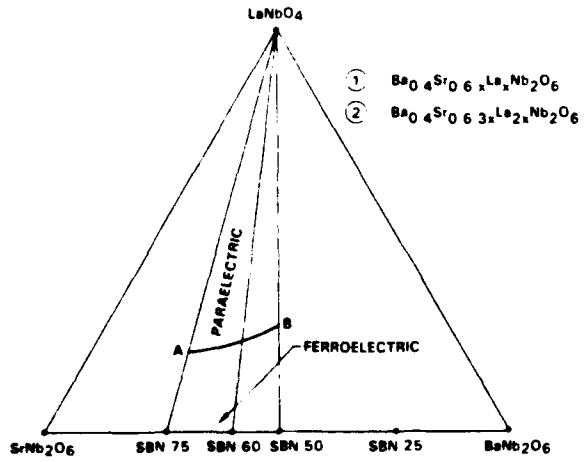

Fig. 2. Ternary phase diagram for the $BaNb_2O_6$-$SrNb_2O_6$-$LaNbO_4$ solid solution system.

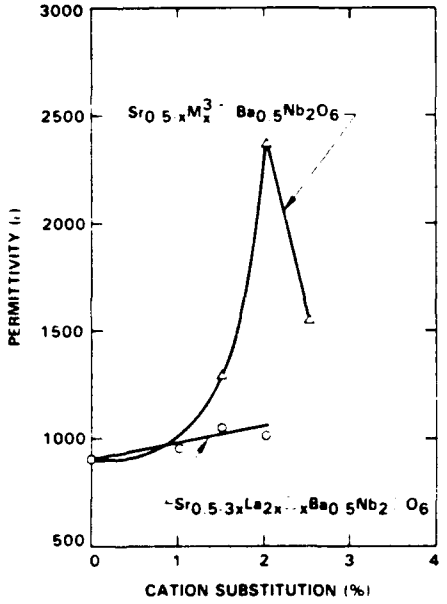

Fig. 3. Room temperature dielectric constant for La-modified SBN : 50 ceramics.

solubility limit for these modifications of SBN is upwards of 20 mol%.

Fig. 3 shows the room temperature dielectric constant at 1 kHz for two types of SBN : 50 ceramic modifications using La^{3+}; similar results were obtained for Y^{3+} modifications. Only the type $Sr_{0.5-x}La_xBa_{0.5}Nb_2O_{6+x}$ modification resulted in significant changes in the dielectric constant with increasing La^{3+} or Y^{3+} substitution, this being a consequence of a lower ferroelectric phase transition temperature. Equivalent results were also obtained with rare earth substitutions for Ba^{2+}. Hence, only type 1 modifications were used in subsequent crystal growth work with SBN : 60. Since Sr^{2+} and La^{3+} have similar cationic sizes, Czochralski crystal growth was attempted for La-modified SBN : 60 to avoid potential growth problems which might arise from dissimilar size cations in the same crystallographic site.

2.2. *Growth of La-modified SBN : 60 single crystals*

Because of extensive prior experience in the Czochralski crystal growth of congruently melting SBN : 60 [16], the growth of La-modified SBN : 60 proceeded without undue difficulty. A $Sr_{0.5-x}La_xBa_{0.5}Nb_2O_6$ substitution of La^{3+} for Sr^{2+} was used (type 1 modification), with concentrations varying from 0.5 to 2.0 mol%. High purity starting materials were used exclusively for these growths with the calcined materials thoroughly ball-milled in acetone prior to melting in a 5 cm diameter, 5 cm height platinum crucible. All crystal growths were performed in an RF induction heated furnace operating at 370 kHz.

The incorporation of La^{3+} in the SBN crystal lattice did not cause major changes in the growth conditions. Czochralski growth was performed along the *c*-axis (⟨001⟩) using an automatic diameter control system (proven mandatory for high-quality tungsten bronze crystal growth) and an after-heater geometry. Initially, *c*-axis SBN : 60 crystal seeds were used until La-modified crystals became adequate for use in subsequent growths. Bulk fracture was an early problem in these growths, probably as a result of the multiple site preference of La^{3+} in the 15-, 12- and 9-fold coordinated oxygen octahedra sites of the SBN lattice. This problem was overcome in part by maintaining strictly constant cooling rates after crystal growth.

Fig. 4 shows examples of unmodified and La-modified SBN : 60 crystal boules. Modified crystals were successfully grown up to 2 cm in diameter. A striking feature of these crystals, common to other tungsten bronzes, is the presence of large natural facets. La-modified SBN : 60 boules grow with 24 natural facets, similar to unmodified crystals, with the crystal cross-section becoming more rectangular with increasing lanthanum modification and featuring large ⟨100⟩ and ⟨010⟩ facets, as seen in fig. 4. A rectangular growth habit is not uncommon to crystals in the tungsten bronze family; for example, larger unit cell bronzes such as $Ba_{2-x}Sr_xK_{1-y}Na_yNb_5O_{15}$ (BSKNN) and KLN typically grow in a rectangular shape with 8 well-defined facets [14]. What is unusual about La-modified SBN : 60 crystals is that the crystal unit cell does not change markedly with increasing lanthanum content; for example, a 1.0 mol% La-modified crystal has unit cell dimensions of $a = b = 12.466$ Å, $c = 3.930$ Å compared to $a = b =$

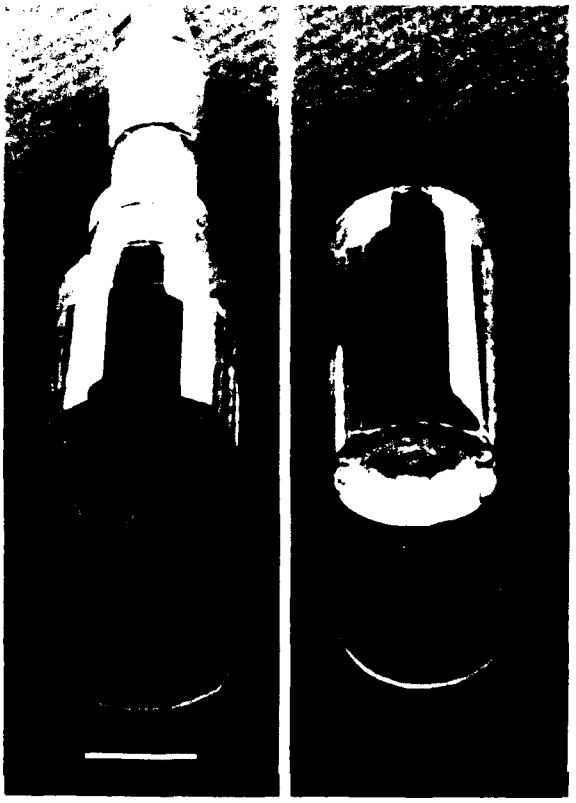

Fig. 4. La-modified (left) and unmodified (right) SBN:60 crystal boules grown by the Czochralski technique. Marker represent 2 cm.

12.465 Å, $c = 3.935$ Å for unmodified SBN:60. Hence, the gradual change in growth habit from a circular to a more rectangular shape with La modification may be a result of the partial occupancy of the otherwise empty 9-fold coordinated lattice site.

Table 1 summarizes the major crystal growth parameters and physical properties of these crystals. Crystal growth beyond 2 mol% modification was not attempted since we wished to maintain a ferroelectric phase at room temperature. Furthermore, the more heavily modified compositions showed major optical striations and were very difficult to grow. Nevertheless, it would be interesting to examine crystals with heavier La modifications since such paraelectric (4/mmm) crystals should have large quadratic electro-optical and possibly large electrostrictive properties.

2.3. Ferroelectric properties

The polar c-axis dielectric properties for a poled. 1 mol% La-modified SBN:60 crystal are shown as a function of temperature in fig. 5. Like unmodified SBN crystals, the polar axis dielectric constant is characterized by a large dielectric anomaly at the ferroelectric phase transition temperature (Curie point), above which the dielectric constant follows a Curie–Weiss law,

$$\epsilon_{33} = C_3(T - \Theta_3), \qquad (1)$$

where $C_3 = 4.3 \times 10^5$ and $\Theta_3 = 38\,^\circ$C. The Curie constant, C_3, remains remarkably unchanged with La substitution up to 2 mol%, with the only change occurring in the Curie temperature, Θ_3, which is 75 °C in unmodified SBN:60. The drop in Θ_3 with La substitution is nearly at approximately 36 °C/mol%, so that for a 1.5 mol% substitution, Θ_3 occurs at room temperature.

As evident in fig. 5, SBN:60/La shows a strong frequency dependence for the polar axis dielectric

Table 1
Growth conditions and properties for pure and La^{3+} modified SNB:60 crystals

	SBN:60	SBN:60/La (1 mol% La)	SBN:60/La (1.5 mol% La)
Crystal symmetric at 20 °C	4mm	4mm	4mm
Growth temperature (°C)	1480 °C	1480 °C	1475 °C
Pulling rate (mm/h)	10	9	6–7
Interface	Smooth and flat	Rough but nearly flat	Rough and concave
Quality	Optical	Optical	Weak striations
Growth habit	Circular	Near-circular	Squarish
Number of facets	24 Facets	24 Facets, (100) prominent	24 Facets (100) prominent
Color	Pale cream	Pale cream	Pale cream

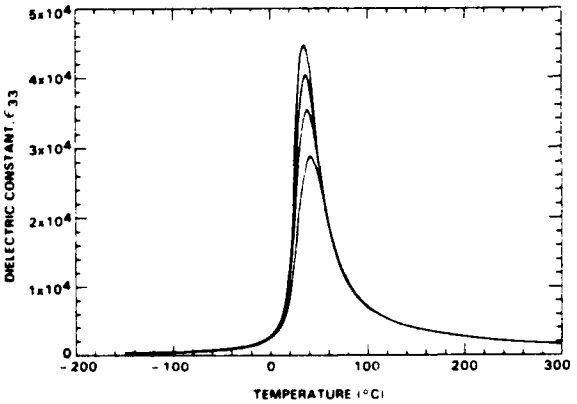

Fig. 5. Polar axis dielectric constant for a poled, 1.0 mol% La-modified SBN : 60 crystal at 100 Hz (upper curve), 1.0 kHz, 10 kHz and 100 kHz (lower curve).

constant near the phase transition. Because of this relaxor behavior, the temperature of the dielectric maximum, T_c, varies with frequency from 34 to 42 °C over a 100 Hz to 100 kHz range, for a 1 mol% La substitution, so that the specification of T_c loses some of its meaning. Relaxor behavior has also been found in unmodified SBN : 60 [10] but the effects are much less pronounced than those in fig. 5. This behavior in SBN : 60 is felt to arise from the lattice site uncertainty of the Sr^{2+} and Ba^{2+} ions between the 15- and 12-fold coordinated oxygen octahedral sites of the partially empty lattice, leading to a distribution of phase transition temperatures in the crystal bulk. In the present case of La substitution, this site uncertainty extends to the 9-fold coordinated site as well, so that more pronounced relaxor effects would be expected.

Because of the lowered phase transition temperature and increased relaxor effects, the room temperature polar axis dielectric constant for 1 mol% La-substituted SBN : 60 is very large at 9600–7000, depending on frequency. These values are roughly an order of magnitude large than the nearly dispersionless value of 920 for unmodified crystals. The corresponding room temperature dielectric loss tangent varies from 0.01 to 0.07 in poled crystals, about a factor of five greater than for unmodified SBN : 60 but still reasonable in light of the close proximity of the phase transition temperature. For 1.5 mol% La substitution, the relaxor effects become very pronounced, with ϵ_{33} = 36000–21000 and tan δ = 0.05–0.28.

Crystal poling was found to be straightforward, with a 5 kV/cm DC poling field being sufficient the pole the crystals at room temperature to a single ferroelectric domain. No advantages were found by poling from the phase transition temperature down to room temperature. The coercive field necessary to initiate ferroelectric domain reversal at room temperature was relatively low at 1–2 kV/cm, a factor for consideration in potential device applications.

The nonpolar a-axis dielectric constant, ϵ_{11}, for a 1 mol% La-modified SBN : 60 crystal is shown as a function of temperature in fig. 6. The dielectric anomaly near 40 °C is typical of SBN : 60 crystals and arises from the onset of nonzero spontaneous polarization along the c-axis [14]. As a result, some frequency dispersion is observed near the peak, but the effect is generally minimal. The a-axis constant follows a Curie–Weiss law above the phase transition temperature, with C_1 = 2.1×10^5 and $\theta_1 = -265 \pm 20$ °C. As in the c-axis case, C_1 is essentially the same as for unmodified SBN : 60, with only Θ_1 varying downward from −245 °C with increasing La substitution. At room temperature, Θ = 640 for 1 mol% La modification, increasing to 700 for 1.5 mol% crystals. The corresponding dielectric loss tangents are low (0.012 or less) and are nearly independent of frequency.

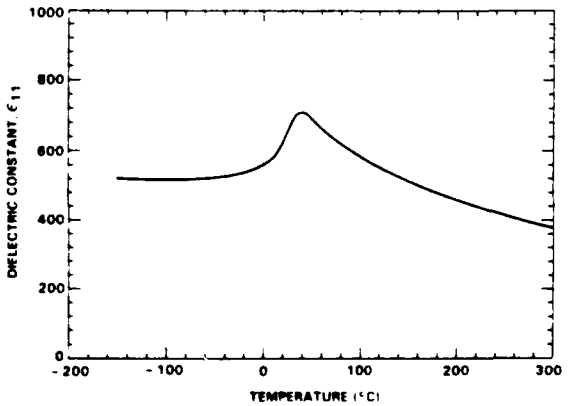

Fig. 6. Nonpolar a-axis dielectric constant for 1.0 mol% La-modified SBN : 60 at 10 kHz. Data at other frequencies are substantially the same.

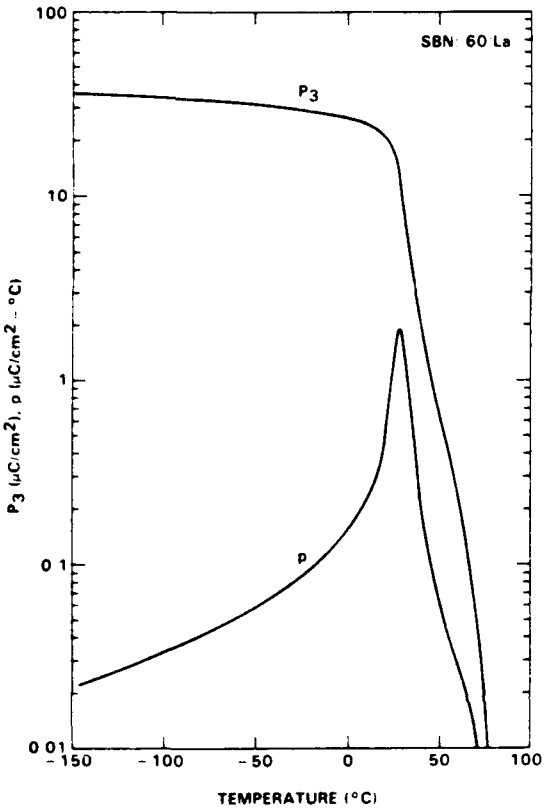

Fig. 7. Polarization, P_3, and the pyroelectric coefficient, p, for 1.0 mol% La-modified SBN : 60.

The net spontaneous polarization along the c-axis, P_3, was measured by integrating the charge released during warming at a uniform rate (2°C/min) under zero bias conditions [12]. The results for 1 mol% La substituted SBN : 60 are shown in fig. 7 along with the pyroelectric coefficient, $p = -dP_3/dT$. As in the case for the dielectric properties, the polarization and the pyroelectric coefficient behave in a manner similar to that for unmodified SBN : 60, differing only in an overall temperature shift of the characteristics due to the change in Θ_3 and a slight broadening of the pyroelectric peak near the phase transition. The pyroelectric maximum occurs at 27°C, 11°C below Θ_3, compared to the 8°C separation typical of unmodified SBN : 60 crystals; this downward shift from Θ_3 is a consequence of the diffuse nature of the ferroelectric transition.

The room temperature values of the spontaneous polarization and the pyroelectric coefficient are summarized in table 2 along with other ferroelectric data for unmodified, 1 mol% and 1.5 mol% La-modified SBN : 60 crystals. The changes in these parameters with composition, as well as the changes in the dielectric properties, are essentially reflections of the changes in the Curie temperature. For example, in the particular case of 1.5 mol% La modification, the very low polarization and large ϵ_{33} are due to the occurrence of the phase transition close to room temperature; consequently, these parameters are also extremely sensitive to small temperature changes.

Table 2
Ferroelectrical properties [a]

	SBN : 60	SBN : 60 / La (1.0 mol% La)	SBN : 60 / La (1.5 mol% La)
Curie point, T_C [b] (°C)	73–76	34–42	17–28
Θ_3 (°C)	75	38	22
C_3 (°C)	4.1×10^5	4.3×10^5	4.3×10^5
Θ_1 (°C)	-245 ± 20°	-265 ± 20°	-275 ± 20°
C_1 (°C)	2.04×10^5	2.1×10^5	2.1×10^5
ϵ_{33} (at 1 kHz)	920	8800	30.000
ϵ_{11} (at 1 kHz)	485	640	700
P_3 (μC/cm²)	28.5	21.1	3.4
p (μC/cm² · °C)	0.097	0.62	0.95
E-O coefficient, r_{33} [c] (10^{-12} m/V)	460	3290	1800

[a] All values are at 20°C, unless otherwise indicated.
[b] Over range 100 Hz to 100 kHz.
[c] Calculated values (see text).

3. Discussion

It is worthwhile to examine the potential utility of La-modified SBN : 60 crystals in potential device applications. For pyroelectric detector considerations, the decrease of the phase transition temperature with La-modification crystal necessarily increases both the polar axis dielectric constant and the pyroelectric coefficient at room temperature, as shown in table 2, so that the longitudinal pyroelectric device figure-of-merit, p/ϵ_{33}, actually declines with increasing La substitution. However, in transverse pyroelectric detector configurations where a low detector impedance (high capacitance) is desirable, La-modified SBN : 60 is clearly superior to unmodified SBN : 60 because of the higher dielectric constant and pyroelectric coefficient available.

The large increase in the room temperature dielectric constant over unmodified SBN : 60 is also significant for electro-optical or nonlinear optical applications. From the phenomenology developed for tetragonal tungsten bronze ferroelectrics [17], the linear electro-optic coefficient, r_{33}, is given by

$$r_{33} = 2 g_{33} P_3 \epsilon_0 \epsilon_{33}, \qquad (2)$$

where g_{33} is the quadratic electro-optic coefficient and ϵ_0 is the permittivity of free space. In the particular case of La-modified SBN : 60, the enhancement of r_{33} due to the dramatic increase of ϵ_{33} at room temperature is partially offset by a corresponding decrease in the spontaneous polarization. Nevertheless, the calculated r_{33} for 1.0 mol% La modification, using $g_{33} = 0.10\ m^4/°C^2$ typical of bronze ferroelectrics, is 3290×10^{-12} m/V at 1 kHz compared to 460×10^{-12} m/V (470×10^{-12}, measured) for unmodified SBN : 60. The lower value of 1800×10^{-12} m/V for 1.5 mol% modification in table 2 results from the substantial decline in the spontaneous polarization at the room temperature ferroelectric phase transition. In this case, it is also difficult to maintain a single ferroelectric domain unless a dc bias field is maintained on the crystal; this would also serve to substantially increase P_3, and therefore, r_{33}.

The large pyroelectric and electro-optic coefficients for La-modified SBN : 60 crystals make these very attractive materials for infrared focal plane array, millimeter wave, electro-optic and nonlinear optical applications. Although heavily modified crystals (≥ 1.5 mol%) have prominent optical striations, more lightly modified crystals have excellent optical quality and can maintain a single ferroelectric domain, after poling, for an indefinite period of time below 35 °C. Lanthanum modifications greater than 1.5 mol% result in crystal which are paraelectric at room temperature, which may be of interest for very low loss, biased pyroelectric detectors or for electrostrictive applications; quadratic electro-optic applications, however, would necessarily require further improvements in crystal optical quality.

Acknowledgements

This work was supported by DARPA (Contract No. N00014-82-C-2246) and by the Office of Naval Research (Contract No. N00014-81-C-0463).

References

[1] O. Eknoyan, C.H. Bulmer, H.F. Taylor, W.K. Burns, A.S. Greenblatt, L.A. Beach and R.R. Neurgaonkar, Appl. Phys. Letters 48 (1986) 13.
[2] G.J. Salamo, M.J. Miller, E.J. Sharp, G.L. Wood and W.W. Clark III, Opt. Commun. 59 (1986) 417.
[3] E.J. Sharp, M.J. Miller, G.L. Wood, W.K. Clark III, G.J. Salamo and R.R. Neurgaonkar, in: Proc. 6th IEEE Intern. Symp. on Applications of Ferroelectrics (ISAF), 1986, p. 51.
[4] G.E. Rakuljic, A. Yariv and R.R. Neurgaonkar, Appl. Phys. Letters 50 (1987) 10.
[5] M.J. Miller, E.J. Sharp, G.L. Wood, W.W. Clark III, G.J. Salamo and R.R. Neurgaonkar, Opt. Letters 12 (1987) 340.
[6] J. Rodriguez, A. Siahmakoun, G. Salamo, M.J. Miller, W.W. Clark III, G.L. Wood, E.J. Sharp and R.R. Neurgaonkar, Appl. Opt. 26 (1987) 1732.]
[7] M.D. Ewbank, R.R. Neurgaonkar, W.K. Cory and J. Feinberg, Appl. Phys. Letters 62 (1987) 374.
[8] B. Bobbs, M. Matloubin, H.R. Fetterman, R.R. Neurgaonkar and W.K. Cory, Appl. Phys. Letters 48 (1986) 1642.
[9] W.W. Ho, W.F. Hall and R.R. Neurgaonkar, Ferroelectrics 56 (1984) 230.

[10] R.R. Neurgaonkar, W.W. Ho, W.K. Cory, W.F. Hall and L.E. Cross, Ferroelectrics 51 (1984) 185.
[11] S.T. Liu and R.B. Maciolek, J. Electron. Mater. 4 (1975) 91.
[12] A.M. Glass, J. Appl. Phys. 40 (1969) 4699.
[13] J.R. Oliver, G. Shoop and R.R. Neurgaonkar, in: Proc. 6th IEEE Intern. Symp. on Applications of Ferroelectrics (ISAF), 1987, p. 485.
[14] R.R. Neurgaonkar and W.K. Cory, J. Opt. Soc. Am. B3 (1986) 274.
[15] K. Megumi, N. Nagatsuma, K. Kashiwada and Y. Furuhata, Mater. Sci. 11 (1976) 1583.
[16] R.R. Neurgaonkar, W.K. Cory and J.R. Oliver, Ferroelectrics 35 (1983) 301.
[17] M. DiDomenico and S.H. Wemple, J. Appl. Phys. 40 (1969) 720.

7.0 A THERMODYNAMIC PHENOMENOLOGY FOR FERROELECTRIC TUNGSTEN BRONZE $Sr_{0.6}Ba_{0.4}Nb_2O_6$ (SBN:60)

Rockwell International
Science Center
SC5345.FR

A thermodynamic phenomenology for ferroelectric tungsten bronze $Sr_{0.6}Ba_{0.4}Nb_2O_6$ (SBN:60)

J. R. Oliver and R. R. Neurgaonkar
Rockwell International Science Center, Thousand Oaks, California 91360

L. E. Cross
Materials Research Laboratory, The Pennsylvania State University, University Park, Pennsylvania 16802

(Received 16 November 1987; accepted for publication 22 February 1988)

The tetragonal tungsten bronze ferroelectrics in the strontium barium niobate system have been extensively studied over many years. As for many of the bronzes, a crude interpretation of the experimental data has been attempted in the past using the simple Landau-Ginsburg-Devonshire expansion of the Gibbs free energy as a Taylor series in powers of the polarization, lumping all the temperature dependence into the lowest order term. In this paper new measurements are presented for the temperature dependence of dielectric polarization, permittivity, and the E-field dependence of the permittivity. It is shown that for a realistic fitting of the data, the Taylor expansion must be taken to at least the eighth power term, and that the coefficients of terms up to the sixth power must be taken as functions of temperature. Since the phenomenology describes equilibrium behavior, it is the total static polarizability that is being explored in this treatment. The nature of this temperature dependence strongly suggests that the phase transition from a macropolar to a macrononpolar state is tetracritical.

I. INTRODUCTION

Tungsten bronze ferroelectric oxides have received considerable attention for many years, with perhaps the best known of these being compositions in the $Sr_{1-x}Ba_xNb_2O_6$ (SBN) solid solution system. Numerous applications have been realized for SBN, particularly in the areas of pyroelectric infrared detection,[1] piezoelectrics,[2,3] electro-optics,[4–8] and photorefractive optics,[8–14] the latter resulting from the evolution of techniques for the growth of high-quality single crystals in the congruently melting $Sr_{0.6}Ba_{0.4}Nb_2O_6$ (SBN:60) composition.[15] As in the case for other ferroelectric materials, much of the experimental data for SBN have been interpreted on the basis of the Landau:Ginsburg:Devonshire (LGD) phenomenology, as in the extensive work by Shrout *et al.*[16] on the elastic, dielectric, and piezoelectric properties of SBN:60.

With some important exceptions, nearly all of these interpretations of ferroelectric behavior have involved simple LGD expansions of the Gibbs free energy as a Taylor series in even powers of the polarization, truncated at the sixth power, with all temperature dependence carried only in the lowest order coefficient.[17] This approach has proven successful for SBN:60,[3,16] although in some instances only rough approximations of the experimental data can be obtained, as in the case of the dielectric properties.

The development of optical quality SBN:60 crystals has made it possible to accumulate very reproducible dielectric and polarization data as a function of temperature. In this paper, we present new measurements of these properties along with measurements of the electric field dependence of the permittivity as a function of temperature. It is shown, that for an accurate fitting to these data in the ferroelectric phase the Taylor expansion of the Gibbs free energy must be taken out to at least the eighth power of the polarization, and that the coefficients of terms up to the sixth power must be taken as strong functions of temperature. Since the phenomenology describes equilibrium behavior, it is the total static polarizability, summing all possible contributions, which is being explored in this treatment.

II. THERMODYNAMIC PHENOMENOLOGY

The free-energy function of interest for a polarizable insulator is the elastic Gibbs function, given by

$$G_1 = U - TS - Xx, \tag{1}$$

where U is the internal energy, T the temperature, S the entropy, X the elastic stress, and x the strain. Under the symmetry constraints of bronze ferroelectrics with a high-temperature tetragonal prototype symmetry $4/mmm$, the change in free energy, ΔG_1, due to nonzero polarization P_i may be written as a power series expansion in the P_i's along the three principal crystallographic axes. Under isothermal conditions and zero stress, the LGD phenomenological elastic Gibbs function in the shortened matrix notation[18] becomes

$$\begin{aligned}\Delta G_1 = 1/\epsilon_0[&\alpha_1(P_1^2+P_2^2)+\alpha_3P_3^2+\alpha_{11}(P_1^4+P_2^4)+\alpha_{12}P_1^2P_2^2+\alpha_{13}(P_1^2+P_2^2)P_3^2+\alpha_{33}P_3^4+\alpha_{111}(P_1^6+P_2^6)\\&+\alpha_{112}(P_1^2P_2^4+P_1^4P_2^2)+\alpha_{113}(P_1^4+P_2^4)P_3^2+\alpha_{133}(P_1^2+P_2^2)P_3^4+\alpha_{123}P_1^2P_2^2P_3^2+\alpha_{333}P_3^6\\&+\alpha_{1111}(P_1^8+P_2^8)+\alpha_{1122}P_1^4P_2^4+\alpha_{1133}(P_1^4+P_2^4)P_3^4+\alpha_{3333}P_3^8],\end{aligned} \tag{2}$$

 0021-8979/88/130037-11$02.40

where the α's have been normalized by the free-space permittivity, ϵ_0, for later convenience. Equation (2) principally differs from earlier treatments[3,16] by the inclusion of terms out to the eighth power of the polarization for reasons which will become evident later.

For nonzero electric fields, E_i, we must examine the complete Gibbs function $\Delta G = \Delta G_1 - (E_1P_1 + E_2P_2 + E_3P_3)$. Setting the first partial derivatives of ΔG with respect to polarization equal to zero then gives the electric field relations along the principal axes:

$$\begin{aligned} E_1 = 1/\epsilon_0[&2\alpha_1P_1 + 4\alpha_{11}P_1^3 + 2\alpha_{12}P_1P_2^2 + 2\alpha_{13}P_1P_3^2 \\ &+ 6\alpha_{111}P_1^5 + \alpha_{112}(2P_1P_2^4 + 4P_1^3P_2^2) + 4\alpha_{113}P_1^3P_3^2 \\ &+ 2\alpha_{133}P_1P_3^4 + 2\alpha_{123}P_1P_2^2P_3^2 + 8\alpha_{1111}P_1^7 \\ &+ 4\alpha_{1122}P_1^3P_2^4 + 4\alpha_{1133}P_1^3P_3^4]. \end{aligned} \tag{3}$$

$$\begin{aligned} E_3 = 1/\epsilon_0[&2\alpha_3P_3 + 2\alpha_{13}(P_1^2 + P_2^2)P_3 + 4\alpha_{33}P_3^3 \\ &+ 2\alpha_{113}(P_1^4 + P_2^4)P_3 + 4\alpha_{133}(P_1^2 + P_2^2)P_3^3 \\ &+ 2\alpha_{123}P_1^2P_2^2P_3 + 6\alpha_{333}P_3^5 \\ &+ 4\alpha_{1133}(P_1^4 + P_2^4)P_3^3 + 8\alpha_{3333}P_3^7]. \end{aligned} \tag{4}$$

The electric field expression for E_2 has been omitted since it is formally equivalent to Eq. (3) for the tetragonal symmetry assumed here.[16] The solutions of these equations with $E_i = 0$ determine the normal ferroelectric states; in the case of tetragonal bronze ferroelectrics, the 3 (or c) axis is the only spontaneously polarizable axis, so that Eqs. (3) and (4) reduce to

$$\begin{aligned} E_1 = 1/\epsilon_0[&2\alpha_1P_1 + 4\alpha_{11}P_1^3 + 2\alpha_{13}P_1P_3^2 + 6\alpha_{111}P_1^5 \\ &+ 4\alpha_{113}P_1^3P_3^2 + 2\alpha_{133}P_1P_3^4 \\ &+ 8\alpha_{1111}P_1^7 + 4\alpha_{1133}P_1^3P_3^4] \\ &(P_2 = 0), \end{aligned} \tag{5}$$

$$\begin{aligned} E_3 = 1/\epsilon_0[&2\alpha_3P_3 + 4\alpha_{33}P_3^3 + 6\alpha_{333}P_3^5 + 8\alpha_{3333}P_3^7] \\ &(P_1 = P_2 = 0). \end{aligned} \tag{6}$$

The dielectric stiffnesses, $\chi_{ii} = \epsilon_{ii}^{-1}$, are then given by

$$\begin{aligned} \chi_{11} = \epsilon_0\frac{\partial E_1}{\partial P_1} = &2\alpha_1 + 12\alpha_{11}P_1^2 + 2\alpha_{13}P_3^2 + 30\alpha_{111}P_1^4 \\ &+ 12\alpha_{113}P_1^2P_3^2 + 2\alpha_{133}P_3^4 \\ &+ 56\alpha_{1111}P_1^6 + 12\alpha_{1133}P_1^2P_3^4 \\ &(P_2 = 0), \end{aligned} \tag{7}$$

or

$$\chi_{11} = 2\alpha_1 + 2\alpha_{13}P_3^2 + 2\alpha_{113}P_3^4 \quad (P_1 = P_2 = 0), \tag{7a}$$

and

$$\begin{aligned} \chi_{33} = \epsilon_0\frac{\partial E_3}{\partial P_3} = &2\alpha_3 + 12\alpha_{33}P_3^2 \\ &+ 30\alpha_{333}P_3^4 + 56\alpha_{3333}P_3^6 \\ &(P_1 = P_2 = 0). \end{aligned} \tag{8}$$

At temperatures well above the ferroelectric Curie point, T_c, $P_3 = 0$ under zero bias conditions and the paraelectric stiffnesses generally follow a linear Curie–Weiss behavior of the form

$$\chi_{11} = 2\alpha_1 = (T - \theta_1)/C_1 \quad (T > T_c), \tag{9}$$

$$\chi_{33} = 2\alpha_3 = (T - \theta_3)/C_3 \quad (T > T_c), \tag{10}$$

with $\theta_1 \ll \theta_3$. For a first-order phase transition $\theta_3 < T_c$, whereas for a second-order transition $\theta_3 = T_c$ under ideal conditions.[17,19]

Generally, there are no restrictions on the temperature dependence of the higher order Devonshire coefficients α_{ii}, α_{ij}, α_{iii}, etc., and indeed for cases such as $BaTiO_3$ some temperature dependence has been found.[20] However, in most treatments of ferroelectric materials, the higher order coefficients are assumed to be temperature invariant, at least over a limited range below T_c, and reasonably good fits to dielectric and spontaneous polarization data can be obtained. Nevertheless, the uniqueness of the Devonshire coefficients is necessarily determined by physically measurable parameters such as the low-frequency dielectric constant, the spontaneous polarization, and the electric field which must rigorously satisfy the dielectric stiffness and electric field equations as well as other derived phenomenological relations. These we shall now examine on the basis of macroscopic experimental data for tungsten bronze SBN:60.

III. TUNGSTEN BRONZE SBN:60

The congruently melting SBN:60 composition is a smaller unit cell bronze with a tetragonal 4-mm crystal structure at room temperature and lattice constants $a,b = 12.465$ Å and $c = 3.935$ Å as determined by x-ray diffraction measurements. The SBN solid solution system is represented by the formula $(A_1)_4(A_2)_2B_{10}O_{30}$ in which both the Sr^{2+} and Ba^{2+} ions occupy the fifteenfold (A_1) and twelvefold (A_2) coordinated oxygen octahedra sites.[21,22] Since only $\frac{5}{6}$ of these sites are occupied, SBN is referred to as an unfilled bronze. The high-temperature prototype symmetry is tetragonal $4/mmm$, placing SBN in the Shuvalov ferroelectric species $4/mmm(1)D4F4mm$.[23]

The SBN:60 solid solution crystals examined were grown by the Czochralski technique[15,24,25] using an automatic-diameter control system to facilitate tight compositional control and high optical quality during bulk crystal growth. Further details may be found in previous papers.[6,8,12] Over 100 growths have now been performed in the SBN system, including undoped and doped crystals (Ce, La, Fe, etc.), and crystal quality has evolved to the point where c-axis boules up to 4 cm diam are now routinely grown, free of detectable imperfections and major optical striations. These crystals have been of sufficiently high optical quality to permit extensive optical measurements such as two- and four-wave mixing and self-pumped phase conjugation.[8–14]

A photograph of a typical SBN:60 crystal boule is shown in Fig. 1. A general characteristic of tungsten bronze crystals is the presence of major facets parallel to the growth axis; in the particular case of SBN:60 c-axis growths there are 24 facets, including (100), (010), (110), etc., a feature which significantly eases the task of crystal orientation and cutting.

IV. EXPERIMENTAL METHOD

The two principal crystallographic axes of interest in SBN:60 are the a or b axes ($\langle 100\rangle$ or $\langle 010\rangle$) and the polar c

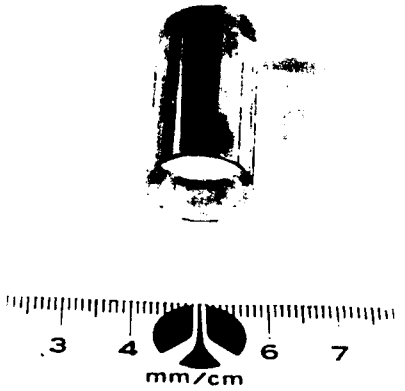

FIG. 1. Czochralski-grown SBN:60 bulk single crystals.

axis (⟨001⟩). Crystal wafers in these orientations were cut with a diamond saw and then mechanically lapped and, in some instances, additionally polished to an optical finish. However, the latter step was not found to be particularly necessary for electrical measurements, as long as the contacts were annealed. We have used sputtered Pt or Au full area contacts almost exclusively in our measurements, and although other materials (such as Al) and contact forming methods (such as fired pastes) are viable alternatives, sputtered noble metal contacts have been found more stable at elevated temperatures and yield highly reproducible electrical measurement data.

Contacted crystal samples were generally annealed in a dry oxygen atmosphere at 450–550 °C for 1–3 h prior to measurement. Although the crystal boules undergo a post-growth anneal at 1300–1400 °C, the second low-temperature anneal establishes a good interface between the contact metallization and the crystal surface, and helps to minimize surface conductivity along the unmetallized edges. Surface damage due to cutting, polishing, and metal deposition appears to be minimized at these relatively low temperatures, and residual internal stress is also probably reduced.

The measurement apparatus for dielectric, conductivity, and polarization measurements consisted of a fully shielded alumina sample mount enclosed in an environmentally sealed alumina chamber. Electrical contact with the test samples was established by small Pt pads which lightly pressed against a portion of the contact metallization using an adjustable spring-loaded alumina rod. Details of the design are given in the paper by Morin, Oliver, and Housley;[26] the apparatus in its present configuration represents evolutionary refinements of the original design. Sample temperature control was facilitated by a Kanthal-wound tube furnace, with temperatures below room temperature achieved by spraying liquid nitrogen onto the sample chamber wall. N_2 gas was used in the chamber below 0 °C and O_2 above at a ~2 psi positive pressure to maintain a dry environment.

All dielectric measurements were made with a calibrated HP4274A bridge covering the frequency range of 100 Hz–100 kHz. dc currents were measured with a Keithley 619 electrometer. All data acquisition, process control, and data analysis were facilitated by a HP9816 desktop computer using an IEEE-488 interface bus.

V. POLAR-AXIS PROPERTIES

The bronze solid solution system $Sr_{1-x}Ba_xNb_2O_6$, $0.25 \leqslant x \leqslant 0.75$, is characterized by a large dielectric anomaly along the polar c axis at the paraelectric/ferroelectric phase transition temperature, T_c. An example is shown in Fig. 2 for the weak-field c-axis dielectric constant, ϵ_{33}, as a function of temperature for an SBN:60 crystal poled to a single ferroelectric domain. A recurring feature of SBN is the significant dielectric dispersion which appears within a 10–15 °C range of T_c (~75 °C) as shown in Fig. 2. This Debye-type relaxation behavior is why SBN solid solution crystals are generally referred to as relaxor ferroelectrics. This behavior is postulated to occur because of the distribution of phase transition temperatures in the bulk of the crystal arising from the site uncertainty of the Sr^{2+} and Ba^{2+} ions in the partially filled lattice. Further evidence for this postulate is provided by comparison with "filled" bronze ferroelectrics, such as $Ba_{2-x}Sr_xK_{1-y}Na_yNb_5O_{15}$(BSKNN),[14] where relaxor behavior is greatly diminished.

For temperatures approximately 20 °C or more on either side of T_c, the dielectric dispersion is small (typically <2% from 100 Hz–100 kHz), as is the dielectric loss ($\tan\delta$ typically 0.007 or less at 20 °C, and less than 0.001 at 120 °C). Room-temperature dark dc conductivity is also very small, typically $10^{-15}\ \Omega^{-1}\ cm^{-1}$ or less, and can only be measured under absolutely stable temperature conditions because of the large pyroelectric currents which can otherwise occur.

SBN:60 crystals which have been thermally depoled by a warming well above 100 °C show the same low dielectric dispersion and loss above T_c, but show a very large dispersion and loss ($\tan\delta = 0.10$–0.25 at 20 °C) which persist well

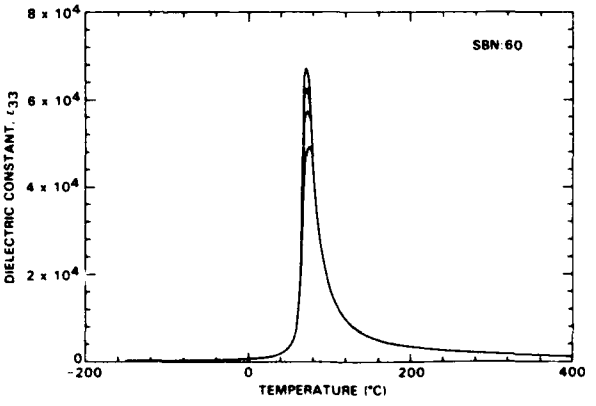

FIG. 2. Polar-axis dielectric constant for a poled SBN:60 crystal at 100 Hz (highest curve), 1, 10, and 100 kHz (lowest curve). T_c = 73–76 °C, depending on frequency.

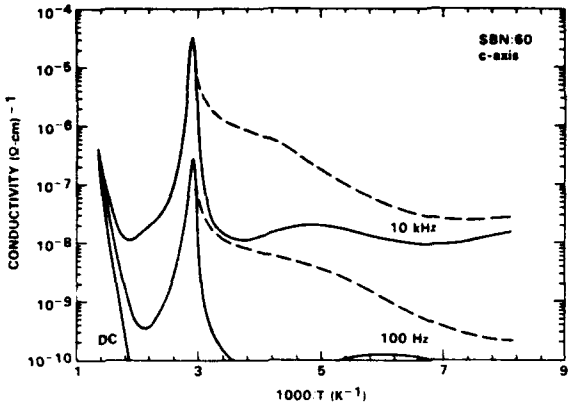

FIG. 3. Arrhenius plots of the polar axis conductivity of SBN:60 at dc, 100 Hz, and 10 kHz. The dashed lines are for a thermally depoled crystal; the solid lines are for the same crystal in a poled condition.

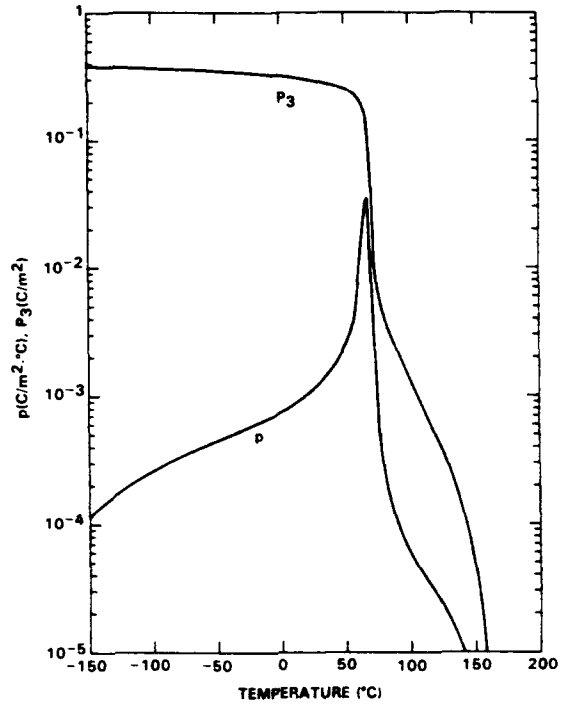

FIG. 4. The polar-axis polarization, P_3, and the pyroelectric coefficient, p, for SBN:60. The high-temperature tail regions tend to vary somewhat with the poling conditions.

below 0 °C. The substantial differences between the poled and depoled ac conductivities are shown in the Arrhenius plots of Fig. 3 at 100 Hz and 10 kHz. The higher conductivities and large dielectric dispersion for depoled crystals are felt to primarily arise from antiparallel domain wall relaxation[27] which progressively freezes out at lower temperatures. A curiosity of SBN compositions is that at low temperatures, typically below -100 °C, the antiparallel ferroelectric domains of a depoled crystal effectively clamp the crystal, resulting in a nearly dispersionless dielectric constant which is less than that for a normally poled crystal.

SBN:60 may be poled to a single ferroelectric domain by applying a 5–10 kV/cm dc field along the polar c axis at room temperature. However, an initial thermally depoled condition is necessary since the inadvertent application of a reversed polarity field to a partially poled crystal can result in the formation of antipolar macrodomains which cannot be fully switched.[28–30] For this work, poling was accomplished by a field-cooling method with the dc field applied from just below T_c down to room temperature or below. Although it would appear advantageous to apply a poling field well above T_c and then cool because of the distributed nature of the phase transition temperature in the crystal bulk, in practice this was found to degrade the room-temperature dielectric losses by as much as a factor of 3 due to space-charge effects and did not result in any significant changes of the measured polarization.

Figure 4 shows the c-axis polarization, P_3, and the pyroelectric coefficient, p, for a poled SBN:60 crystal. These data were obtained during warming at a nominal 3 °C/min rate, with other rates giving substantially the same results. The polarization was determined from the numerically integrated charge released during warming at zero bias. The pyroelectric coefficient was measured simultaneously with the polarization[1,19] using

$$p = -\frac{dP_3}{dT} = -\frac{J_P}{r_T}, \tag{11}$$

where r_T is the rate of temperature change and J_P is the measured current density. Although either form of Eq. (11) may be used to determine p, numerical differentiation of the polarization data was found less noisy since it was less affected by small fluctuations in the thermal ramp rate.

The pyroelectric maximum for SBN:60 occurs at 67 °C (Fig. 4), roughly 8 °C below T_c, and the net polarization persists well above T_c because of the distribution of phase transition temperatures; this distribution is estimated to have a Gaussian half-width of 8 °C. At room temperature, $P_3 = 0.28$ C/m^2 and $p = 9.7\times10^{-4}$ C/m^2 °C, values which are comparable to other published results.[1,28] Secondary pyroelectric contributions to these data due to thermal dilatation are expected to be small except very close to T_c.[31]

A. Phenomenological fitting

From the standpoint of the thermodynamic phenomenology, it is preferable to examine the polar axis dielectric constant of SBN:60 in terms of the dielectric stiffness, $\chi_{33} = \epsilon_{33}^{-1}$, as shown in Fig. 5. The dielectric stiffness accurately follows a linear Curie–Weiss law both above and below T_c over a wide temperature range, with

$$\epsilon_{33} = C_3/(T-\theta_3) \quad (T>\theta_3)$$
$$= C_{3f}/(\theta_{3f}-T) \quad (T<\theta_{3f}), \tag{12}$$

where in the paraelectric phase $C_3 = 4.1\times10^5$ °C and $\theta_3 = 75$ °C, and in the ferroelectric phase $C_{3f} = 4.5\times10^4$ °C and $\theta_{3f} = 69$ °C. The general behavior of the dielectric stiff-

ness suggests a near-second-order phase transition; the fact that $\theta_{3f} \neq \theta_3 \neq T_c$ is felt to be due to the finite distribution of phase transition temperatures in SBN crystals. Indeed, for "filled" bronzes such as BSKNN, this difference amounts to, at most, 1–2 °C.[14]

The linear behavior of the dielectric stiffness over such a wide temperature range below T_c is unusual compared to other ferroelectric materials such as $LiNbO_3$ and $BaTiO_3$.[19,20] A quick inspection of the electric field and dielectric stiffness expressions in Eqs. (6), (8), and (10) shows that for a stiffness expansion truncated at the fourth power of P_3 and temperature invariant α_{33} and α_{3333}, only a $\sim$4:1 ratio for C_3:C_{3f} is predicted in the low-temperature limit (P_3 large), compared to the $\sim$9:1 ratio measured. Adiabatic versus isothermal considerations can modify the predicted results,[17,19] but only weakly due to the slow variation of the spontaneous polarization well below T_c.

An examination of the spontaneous polarization (Fig. 4) shows a linear temperature dependence for P_3^6 over a very wide temperature range, as shown in Fig. 6. Deviations from linearity occur only very close to T_c and at the low-temperature extreme. Formally,

$$P_3 = P_{30}(\theta_{3f} - T)^{1/6}, \tag{13}$$

with $\theta_{3f} = 69$ °C, as before, and $P_{30} = 0.150$ C/m^2 °C$^{1/6}$. From Eq. (11), the pyroelectric coefficient is then

$$p = P_{30}/6(\theta_{3f} - T)^{5/6} = P_3/6(\theta_{3f} - T), \tag{14}$$

which is experimentally satisfied over an equally wide temperature range.

The temperature dependence of p in Eq. (14) may be compared with the phenomenology by taking the derivative with respect to temperature of the electric field expression in Eq. (6) under zero field conditions. For temperature invariant higher order coefficients and α_3 defined by Eq. (10), we have

$$0 = \frac{1}{C_3} P_3 + \left(\frac{T - \theta_3}{C_3} + 12\alpha_{33}P_3^2 + 30\alpha_{333}P_3^4 + 56\alpha_{3333}P_3^6\right)\frac{dP_3}{dT}. \tag{15}$$

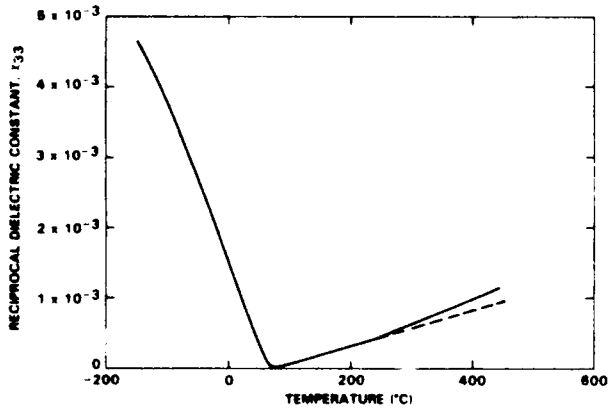

FIG. 5. The polar-axis reciprocal dielectric constant at 10 kHz for poled SBN:60.

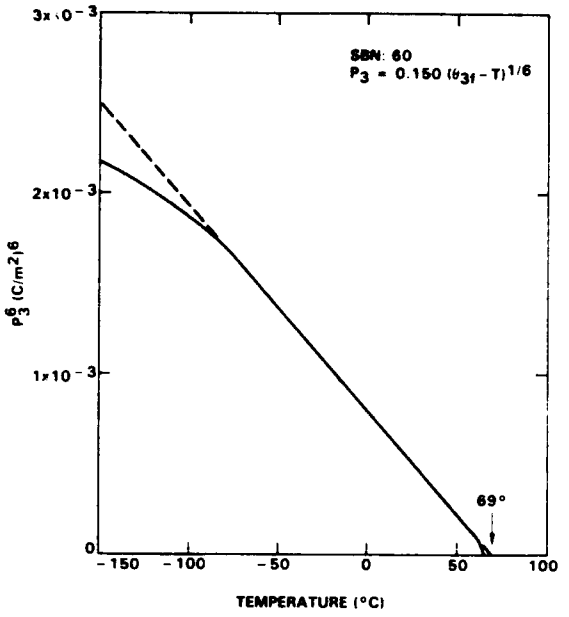

FIG. 6. Plot of the sixth power of P_3 vs temperature, showing a wide linear region below the zero intercept at 69 °C.

Comparing this with the dielectric stiffness expression in Eq. (8), Eq. (15) reduces to

$$p = -\frac{dP_3}{dT} = \frac{\epsilon_{33}P_3}{C_3}. \tag{16}$$

Using the empirical relation for ϵ_{33} given in Eq. (12) for $T < \theta_{3f}$, Eq. (16) becomes

$$p = C_{3f}P_3/C_3(\theta_{3f} - T) = P_3/9.11(\theta_{3f} - T), \tag{17}$$

a relationship which is in vast disagreement with the observed behavior of Eq. (14). Note that Eqs. (16) and (17) are correct for any number of higher order Devonshire coefficients, as long as they remain independent of temperature. In the particular case of SBN:60, this assumption is clearly not valid.

The dielectric, pyroelectric, and polarization behaviors described here for SBN:60 have been consistently found in a large number of crystal samples, with relatively minor variations in the physical constants being found from one crystal growth to another. Effects due to sample geometry are also not significant; excellent agreement in the properties has been found for samples from 0.35 mm up to several mm in thickness, indicating that contact layer effects do not play an important role.

It is evident from the polar-axis behavior of SBN:60 that the phenomenology for the Gibbs free energy must be taken out to at least the eighth power of P (sixth power in dielectric stiffness) with temperature-dependent higher order coefficients. Ironically, a reasonable sixth-order least-squares fit to the dielectric data can still be achieved over a moderate temperature range using temperature-independent coefficients.[16] However, the pyroelectric data clearly show that the relationship between p and P_3 [Eq. (14)] is *independent*

of the Curie–Weiss coefficient C_3, in violation of the phenomenology for temperature-independent higher order coefficients [Eqs. (16) and (17)]. This situation is not unique to undoped SBN:60; we have found equivalent behavior in other SBN compositions (e.g., SBN:50), doped crystals (e.g., La^{3+}), and more importantly, for other ferroelectric bronzes, including compositions in the BSKNN system.[14]

The measured temperature dependencies of the spontaneous polarization and the polar-axis dielectric stiffness are highly suggestive of higher order thermodynamic coefficients of the form

$$\alpha_{33} = \alpha'_{33}(\theta_3 - T)^{2-3},$$
$$\alpha_{333} = \alpha'_{333}(\theta_3 - T)^{1-3},$$
$$\alpha_{3333} = \alpha'_{3333},$$

which qualitatively at least, will then satisfy the observed temperature dependence of ϵ_{33}. The measured relationship between p and P_3 [Eq. (14)] will also be satisfied, but unfortunately without yielding any information about the magnitudes of α'_{33}, etc. However, the postulated temperature dependencies may be unnecessarily strict since the dielectric stiffness and electric field relations involve the sum and difference of at least four (potentially large) terms in the ferroelectric phase. Hence, an additional experimental method is needed to determine the thermodynamic coefficients in an unequivocal manner.

B. The linear electro-dielectric effect in SBN:60

The extension of the LGD phenomenology out to the eighth power of P_3 in the Gibbs free-energy expansion necessarily leads to an underdetermined set of equations based on the physically measurable parameters E_3 and ϵ_{33}, so that no unique values for the higher order coefficients can be established. One solution to this problem is to examine the behavior of the dielectric constant at several different applied fields; this will lead, for example, to upward shifts of the phase transition temperature for applied fields of the same polarity as the poling field.[17] This technique has been used by many authors to investigate ferroelectric materials, including the excellent work by Glass[1] on SBN compositions and the work by Burns *et al.*[12] to determine the values of the sixth-order Devonshire coefficients for La-modified $Sr_2KNb_5O_{15}$ crystals. Unfortunately, this type of analysis is necessarily limited to a small temperature range near T_c, and is further complicated by finite distributions of transition temperatures in materials such as SBN.

An alternative technique is to examine small changes in the dielectric constant with changes in the applied field at fixed temperatures; this method was successfully used by Drougard, Landauer, and Young[20] to establish the strong temperature dependence of the fourth power coefficient in $BaTiO_3$ using a dynamic low-frequency biasing technique above T_c. This method may also be applied below T_c as long as instrument sensitivity and accuracy are sufficient to measure $\Delta\epsilon_{33}$. In the particular case of the eighth-order phenomenology presented here, the change in the dielectric stiffness with applied electric field along the c axis may be calculated from Eq. (8):

$$\frac{\partial\chi_{33}}{\partial E_3} = (24\alpha_{33}P_3 + 120\alpha_{333}P_3^3 + 336\alpha_{3333}P_3^5)\frac{\partial P_3}{\partial E_3}. \tag{18}$$

For small changes in E_3, $\partial P_3/\partial E_3 = \epsilon_0\epsilon_{33}$, so that Eq. (18) may be written as

$$\frac{\partial\chi_{33}}{\partial E_3} = \frac{\epsilon_0\epsilon_{33}}{P_3}(24\alpha_{33}P_3^2 + 120\alpha_{333}P_3^4 + 336\alpha_{3333}P_3^6). \tag{19}$$

This equation, combined with the relations for the electric field [Eq. (6)] and dielectric stiffness [Eq. (18)], completes the set of equations necessary to determine the higher order coefficients. Under the constraint of small linear changes of χ_{33} with applied field, the solutions are

$$\alpha_{33} = \frac{1}{32\epsilon_{33}P_3^2}\left(\frac{P_3}{\epsilon_0}\frac{\partial\chi_{33}}{\partial E_3} + 24\epsilon_{33}\frac{(\theta_3 - T)}{C_3} - 11\right),$$
$$\alpha_{333} = \frac{-1}{24\epsilon_{33}P_3^4}\left(\frac{P_3}{\epsilon_0}\frac{\partial\chi_{33}}{\partial E} - 12\epsilon_{33}\frac{(\theta_3 - T)}{C_3} - 9\right),$$
$$\alpha_{3333} = \frac{1}{64\epsilon_{33}P_3^6}\left(\frac{P_3}{\epsilon_0}\frac{\partial\chi_{33}}{\partial E} + 8\epsilon_{33}\frac{(\theta_3 - T)}{C_3} - 7\right). \tag{20}$$

To this point, we have made no assumptions regarding any specific temperature dependencies, except for the paraelectric dielectric stiffness, $(T - \theta_3)/C_3$. In the particular case of SBN:60, we may substitute for the temperature dependence of P_3 and ϵ_{33}, and with the approximation $\theta \cong \theta_3 \cong \theta_{33}$, the expressions in Eq. (20) become

$$\alpha_{3333} \cong \frac{1}{64C_3P_{s0}^6}\left(\frac{P_3}{\epsilon_0}\frac{\partial\chi_{33}}{\partial E_3} + \frac{8C_3}{C_3} - 7\right), \text{ etc.},$$

where C_3 and P_{s0} are as defined earlier. Hence, if $\partial\chi_{33}/\partial E_3$ varies with temperature as P_3^{-1}, α_{3333} is a constant. Similarly, α_{33} and α_{333} will vary, respectively, with temperature as $(\theta - T)^{-1}$ and $(\theta - T)^{1-3}$, as suggested earlier. However, note that the higher order coefficients need not follow any specific simple functions of temperature, but need only satisfy the general expressions given in Eq. (20).

The linear electro-dielectric effect, $\partial\chi/\partial E_3$, is the low-frequency analog of the linear electro-optic effect in ferroelectric crystals, and it is a particularly powerful test for the validity of truncated free-energy power expansions. For example, rearrangement of the third expression in Eq. (20) gives

$$\frac{\partial\chi_{33}}{\partial E_3} = \frac{\epsilon_0}{P_3}\left(64\epsilon_{33}\alpha_{3333}P_3^6 - 8\epsilon_{33}\frac{(\theta_3 - T)}{C_3} + 7\right), \tag{21}$$

so that by setting $\alpha_{3333} = 0$, the electro-dielectric response for a sixth-order Gibbs free-energy expansion may be calculated. In the particular case of SBN:60 at 20 °C, with $\epsilon_{33} = 920$ and $P_3 = 0.285$ C/m^2, the calculated sixth-order response is 190×10^{-12} m/V. The measured value, constant for linear dielectric changes of up to several percent, is 418×10^{-12} m/V, more than twice the calculated sixth-order value. This discrepancy cannot be accounted for by adiabatic or contrapiezoelectric corrections since these amount to, at most, a 3%–4% correction to the calculated value. This particular result is what finally confirmed our recent

suspicions that a sixth-order LGD phenomenology was inadequate to characterize SBN compositions, and perhaps the tungsten bronze crystal family in general.

A full series of electro-dielectric measurements were carried out from $-140\,^{\circ}\mathrm{C}$ to T_c on poled SBN:60 crystals from different growths. All measurements were made at fixed temperatures to insure equilibrium conditions. Although the response times for changes in applied field were short below 50 °C (on the order of the bridge-balancing time of ~ 1 s or less), these increased to tens of seconds near T_c, rendering methods such as low-frequency dynamic biasing to be of limited value. Nevertheless, the latter has appealing features and may be explored in future work. In the present work, all electro-dielectric measurements were performed using static electric fields of alternating polarity.

Representative electro-dielectric response data for SBN:60 are shown in Fig. 7. The higher order Devonshire coefficients were calculated from these data and from measured ϵ_{33} and P_s values using Eq. (20), and are plotted on a log-log scale versus $(\theta_{3f} - T)$ in Fig. 8. These coefficients are well characterized by the postulated temperature dependencies, with

$$\alpha_3 = -1.22 \times 10^{-6}(\theta_c - T),$$
$$\alpha_{33} = 1.54 \times 10^{-4}(\theta_{3f} - T)^{-2.4} \quad (\mathrm{m}^2/\mathrm{C})^2,$$
$$\alpha_{333} = -1.03 \times 10^{-2}(\theta_{3f} - T)^{-1.5} \quad (\mathrm{m}^2/\mathrm{C})^4,$$
$$\alpha_{3333} = 2.20 \times 10^{-1} \quad (\mathrm{m}^2/\mathrm{C})^6.$$

The solid curve in Fig. 7 is calculated from Eq. (21) using the value of α_{3333} given above.

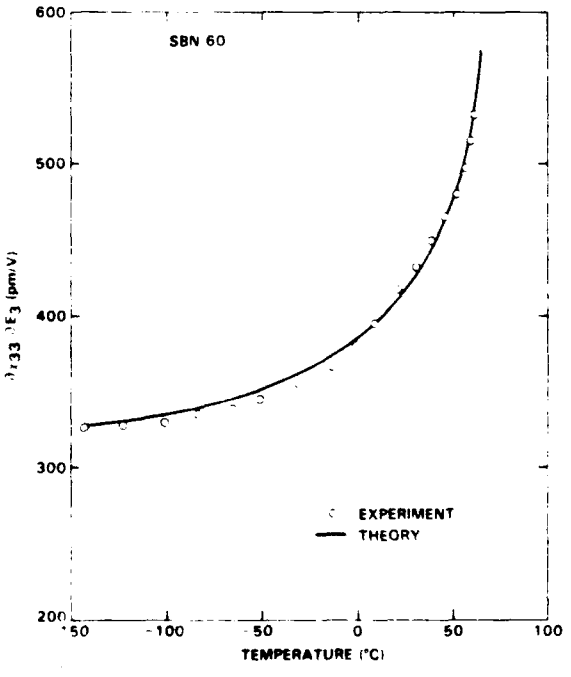

FIG. 7. The polar-axis linear electro-dielectric response of poled SBN:60. The solid line is the theoretical curve based on the derived phenomenological constant α_{3333}.

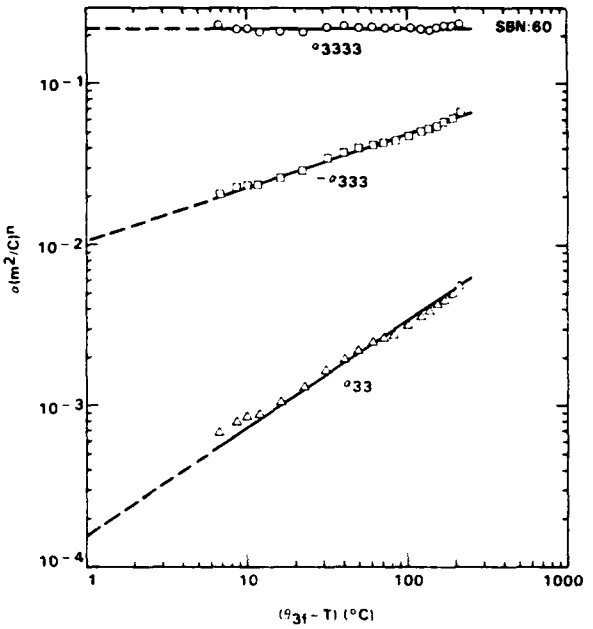

FIG. 8. Log-log plots of the higher order c-axis Devonshire coefficients vs $(\theta_{3f} - T)$. The coefficients follow a $(\theta_{3f} - T)^n$ temperature dependence, with $n = 0$, 1, and 2.

The electro-dielectric response was found to be independent of applied voltage, as expected, for dielectric changes up to 3%–4%; the maximum applied voltage was adjusted with temperature to maintain adequate sensitivity and linearity. However, close to T_c no consistent data could be obtained due to long-term drifts. In spite of the long equilibration times necessary after temperature changes near T_c (~ 1 h), the dielectric data were found to be highly reproducible on cooling, indicating that a fully poled, single ferroelectric domain condition can be maintained in SBN:60 even after long-term exposures to elevated temperatures near T_c.

Figure 9 shows the calculated crystal free energy, ΔG_1, as a function of polarization. At room temperature, the depth of the potential well is only ~ 1 meV per unit cell, substantially below the thermal energy, kT, thus illustrating the cooperative coupling of microdomains necessary to maintain a uniform macrodomain state. The calculated free energy is absolutely stable over the entire temperature range; metastable states for $\Delta G = \Delta G_1 - E_3 P_3$ do exist for reverse polarity fields, but these are inaccessible since they lie at energies above those for the absolutely stable states. Calculated P_3 vs E_3 hysteresis loops for SBN:60 show a coercive switching field of approximately 20 kV/cm at room temperature, a factor of 8 larger than the ~ 2.5 kV/cm encountered experimentally. However, this result is not surprising since the phenomenological model does not attempt to account for the kinetics of microdomain reversal.[33,34]

The electro-dielectric character of SBN:60 crystals was also examined above the ferroelectric phase transition temperature. In this phase, P_s is small or zero at zero bias; hence, using $P_3 \cong \Delta P_3 = \epsilon_0 \epsilon_{33} \Delta E_3$ in Eq. (8), and ignoring higher order terms,

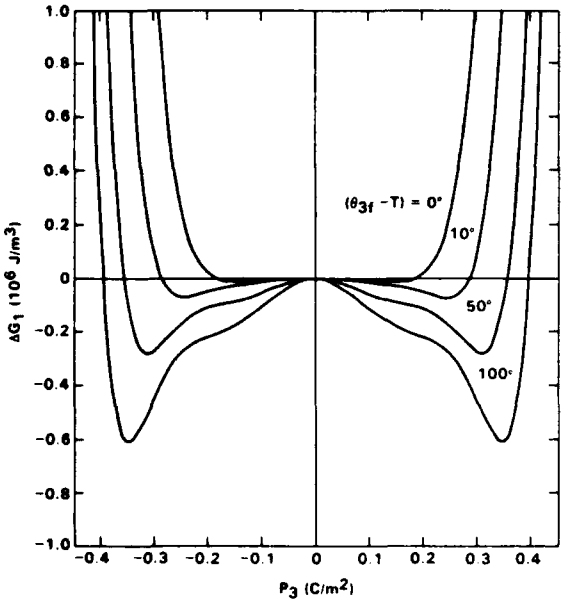

FIG. 9. Calculated curves for the Gibbs free energy of SBN:60 at four temperatures, showing absolute stability for the energy minima at $P_3 = \pm P_s$.

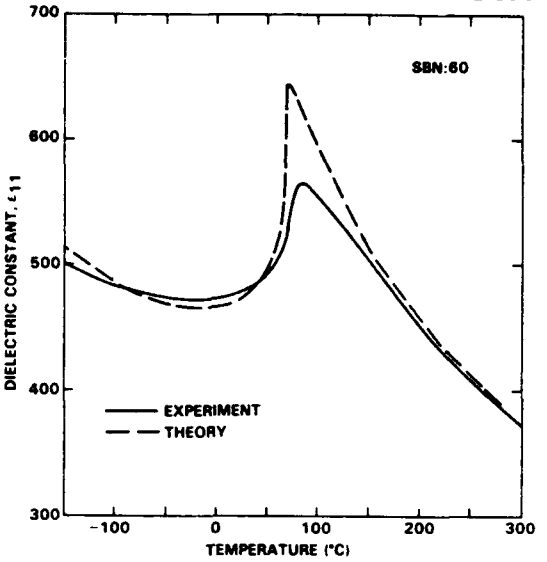

FIG. 10. The a-axis dielectric constant of SBN:60 at 10 kHz. Data at other frequencies are essentially identical. The dashed curve is calculated from the phenomenological model using temperature-independent higher order coefficients.

$$\Delta\chi_{33}/\Delta E_3 \cong 24\alpha_{33}\epsilon_0^2\epsilon_{33}^2\Delta E_3 \quad (T > T_c), \tag{22}$$

or

$$\Delta\epsilon_{33}/\epsilon_{33} \cong -24\alpha_{33}\epsilon_{33}^3(\epsilon_0\Delta E_3)^2. \tag{23}$$

Therefore, $\Delta\epsilon_{33}/\epsilon_{33}$ is expected to vary quadratically with applied electric field and rapidly diminish above T_c with the third power of ϵ_{33}. This behavior was found in SBN:60, but some asymmetry with $\pm\Delta E_3$ was seen in poled crystals at temperatures as much as 40 °C above T_c. A more symmetric response was found after thermal depoling under shorted conditions, although measurements below 95 °C remained unreliable due to long-term drifts, presumably due to crystal repoling. From the measurements over the temperature range of 100–150 °C, the averaged value of α_{33} calculated from Eq. (23) is

$$\alpha_{33} \cong -1.4\times10^{-4}(\mathrm{m}^2/\mathrm{C})^2 \quad (T > T_c),$$

a value opposite in sign to the $T < T_c$ value. Although it was difficult to establish any temperature dependence for α_{33} in the paraelectric phase, it seems reasonable to presume that α_{33} changes sign somewhere near T_c with no abrupt discontinuities. Such a sign change may also occur for α_{333}, but this could not be determined from these measurements.

VI. NONPOLAR PROPERTIES

We now turn attention to the dielectric properties of SBN:60 along the nonpolar a or b axis. The weak-field dielectric stiffness at zero bias is given in Eq. (7a) and repeated here for convenience:

$$\chi_{11} = \chi_{22} = (T-\theta_1)/C_1 + 2\alpha_{13}P_3^2 + 2\alpha_{133}P_3^4 \quad (P_1 = P_2 = 0). \tag{24}$$

A dielectric anomaly is therefore anticipated for the nonpolar directions as a result of the onset of the spontaneous polarization, P_3. A complicating factor in the measurement of the nonpolar dielectric properties is the large dielectric anisotropy of most tetragonal ferroelectric bronzes, so that incomplete contact coverage or slight axial misalignment can cause erroneous results, particularly near T_c. Fortunately, we were able to obtain a nearly perfectly oriented a-axis crystal wafer (as evidenced by x-ray diffraction and ac conductivity measurements), and its dielectric behavior is shown on an expanded scale in Fig. 10. Corresponding Arrhenius plots of the a-axis conductivity at 0.1, 1.0, and 10 kHz are presented in Fig. 11, showing the virtual absence of major conductivity peaks near T_c.

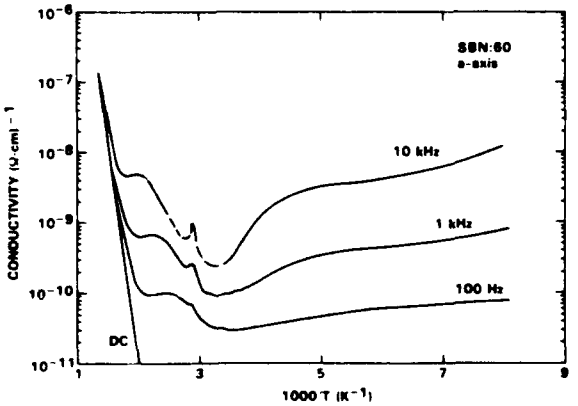

FIG. 11. Arrhenius plots of the a-axis conductivity for SBN:60 at dc, 100 Hz, 1 kHz, and 10 kHz; much of the 100-kHz conductivity was below instrument sensitivity. Note the virtual absence of a large conductivity peak at T_c.

The a-axis dielectric dispersion over 100 Hz–100 kHz was found to be minimal except at the temperature extremes where it increased to 2%–5%. Dielectric losses were similarly low, with $\tan\delta = 0.003$ or less over most of the temperature range, rising primarily above 300 °C due to the onset of significant dc conductivity. At room temperature, the dark dc conductivity was typically $5\times10^{-16}\,\Omega^{-1}\,\mathrm{cm}^{-1}$ or less.

As expected, changes in ϵ_{11} with applied field were unmeasurable because of the small induced polarization $\Delta P_1 = \epsilon_0\epsilon_{11}\Delta E_1$; hence, the values of coefficients such as α_{11} and α_{111} in Eq. (7) ($P_1 \neq 0$) could not be determined. This is of little consequence, since these coefficients do not contribute to the dielectric stiffness [Eq. (24)] or the Gibbs free energy [Eq. (2)] at zero bias ($P_1 = P_2 = 0$).

The dielectric stiffness expression in Eq. (24) could be fitted to the measured data under the assumption of temperature invariant α_{11} and α_{133}. The calculated curve is shown as the dashed line in Fig. 10 based on the following constants:

$$C_1 = 2.04\times10^5,$$
$$\theta_1 = -245 \pm 20\,^\circ\mathrm{C},$$
$$\alpha_{11} = 3.78\times10^{-3}\ (\mathrm{m}^2/\mathrm{C})^2,$$
$$\alpha_{133} = 1.40\times10^{-2}\ (\mathrm{m}^2/\mathrm{C})^4.$$

The calculated fit to the a-axis dielectric data is generally quite good (less than 3.5% error) except near T_c. Perhaps the most interesting discrepancy is the roughly 10 °C difference between the theoretical and measured dielectric maxima. The a-axis dielectric peak is also higher in temperature than the c-axis peak by 6–8 °C. The shift in temperature between the theoretical and experimental maxima of ϵ_{11} may be accounted for, at least in part, by fluctuations in P_3 such that $\langle P_3\rangle \cong 0$, but $\langle P_3^2\rangle \neq 0$, above T_c. This would also help to explain the small discrepancies in the theoretical and measured values for the paraelectric phase well above T_c.

VII. DISCUSSION

The thermodynamic phenomenology developed for SBN:60 may be applied to the calculation of other important crystal properties such as the entropy, S, and the excess heat capacity. Using the crystal free-energy expression in Eq. (2) with $P_1 = P_2 = 0$ and the measured temperature dependencies of the coefficients, the entropy is given by

$$S = -\left(\frac{\partial\Delta G_1}{\partial T}\right)_{P_3}$$
$$= \frac{P_3^2}{\epsilon_0}\left(-\frac{1}{2C_1} + \frac{2}{3}\alpha_{33}^0(\theta_{3f}-T)^{-1/3} \times P_3^2 + \frac{1}{3}\alpha_{333}^0(\theta_{3f}-T)^{-2/3}P_3^4\right). \quad (25)$$

Inserting the measured temperature dependence of P_3 into Eq. (25), we have

$$S = -0.14(\theta_{3f}-T)^{1.1}\ \mathrm{cal/mol\,^\circ C}, \quad (26)$$

and therefore the excess heat capacity due to nonzero polarization below T_c is

$$c_e - c_P^0 = T\left(\frac{\partial S}{\partial T}\right)_E$$
$$= 0.047\ T(\theta_{3f}-T)^{-2/3}\ \mathrm{cal/mol\,^\circ C}. \quad (27)$$

The excess heat capacity is thus expected to peak sharply as the phase transition temperature is approached from below, in qualitative agreement with the experimental results by Glass[1] on early SBN crystals. However, very close to the transition, the calculated excess heat capacity represents a substantial fraction of the background lattice heat capacity of 30–40 cal/mol °C, whereas the measured values represent only a few percent of the total. Our own preliminary heat capacity results show similar behavior. However, this is not entirely unexpected since the phenomenological model does not account for a distribution of phase transition temperatures, but rather presents an average of the macroscopic crystal behavior for regions well above and below the transition region.

The Gibbs free-energy function for SBN:60 possesses continuous first derivatives with respect to P,T and discontinuous second derivatives, making SBN:60 a second-order phase transition ferroelectric. However, it is interesting to note that the temperature behavior of the heat capacity is of the form expected for a classic first-order transition,[19] this being due to the strong temperature dependencies of the higher order Devonshire coefficients. Since these coefficients tend to zero as $T\to\theta$, the phenomenology suggests that the transition from macropolar to macrononpolar is tetracritical in SBN:60.

The highly regular temperature dependencies of the major physical properties for SBN:60 permit the straightforward evaluation of several parameters relevant to device applications. For example, the commonly accepted figure of merit for longitudinal pyroelectric infrared (IR) detectors is p/ϵ_{33}. Using Eqs. (12) and (14),

$$p/\epsilon_{33} = P_{30}(\theta_{3f}-T)^{1/6}/6C_{3f}, \quad (28)$$

indicating that this figure of merit varies only weakly with the separation between the operating temperature, T, and the transition temperature. Equation (28) is also valid for other SBN compositions (e.g., SBN:50, SBN:75), with differences principally occurring in the value of θ_{3f} and, to a lesser extent, P_{30}.

Another parameter of interest for optical applications is the linear electro-optic coefficient, r_{ij}. The linear electro-optic effect in bronze ferroelectrics may be considered a prototypic quadratic effect biased by the nonzero spontaneous polarization in the ferroelectric phase.[35] Hence, along the polar c axis,

$$r_{33} = 2g_{33}P_3\epsilon_0\epsilon_{33} = 2g_{33}P_{30}\epsilon_0C_{3f}/(\theta_{3f}-T)^{5/6}, \quad (29)$$

where g_{33} is the quadratic electro-optic coefficient. Measurements of g_{33} on SBN crystals[36] have shown this to be essentially independent of temperature, with a value of $\sim0.10\ \mathrm{m}^4/\mathrm{C}^2$, so that at room temperature the calculated linear coefficient for SBN:60 is $r_{33} = 464\times10^{-12}$ m/V. This value is in excellent agreement with room-temperature measurements at optical wavelengths,[8,12,14] although data at other temperatures are presently lacking. However, considerable data for the temperature dependence of r_{33} have been ob-

tained for SBN:60 at millimeter-wave frequencies (30–90 GHz).[7,37] At room temperature, the equivalent r_{33} value is 1600–2700 $\times 10^{-12}$ m/V, with the spread in value due partly to complications arising from moderate dielectric losses. At 77 K, where the dielectric losses are considerably lower, $r_{33} = 725 \times 10^{-12}$ m/V, in general agreement with the temperature dependence predicted in Eq. (29). These large values indicate that g_{33} is substantially higher at millimeter-wave frequencies, with a computed value of approximately 0.60 m^4/C^2.

The linear electro-optic effect at optical and millimeter-wave frequencies is the high-frequency equivalent of the low-frequency linear electro-dielectric effect. However, it must be cautioned that although the room-temperature value for r_{33} at optical frequencies is similar to the electro-dielectric value (418×10^{-12} m/V), their functional origins are vastly different. This is reflected in the temperature dependencies, with the linear electro-dielectric effect in SBN:60 following a $(\theta_1 - T)^{-1.6}$ dependence, as may be deduced from Eq. (21), whereas r_{33} follows a much stronger $(\theta_1 - T)^{-5.6}$ power law. Nevertheless, these two effects do share a common strong dependence on the value of the low-frequency dielectric constant, ϵ_{33}.

In the derivation of the phenomenological constants for SBN:60, we have made use of the measured c-axis dielectric properties in the paraelectric phase to determine the Curie–Weiss constants C_1 and θ_1, as discussed in Sec. V. These constants were determined from the linear inverse susceptibility region which exists above T_c up to approximately 250 °C (Fig. 4). However, above 250 °C there exists a second linear Curie–Weiss region, with constants $C_1' = 2.8 \cdot 10^5$ and $\theta_1' = 134$ °C, the latter being substantially above the phase transition temperature. It has been postulated in the work by Burns and Dacol[38,39] on bronze $Sr_2KNb_5O_{15}$ (SKN), and more recently in their work with Bhalla *et al.*[40] on SBN, that observed deviations of the optical refractive index from a linear temperature dependence above T_c may arise from fluctuations in the polarization such that $\langle P_3 \rangle = 0$, but $\langle P_3^2 \rangle \neq 0$, over a large temperature range. This would necessarily affect the low-frequency dielectric properties as well, and may account for the change in slope of χ_{33} in the paraelectric region below 250 °C.

This, then, raises the question regarding which values of C_1 and θ_1 to use in the development of the c-axis phenomenology for the ferroelectric phase. However, evaluation of the ferroelectric phenomenology using the alternative constants from the high-temperature paraelectric region shows a rapid divergence of all of the higher order c-axis Devonshire coefficients near the phase transition, leading to metastable energy states and anomalous calculated hysteresis loops. This is in sharp contrast to the well-behaved, predictable temperature dependencies shown in Sec. V. This result, combined with the phenomenological similarities determined for other tungsten bronzes such as BSKNN,[41] leads us to conclude that the lower temperature Curie-Weiss region provides a more valid description of the macroscopic paraelectric behavior of SBN:60 as it applies to the temperature dependence of α_3 in the ferroelectric phase.

The presence of fluctuating polar microdomains in the paraelectric phase below 300 °C would also serve to explain the deviation of ϵ_{11} from the extrapolated high-temperature Curie-Weiss behavior, as shown in Fig. 10. An average rms polarization, $P_d = \langle P^2 \rangle^{1/2}$, may be calculated from a least-squares fit of Eq. (24) to the measured a-axis paraelectric data using the temperature-independent values for α_1, and α_{111} calculated earlier. Such a fit shows a substantial nonzero P_d which declines nearly linearly with temperature up to ~250–300 °C, in qualitative agreement with the results from optical index measurements.[40] However, the calculated magnitude of P_d critically depends upon the chosen values for the Curie–Weiss parameters C_1 and θ_1 in Eq. (24), and hence cannot be determined with particular confidence. This uncertainty also exists to some extent in the interpretation of the refractive index data, as it also depends upon the chosen extrapolation of a linear high-temperature region.[38–40]

While this analysis is adequate to qualitatively account for the deviation of ϵ_{11} from Curie–Weiss behavior in the paraelectric phase, the situation is more complicated along the c axis. In this direction, any spatially fluctuating (and possibly dynamically inverting) polar microdomains would be perturbed by an ac measurement field, E_3, and thus would significantly contribute to the macroscopic dielectric polarizability.[7] At the lowest order this would qualitatively lead to an apparent change in the Curie–Weiss behavior of α_3 [Eqs. (6) and (8)], with the higher order terms contributing to the measured dielectric behavior by a considerably smaller amount. By inference from the discussion of ferroelectric stability given above, this contribution from fluctuating microdomains would necessarily extrapolate well into the ferroelectric region below T_c. Further support for this hypothesis is provided by millimeter-wave measurements, which show anomalous c-axis dielectric losses at room temperature which diminish on further cooling to 77 K.[7,37]

VIII. CONCLUSIONS

The experimental data for ferroelectric SBN:60 show that for a more realistic fitting of the data, the Taylor series expansion of the Gibbs free energy must be taken out to at least the eighth power of the polarization, and that the coefficients of terms up to the sixth power must be taken as functions of temperature. This phenomenological description should provide a foundation for future comparisons with other compositions in the bronze crystal family, and may also assist in uncovering potentially anomalous ferroelectric behavior in materials which otherwise may appear to have well-behaved dielectric and polarization properties. It is noteworthy, however, that a more classical sixth-order phenomenology with temperature invariant higher order coefficients still provides a useful, approximate description for many of the measured properties,[16] and has proven particularly effective for comparisons with other crystal families.[36]

The extended eighth-order phenomenology is that of a simple proper crystalline ferroelectric. The highly regular behavior of the phenomenology suggests that this description is perfectly adequate to account for the observed ferroelectric properties in SBN:60. However, there has been some suggestion that SBN may be an incommensurate phase tran-

sition ferroelectric.[42] Although the present phenomenology does not preclude such a possibility, neither does it suggest it since the computed energy states remain absolutely stable over the entire temperature range. In either case, the phenomenology should prove useful in developing a much clearer theoretical description for the ferroelectric behavior in SBN crystals, and perhaps for other bronze crystal systems as well.

ACKNOWLEDGMENTS

The authors wish to thank W. K. Cory for his patient work on the Czochralski crystal growth technology used for the development of high-quality SBN crystals. This research on the phenomenology of SBN was supported by the Office of Naval Research (Contract No. N00014-81-C-0463).

[1]A. M. Glass, J. Appl. Phys. **40**, 4699 (1969).
[2]R. R. Neurgaonkar, M. H. Kalisher, T. C. Lim, E. J. Staples, and K. L. Keester, Mater. Res. Bull. **15**, 1235 (1980).
[3]R. R. Neurgaonkar, DARPA Final Report, Contract No. F49620-78-C-0093 (1982) (unpublished).
[4]G. Burns, IEEE Trans. Electron Devices **ED-16**, 506 (1969). Includes an extensive bibliography of early tungsten bronze papers.
[5]K. Tada, T. Murai, M. Aoki, K. Muto, and K. Awazu, Jpn. J. Appl. Phys. **11**, 1622 (1972).
[6]R. R. Neurgaonkar, W. K. Cory, and J. R. Oliver, Ferroelectrics **51**, 3 (1983).
[7]W. F. Hall, W. W. Ho, R. R. Neurgaonkar, and W. K. Cory, in *Proceedings of the 6th IEEE International Symposium on Applications of Ferroelectrics (ISAF)*, edited by V. Wood (IEEE, New York, 1986), p. 469.
[8]R. R. Neurgaonkar, J. R. Oliver, W. K. Cory, and L. E. Cross, in *Advances in Materials for Active Optics*, edited by S. Musikant (SPIE, Bellingham, WA, 1985), Vol. 567, p. 11.
[9]B. Fischer, M. Cronin-Golomb, J. O. White, A. Yariv, and R. R. Neurgaonkar, Appl. Phys. Lett. **40**, 863 (1982).
[10]G. Salamo, M. J. Miller, W. W. Clark III, G. L. Wood, and E. J. Sharp, Opt. Commun. **59**, 417 (1986).
[11]E. J. Sharp, M. J. Miller, G. L. Wood, W. W. Clark III, G. J. Salamo, and R. R. Neurgaonkar, in *Proceedings of the 6th IEEE International Symposium on Applications of Ferroelectrics (ISAF)*, edited by V. Wood (IEEE, New York, 1986), p. 51.
[12]R. R. Neurgaonkar and W. K. Cory, J. Opt. Soc. Am. B **3**, 274 (1986). Includes an extensive bibliography of early and more recent papers on tungsten bronze ferroelectrics.
[13]G. Rakuljic, A. Yariv, and R. R. Neurgaonkar, Opt. Eng. **25**, 1212 (1986).
[14]R. R. Neurgaonkar, W. K. Cory, J. R. Oliver, M. D. Ewbank, and W. F. Hall, Opt. Eng. **26**, 392 (1987).
[15]K. Megumi, N. Nagatsuma, K. Kashiwada, and Y. Furuhata, Mater. Sci. **11**, 1583 (1976).
[16]T. R. Shrout, L. E. Cross, P. Moses, H. A. McKinstry, and R. R. Neurgaonkar, in *Proceedings of the IEEE 1980 Ultrasonics Symposium* (IEEE, New York, 1980), p. 414.
[17]A. F. Devonshire, Adv. Phys. **3**, 85 (1954).
[18]See, for example, J. F. Nye, *Physical Properties of Crystals* (Clarendon, Oxford, 1969).
[19]M. E. Lines and A. M. Glass, *Principals and Applications of Ferroelectrics and Related Materials* (Clarendon, Oxford, 1977).
[20]M. E. Drougard, R. Landauer, and D. R. Young, Phys. Rev. **98**, 1010 (1955).
[21]M. H. Francombe, Acta Cryst. **13**, 131 (1960).
[22]P. B. Jamieson, S. C. Abrahams, and J. L. Bernstein, J. Chem. Phys. **48**, 5048 (1968).
[23]L. A. Shuvalov, Proc. Second Int'l Meeting on Ferroelectricity, J. Phys. Soc. Jpn. **28**, (Suppl.), 38 (1970).
[24]A. A. Ballman and H. Brown, J. Cryst. Growth **1**, 311 (1967).
[25]R. B. Maciolek and S. T. Liu, J. Electron. Mater. **2**, 191 (1973).
[26]F. J. Morin, J. R. Oliver, and R. M. Housley, Phys. Rev. B **6**, 4434 (1977).
[27]R. Clarke and J. C. Burfoot, J. Phys. D **8**, 1115 (1975).
[28]I. Camlibel, J. Appl. Phys. **40**, 1690 (1969).
[29]T. W. Cline and L. E. Cross, J. Appl. Phys. **49**, 4298 (1978).
[30]G. Borchardt, J. v. Cieminski, and G. Schmidt, Phys. Status Solidi A **76**, K1-41 (1983).
[31]A. S. Bhalla and L. E. Cross, Ferroelectrics **38**, 935 (1981).
[32]G. Burns, D. F. O'Kane, E. A. Giess, and B. A. Scott, Solid State Commun. **6**, 223 (1968).
[33]M. Hayashi, J. Phys. Soc. Jpn. **33**, 616 (1972).
[34]L. Godefroy, Ferroelectrics **35**, 207 (1981).
[35]M. DiDomenico and S. H. Wemple, J. Appl. Phys. **40**, 720 (1969).
[36]R. R. Neurgaonkar and L. E. Cross, DARPA Semi-Annual Technical Reports No. 1 (1983) and No. 5 (1985), Contract No. N00014-82-C-2466 (unpublished).
[37]R. R. Neurgaonkar, J. R. Oliver, L. E. Cross, and W. F. Hall, ONR Annual Report No. 5, Contract No. N00014-81-C-0463 (1985) (unpublished).
[38]G. Burns, Phys. Rev. B **13**, 215 (1976).
[39]G. Burns and F. H. Dacol, Phys. Rev. B **30**, 4012 (1984).
[40]A. S. Bhalla, R. Guo, L. E. Cross, G. Burns, F. H. Dacol, and R. R. Neurgaonkar, Phys. Rev. B **36**, 2030 (1987).
[41]J. R. Oliver, R. R. Neurgaonkar, and L. E. Cross (unpublished).
[42]J. Schneck, J. C. Toledano, R. Whatmore, and F. W. Ainger, Ferroelectrics **36**, 327 (1981).

8.0 GROWTH OF GRAIN-ORIENTED TUNGSTEN BRONZE SBN FILMS ON Si

GROWTH OF GRAIN-ORIENTED TUNGSTEN BRONZE SBN FILMS ON Si

R. R. Neurgaonkar, I. S. Santha and J. R. Oliver
Rockwell International Science Center
Thousand Oaks, CA 91360

ABSTRACT

This paper reports preliminary results on the growth of grain-oriented tungsten bronze Ce-doped $Sr_{1-x}Ba_xNb_2O_6$ (SBN) thin films on (100)-oriented Si substrates. We maintained the grain orientation in these films up to 4 μm in thickness, using high oxygen pressure and annealing to 700°C. The films are smooth and have excellent surface quality which permits accurate ferroelectric measurements. The temperature dependence of the dielectric constant indicates the phase transition is near 30°C, with a dielectric constant of 1400 at room temperature. The spontaneous polarization for these films is 1.3 μcoul/cm^2 at room temperature and 6.5 μcoul/cm^2 at -125°C.

INTRODUCTION

The integration of ferroelectric thin films with semiconductor substrates is important for optoelectronic applications. Progress has been made in developing deposition techniques; however, grain-orientation has proven to be difficult to achieve on semiconductor substrates. We report here the successful deposition of tungsten bronze (T. B.) SBN ferroelectric thin films on Si substrates in which good grain-orientation was obtained.

The T. B. SBN solid solution exists on the binary $SrNb_2O_6$-$BaNb_2O_6$ system with the highest electro-optic and piezoelectric coefficients for the $Sr_{0.75}Ba_{0.25}Nb_2O_6$ (SBN:75) composition (1-3). At Rockwell, we have been developing ferroelectric crystals in the tungsten bronze family for photorefractive and electro-optic applications since 1978 (4-10). Recently, we have focused our attention on developing single crystal and grain-oriented T. B. thin films for photorefractive, electro-optic and electronic memory applications. Earlier we had demonstrated the growth of single crystal SBN and SKN thin films on SBN:60 substrates by the LPE technique for SAW device applications (11, 12). The growth of polycrystalline SBN films on glass and Si substrates has been reported recently by McKinzie et al (13-16), using the sol-gel process. The ferroelectric properties that can be achieved in such films are greatly reduced from those found in single crystals of the same composition. For this reason, we are pursuing the magnetron sputtering technique for the growth of various tungsten bronze films to achieve good grain orientation on semiconducting substrates. This paper reports the results for SBN films grown on Si.

EXPERIMENTAL PROCEDURE

Ce^{3+}-doped ferroelectric tungsten bronze SBN thin films were sputtered using a single 3" target consisting of sintered BaO, SrO, CeO_2 and Nb_2O_5. Initial experiments indicated that the use of a stoichiometric target (SBN:75) produced nonferroelectric SBN films with an excess of Ba^{2+}. To maintain stoichiometry in the film, we incorporated 20% excess Sr^{2+} in the target to produce ferroelectric SBN films having a composition close to SBN:75. The final targets were prepared using ceramic sintering or hot-pressing; well-mixed powders were cold pressed and then sintered or hot-pressed at 1300°C.

The SBN thin films were deposited with an MRC rf sputtering instrument; the sputtering conditions are summarized in Table 1. (100)-oriented Si substrates

of 10 x 10 x 1 mm were used for this study with platinum as an electrode on one surface. The substrate temperature was maintained below 300°C to avoid the oxidation of Si. The films were annealed in argon and then in oxygen below 700°C to achieve the desired tungsten bronze tetragonal structure (4mm).

X-ray diffraction was used to check the crystal structure and lattice constants of the films. The phase transition temperature, dielectric constant and spontaneous polarization were measured using standard ferroelectric measurement techniques (5, 6).

RESULTS AND DISCUSSION

Since SBN:75 exhibits large spontaneous polarization at room temperature (P_3 > 24 coul/cm^2) and a large electro-optic coefficient (r_{33} = 1400 x 10^{-12} m/V), this composition is very promising for applications including spatial light modulators (SLM's), guided wave optics, photorefractive devices and electronic memories. SBN:75 has an excellent lattice-match with Si in one of the possible orientations (a/ $\sqrt{2}$ = 3.901 Å). In the present work, we selected this orientation to fabricate grain-oriented SBN films on Si. A platinum electrode was sputtered on the growth surface with a thickness of less than 1000 Å. The substrates were mounted on a heating block with a stainless steel mask of 0.2 mm thickness. Substrate temperature was monitored by a Pt-Pt Rh thermocouple inserted into the center of the substrate holder. The sputtering conditions are summarized in Table 1.

TABLE 1

Target-Substrate Distance:	5 cm
Sputtering Gas:	Ar:O_2
Substrate Temperature:	100 - 300°C
Deposition Rate:	10 - 15 Å/min.
Annealing Temperature:	600 - 800°C

Figure 1 shows the x-ray diffraction patterns of SBN films grown on Si

substrates for growth temperatures of 100° and 300°C, followed by annealing at 675°C. As shown in Figure 1b, excellent grain-orientation was achieved for films annealed above 600°C. Below this temperature, the films were essentially amorphous. We have also demonstrated the growth of grain-oriented perovskite PLZT and tungsten bronze PBN:60 and PSKNN thin films on Si substrates with good success (17, 18), but in these cases the annealing temperature was near 600°C. Our current work indicates that grain orientation in these films strongly depends on the $Ar:O_2$ ratio during deposition as well as annealing. If the oxygen partial pressure is sufficiently low, Nb^{5+} converts to Nb^{4+} and this prevents the formation of the tungsten bronze phase. For this reason, we maintained a high oxygen pressure during annealing. Furthermore, we observed that the grain orientation is also very sensitive to the film thickness. Currently we have been successful in maintaining complete grain-orientation up to 3-4 μm with excellent film quality. Beyond this limit, mixed orientation films were observed with the (001)-oriented x-ray diffraction being dominant. This thickness is sufficient for various optoelectronic applications; whereas for electronic memories, thicknesses in the range of 1000 to 3000 Å are required.

Lattice constant measurements on both (001)-oriented and polycrystalline SBN films show a = 12.456 Å and c = 3.912 Å indicating that the film composition is close to SBN:75. However, these results suggest that the films are still slightly Ba^{2+}-rich and can be adjusted to the desired composition by adjusting the Ba:Sr ratio in the target. The film surface and quality are quite adequate to make both ferroelectric and optical measurements, and the addition of Ce^{3+} did not degrade the film quality or change the growth conditions. This dopant was incorporated in the films to enhance their photorefractive properties; however, for linear electro-optical applications (e. g., modulators), such doping would not be utilized.

Figure 2 shows the temperature dependence of the weak-field dielectric constant at 10 kHz for 1.0 μm SBN film, using the substrate Pt metallization and an 0.018 cm^2 Pt surface contact as electrodes. The temperature of the dielectric maximum, T_c, varies with frequency from 27 - 42°C over a 100 Hz - 100 kHz range, typical of a broadened relaxor phase transition. At room temperature the dielectric constant varies from 1430 - 1170 over the same frequency range. The corresponding room temperature dissipation factor is 0.022 - 0.340 with frequency, with the high loss value at 100 kHz resulting primarily from the series sheet

resistance of the substrate metallization. Although this is a nominally SBN:75 film composition, the addition of Ce^{3+}, combined with a mild compressive stress on the film due to differing film/substrate thermal expansion coefficients, along with potential film compositional nonuniformity, result in a broadened ferroelectric phase transition located well below the usual 75 - 78°C transition temperature for SBN:60. Nevertheless, the dielectric constant shows a very well-defined peak typical of an SBN ferroelectric, a feature not often found in many ferroelectric thin films.

Figure 3 shows the temperature dependence of the spontaneous polarization, P_s, measured by the integration of the short-circuit current density during warming at a constant rate of 3°C/min. Prior to measurement, the film was poled with an applied dc field of 40 kV/cm during cooldown from room temperature. The absence of an abrupt change in P_s near T_c again reflects the broadened distribution of phase transition temperatures in the film; this broadening results in the persistence of measurable polarization well above 100°C. Although P_s is only 1.3 microcoulombs/cm^2 at room temperature, it rises nearly linearly with decreasing temperature to a value of 6.5 microcoulombs/cm^2 at -125C. These polarization values are among the highest reported thus far for SBN thin films.

The comparatively low spontaneous polarization at room temperature results in a slim-loop P vs. E hysteresis, as shown in Figure 4(a). The reversible polarization, P_r, is 0.6 microcoulombs/cm^2, roughly one-half the value of P_s measured by thermal depolarization. However, at -95°C (Figure 4(b)), the loop begins to square out, with P_r = 4.6 microcoulombs/cm^2 and a coercive field E_c = 38 kV/cm. The reversible polarization agrees well with the measured P_s at -95°C (Figure 3); this correspondence holds true over most of the temperature range below 0°C.

No significant switching fatigue was observed in these films for up to 5×10^5 switching cycles at 50 Hz and temperatures at or below 23°C. What is noteworthy is that these SBN films can sustain electric fields of 150 kV/cm without breakdown, and still higher fields (> 200 kV/cm) at low temperatures.

CONCLUSIONS

We have presented x-ray and ferroelectric data for Ce^{3+}-doped SBN:60 thin films grown by sputtered deposition on Pt-metallized Si substrates. These films show good grain orientation with the polar c-axis normal to the film surface, and good dielectric and polarization properties. The present films, however, are limited by low spontaneous polarization at room temperature due to a broadened distribution of phase transition temperatures. This is due, in part, to possible excessive Ce^{3+} content in the films, combined with some degree of compositional nonuniformity. Nevertheless, the room temperature polarization of 1.3 microcoulombs/cm^2 ranks among the highest values measured in SBN films, and the dielectric constant is consistent with values found in high quality SBN single crystals. With continued improvement in film stoichiometry, compositional uniformity and grain orientation, these sputtered SBN thin films have the potential for effective use in a number of integrated electro-optical and photorefractive device applications.

ACKNOWLEDGMENTS

This work was supported by DARPA (Contract No. F49620-90-C-0084) and by the Office of Naval Research (Contract No. N00014-81-C-0463). The authors thank Prof. L. Eric Cross of the Pennsylvania State University for his useful discussions and suggestions during the course of this work.

REFERENCES

1. A. A. Ballman and H. Brown, J. Cryst. Growth, 1, 321, 1967.

2. P. B. Lenzo, E. G. Spencer and A. A. Ballman, Appl. Phys. Lett., 11, 23, 1968.

3. R. R. Neurgaonkar and L. E. Cross, Mat. Res. Bull., 21, 893, 1986.

4. R. R. Neurgaonkar, M. H. Kalisher, T. C. Lim, E. J. Staples and K. L. Keester, Mat. Res. Bull., 15, 1305, 1980.

5. R. R. Neurgaonkar and W. K. Cory, J. Opt. Soc. Am., 3(B), 276, 1986.

6. R. R. Neurgaonkar, W. K. Cory, J. R. Oliver, M. D. Ewbank and W. F. Hall, J. Opt. Eng., 26(5), 392, 1987.

7. R. R. Neurgaonkar, W. K. Cory, J. R. Oliver, W. W. Clark III, G. L. Wood, M. J. Miller and E. J. Sharp, J. Cryst. Growth, 84, 629, 1987.

8. R. R. Neurgaonkar, W. K. Cory, J. R. Oliver, E. J. Sharp, G. L. Wood, M. S. Miller, W. W. Clark III, and G. J. Salamo, Mat. Res. Bull., 23, 1459, 1988.

9. R. R. Neurgaonkar, W. K. Cory, J. R. Oliver, E. J. Sharp, M. J. Miller, W. W. Clark III, G. L. Wood and G. J. Salamo, Mat. Res. Bull., 24, 589, 1989.

10. R. R. Neurgaonkar, W. K. Cory, J. R. Oliver and L. E. Cross, Mat. Res. Bull., 24, 1025, 1989.

11. R. R. Neurgaonkar and E. T. Wu, Mat. Res. Bull., 22, 1095, 1987.

12. R. R. Neurgaonkar, J. R. Oliver and L. E. Cross, Mat. Lett., 6, 152, 1988.

13. R. Xu, Y. H. Xu, C. J. Chen, and J. D. Mackenzie, J. Mater. Res., 5(5), 916 (1990).

14. C. J. Chen, Y. H. Xu, R. Xu, and J. D. Mackenzie, J. Appl. Phys., 69, 1763 (1991).

15. Y. H. Xu, C. J. Chen, R. Xu, and J. D. Mackenzie, Phys. Rev. B., accepted for publication in July 1, 1991 issue.

16. C. J. Chen, Y. H. Xu, R. Xu, and J. D. Mackenzie, *Electro-optics and Nonlinear Optic Materials*, Ceramic Transaction, 14, 211 (1990).

17. R. R. Neurgaonkar, I. S. Santha and J. R. Oliver, J. Mat. Science, 25, 2053, 1990.

18. R. R. Neurgaonkar, I. S. Santha and J. R. Oliver, private communication.

FIGURE CAPTIONS

Figure 1 — Growth of grain-oriented tungsten bronze SBN thin films.

Figure 2 — Weak-field dielectric constant and tan δ at 10 kHz for an unpoled SBN:75 thin film.

Figure 3 — Spontaneous polarization vs. temperature for an SBN:75 thin film poled at 40 kV/cm.

Figure 4 — Polarization vs. electric field at 50 Hz for a 1.0 μm SBN:75 film: (a) at 23°C; (b) at -95°C. (Scales: horizontal - 50 kV/cm/div., vertical - 5 μcoul/cm^2/div.)

Tungsten Bronze SBN Thin Films on Si

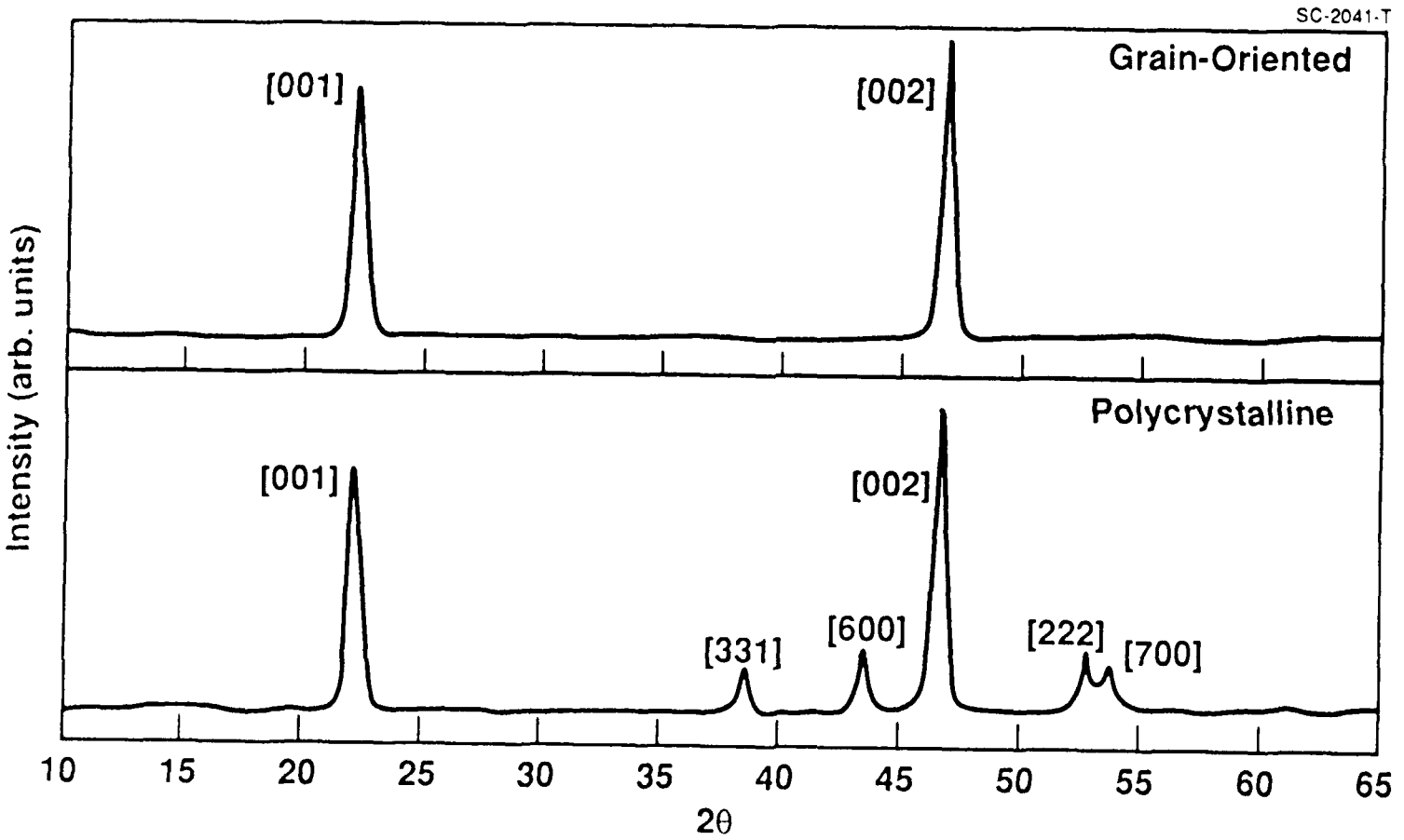

Figure 1. Growth of grain-oriented tungsten bronze SBN thin films.

Rockwell International
Science Center

Temperature Dependent Dielectric Constant

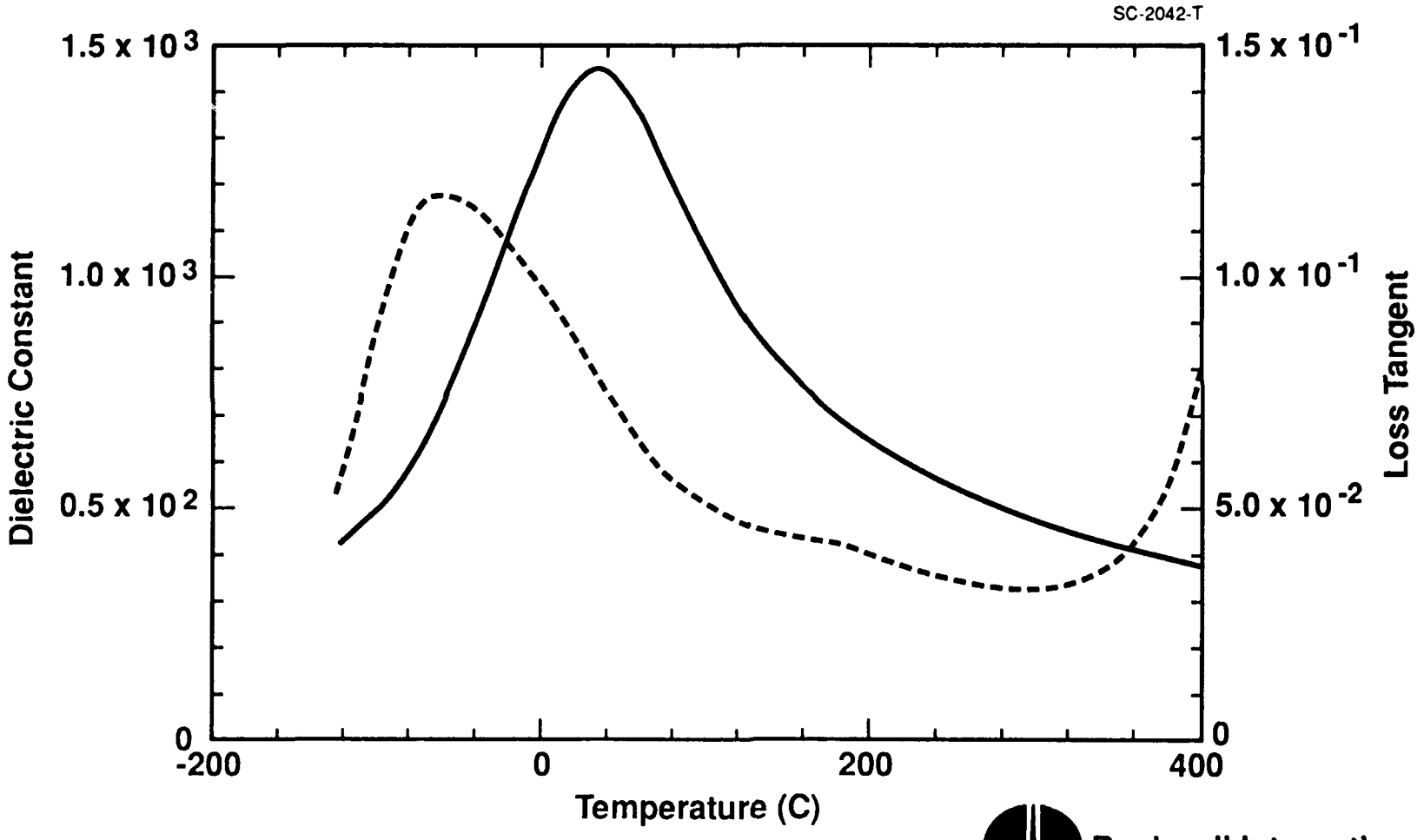

Figure 2. Weak-field dielectric constant and tan δ at 10 kHz for an unpoled SBN:75 thin film.

Polarization as a Function of Temperature

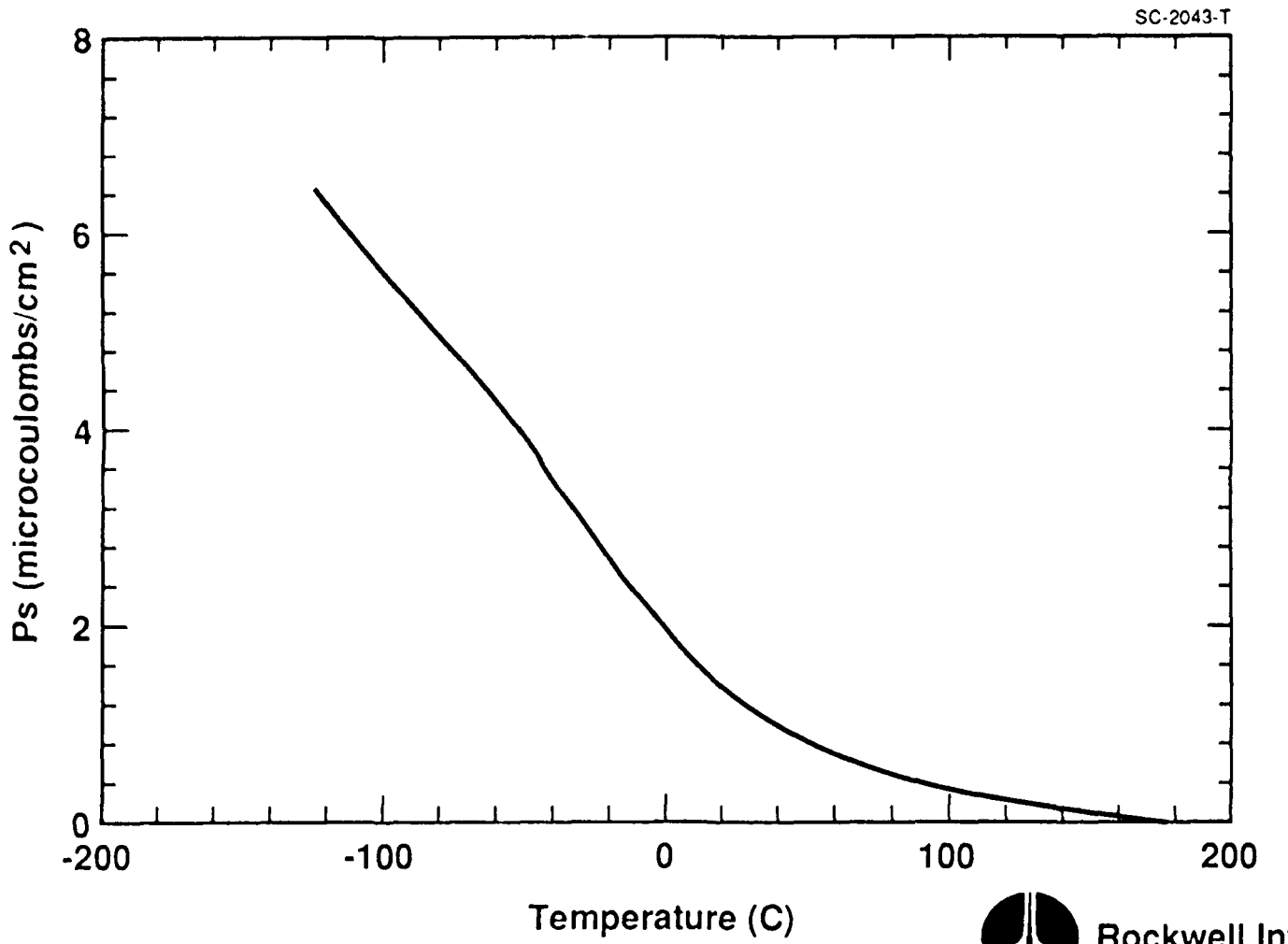

Figure 3. Spontaneous polarization vs. temperature for an SBN:75 thin film poled at 40 kV/cm.

Rockwell International
Science Center

SPONTANEOUS POLARIZATION VS. FIELD

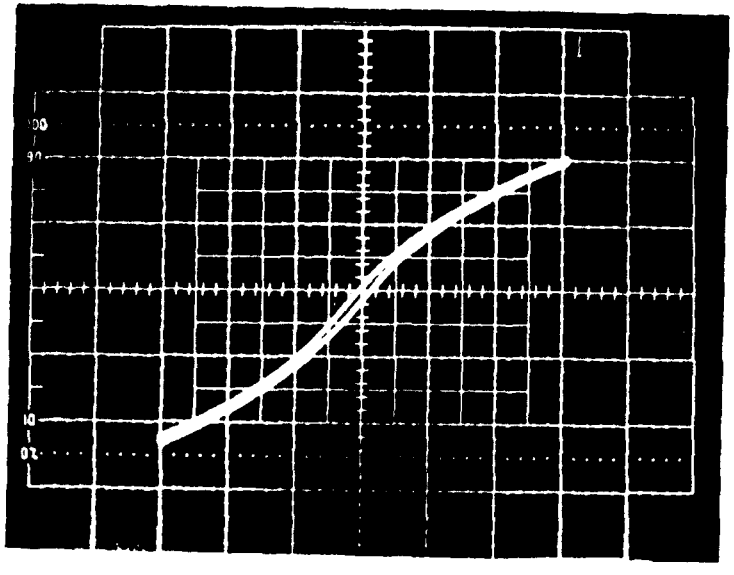

(a)

Measured at RT

SC53402

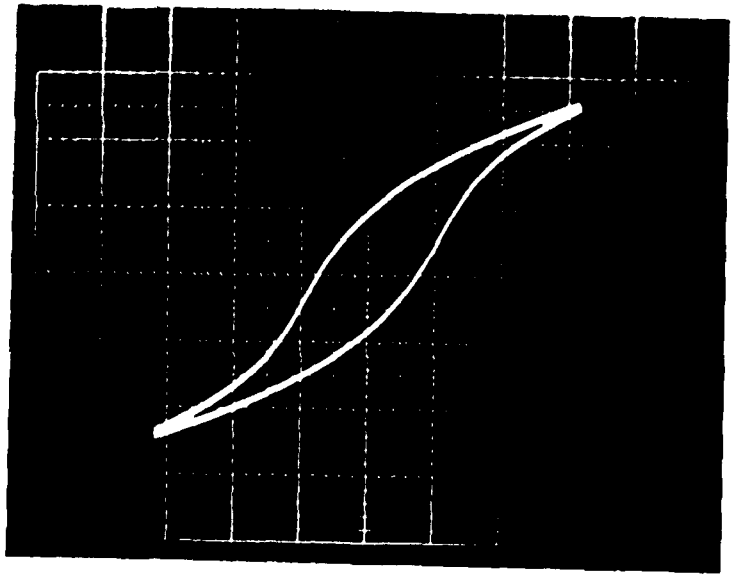

(b)

Measured below RT

Figure 4. Polarization vs. electric field at 50 Hz for a 1.0 μm SBN:75 film: (a) at 23°C; (b) at -95°C. (Scales: horizontal -50 kV/cm/div., vertical - 5 μcoul/cm^2/div.)

Rockwell International
Science Center

9.0 LPE GROWTH OF FERROELECTRIC TUNGSTEN BRONZE $Sr_2KNb_5O_{15}$ THIN FILMS

Volume 6, number 5,6 MATERIALS LETTERS March 1988

LPE GROWTH OF FERROELECTRIC TUNGSTEN BRONZE $Sr_2KNb_5O_{15}$ THIN FILMS

R.R. NEURGAONKAR, J.R. OLIVER
Rockwell International Science Center, Thousand Oaks, CA 91360, USA

and

L.E. CROSS
Materials Research Laboratory, The Pennsylvania State University, University Park, PA 16802, USA

Received 15 December 1987

Ferroelectric tungsten bronze $Sr_2KNb_5O_{15}$ (SKN) thin films have been grown by liquid phase epitaxy on (100), (110) and (001) orientations of tungsten bronze $Sr_{0.6}Ba_{0.4}Nb_2O_6$ (SBN:60) substrates using vanadium-containing solvents. Single-crystal film growths of up to 25 μm thickness were achieved with very good film quality in all growth directions, due in part to the excellent lattice match with SBN:60. Surface acoustic wave (SAW) measurements show electro-mechanical coupling of up to 1.30×10^{-4}, comparable to values measured in other tungsten bronze ferroelectrics. The high dielectric constants available in these films also indicate potentially very large linear electro-optic effects which are roughly an order of magnitude greater than for $LiNbO_3$.

1. Introduction

The solid solution $Sr_2KNb_5O_{15}$ (SKN) is a tetragonal (4mm) tungsten bronze ferroelectric which exists in the $SrNb_2O_6$–$KNbO_3$ pseudobinary system [1–3]. SKN has been of practical interest for several device applications because of its potentially large electro-optic and electro-mechanical properties [4–7]. In particular, extensive efforts have been made to grow SKN in bulk single-crystal form for surface acoustic wave (SAW), electro-optic and millimeter wave device applications. Although we have been able to grow small crystals of reasonable quality by the Czochralski technique in our own work, improvements in homogeneity, optical quality and crystal size have been hampered by the K^+ volatility at the growth temperature and by bulk crystal fracture during cooldown.

An alternative growth method for this ferroelectric bronze is liquid phase epitaxy (LPE) which has been successfully utilized to grow tungsten bronze $Sr_{0.5}Ba_{0.5}Nb_2O_6$ (SBN:50), ilmenite $LiNbO_3$ and $LiTaO_3$ thin films for SAW evaluation [8–11]. In this paper, we report the LPE growth of SKN thin films on $Sr_{0.6}Ba_{0.4}Nb_2O_6$ (SBN:60) substrates, the latter being chosen because of its close lattice match to SKN.

2. LPE flux systems

The successful LPE growth of volatile solid solutions such as SKN requires the development of an appropriate flux system permitting relatively low-temperature growths without the occurrence of spontaneous nucleation during supercooling. Based on our prior work on the LPE growth of tungsten bronze SBN compositions [8], KVO_3 solvents appear to have the best potential for SKN film growth since V^{5+} does not incorporate into the tungsten bronze lattice. In particular, the flux system KVO_3–SBN was found to form tetragonal SKN over a wide compositional range due to the exchange of Ba for K and the formation of BaV_2O_6 and SKN [8]. The phase diagram for this system, with KVO_3 and SBN:50 as end members, was established by DTA

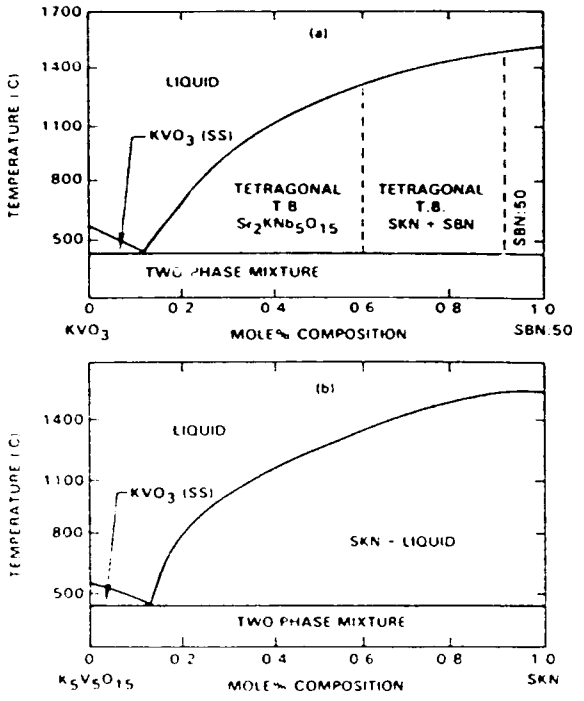

Fig. 1. LPE flux systems for tungsten bronze SKN film growth: (a) KVO_3–SBN:50, (b) $K_5V_5O_{15}$–SKN.

measurements and X-ray diffraction analysis to determine the structure and lattice constants of the major phases, and is shown in fig. 1. Additional dielectric measurements were carried out on sintered ceramics obtained from several flux compositions to determine the composition of the major phase, i.e. either SBN or SKN, the latter having a typically large room-temperature dielectric constant and high Curie point (>150°C). For the KVO_3–SBN:50 system, single-phase SKN was found over a wide compositional range up to 60 mole% SBN:50 (fig. 1a), with ceramic samples showing a ferroelectric transition temperature of $T_c = 154$–156°C and large room-temperature dielectric constants of approximately 1300, ruling out SBN as a possible phase. In the compositional range of 60–90 mole% SBN:50, mixed phases of SKN and SBN were found, and above 90 mole% SBN:50, only SBN compositions were found with very high melting temperatures.

The flux system $K_5V_5O_{15}$–$Sr_2KNb_5O_{15}$ was also examined for possible use in LPE film growth. Because of the absence of Ba^{2+} in this system, single-phase bronze SKN was found in the entire compositional region above 13 mole% SKN concentration, as shown in the phase diagram of fig. 1b. As in the case of the previous flux system, ceramics derived from the $K_5V_5O_{15}$–SKN system showed a high transition temperature of $T_c = 162$°C and large room-temperature dielectric constants of approximately 1100. However, the overall melting temperatures were somewhat lower in this flux system, as can be seen in fig. 1.

3. LPE thin film growth

Since both the KVO_3–SBN:50 and $K_5V_5O_{15}$–SKN flux systems show the formation of single-phase SKN compositions at suitably low melting temperatures, both systems were used for the LPE growth of SKN thin films. The particular flux compositions 0.75 KVO_3–0.25 SBN:50 and 0.80 $K_5V_5O_{15}$–0.20 SKN were chosen for film growth based on their low melting temperatures and the close lattice match of the resulting crystals to stoichiometric $Sr_2KNb_5O_{15}$. The measured crystal lattice constants in these cases were $a,b = 12.469$ Å, $c = 3.943$ Å for the 0.75 KVO_3–0.25 SBN:50 flux system and $a,b = 12.473$ Å, $c = 3.943$ Å for 0.80 $K_5V_5O_{15}$–0.20 SKN. These values compare very closely with $a,b = 12.471$ Å, $c = 3.942$ Å for stoichiometric SKN.

Reagent grade carbonates and oxides of 99.95% purity were used as starting materials, with film growths performed in a vertical tube furnace controllable to within ±1°C. In each case, the calcined flux was melted in a 100 cm³ platinum crucible and held overnight at approximately 100°C above the melting temperature to achieve complete homogeneity. The molten solution was then cooled at a rate of 10°C/h back down to the melting temperature where it was allowed to equilibrate. Finally, oriented substrates were then individually dipped into the melt for LPE film growth; after the required growth time had elapsed, the substrates were removed from the melt and then slowly cooled to room temperature. Adhering flux was removed using dilute HCl followed by water rinsing. Further details may be found in earlier papers [8–12].

Essential to the successful growth of high-quality epitaxial thin films is the use of closely lattice-

matched substrates. In the case of SKN, a close lattice match exists with tungsten bronze SBN:60 along both ⟨100⟩ ($a,b=12.468$ Å) and ⟨001⟩ ($c=3.938$ Å) orientations. SBN:60 is a congruently melting bronze solid solution which can be grown in exceptionally high quality by the Czochralski technique in crystal boules up to 3 cm diameter [13–15]. Therefore, SBN:60 is particularly suited for the LPE growth of SKN thin films of the highest possible quality.

SBN:60 substrate wafers with ⟨100⟩, ⟨110⟩ and ⟨001⟩ orientations were used to evaluate film growth rates and film quality. After cutting with diamond saw, each crystal wafer was lapped and then optically polished on one surface, followed by cleaning in dilute acid. LPE growth of SKN films was found to be faster along ⟨001⟩ for both flux systems, with a growth rate of typically 1–2 μm/min compared to 0.5 μm/min or less for ⟨100⟩ or ⟨110⟩. This is consistent with our observations on Czochralski bulk single-crystal growth of tungsten bronze ferroelectrics where ⟨001⟩ is the preferred growth direction [13–15]. However, optical and X-ray diffraction evaluations of these films showed somewhat better film quality for the ⟨100⟩ and ⟨110⟩ orientations because of their slower growth rates. Nevertheless, all of these SKN thin films were found generally superior to previous SBN:50 growths on SBN:60 substrates [8] due to the improved lattice match between SKN and SBN:60, with SKN films of up to 15–25 μm thickness showing no significant compromise of film quality. This result reflects the general observation that the lattice mismatch tolerance factor for good quality tungsten bronze films appears to be relatively low at 0.3% or less.

The crystallinity, phase purity and lattice constants of the SKN fims were evaluated by X-ray diffraction measurements. Since SKN and SBN:60 have nearly the same lattice constants, it was neccessary to use very slow scanning rates (1/8 to 1/4°/min) to separate the diffraction peaks arising from the SKN film and the underlying substrate. Fig. 2 shows the relative intensity of the Cu $K\alpha_1$ and $K\alpha_2$ diffraction peaks for the (800) reflection in films of successively greater thickness. In the figure, the primed lines indicate diffraction due to the SKN film, and the unprimed lines due to the underlying substrate. The latter are seen to disappear for film thicknesses greater than 10 μm. Film crystallinity was generally

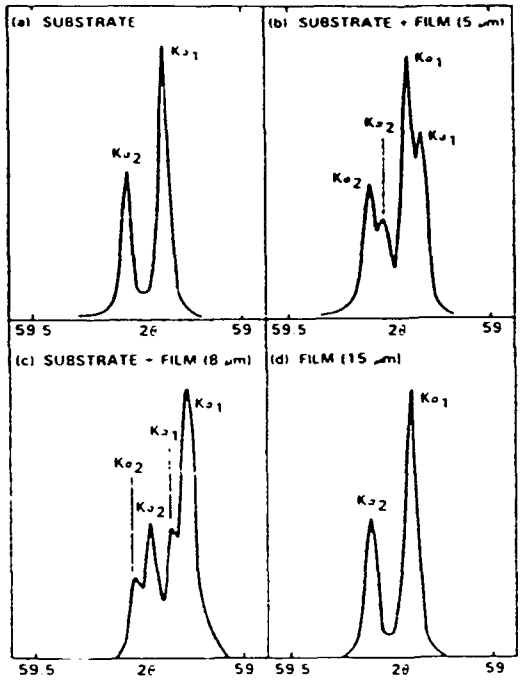

Fig. 2. Cu $K\alpha_1$ and $K\alpha_2$ X-ray diffraction peaks for the (800) line as a function of SKN film thickness. The unprimed peaks are due to the SBN:60 substrate material.

very good, as indicated by the sharpness of the film diffraction peaks in fig. 2.

Table 1 summarizes the growth conditions and major physical properties for the SKN films grown from each flux system. The film lattice constants were established from the (400), (600) and (800) X-ray reflections from (100)-oriented films and the (001), (002) and (004) reflections from (001)-oriented films. The measured constants are in excellent agreement with the values obtained from stoichiometric $Sr_2KNb_5O_{15}$ ceramics. The SAW electro-mechanical coupling constants, K^2, were measured on poled ⟨001⟩ SKN thin films using the method of Staples [16]. Poling to a single ferroelectric domain was accomplished by cooling from the SKN transition temperature with a 4 kV/cm field applied across the substrate/film combination. The measured SAW coupling constants at room temperature for acoustic propagation along ⟨100⟩ were $(110–130)\times10^{-4}$, depending primarily on the flux used for growth (table 1). Although these values are smaller than for SBN:60 (180×10^{-4}) and $Pb_2KNb_5O_{15}$ (188×

Table 1
Physical properties of SKN films grown by LPE

	Substrate SBN:60	SKN films	
		0.75 KVO_3–0.25 SBN:50	0.80 $K_3V_5O_{15}$–0.20 SKN
growth temperature (°C)	–	920–925	880–890
growth rate (μm/min)			
⟨001⟩	–	1–2	1–2
⟨100⟩ or ⟨110⟩	–	≥0.5	≥0.5
lattice constants (Å) and substrate mismatch			
a,b	12.465	12.469 (0.032%)	12.473 (0.064%)
c	3.938	3.943 (0.127%)	3.943 (0.127%)
Curie point (°C)	75	153	162
Dielectric constant at 20°C			
ϵ_{11}	475	≈1000	≈1000
ϵ_{33}	920	≈1200	≈1200
SAW coupling, K^2 (⟨100⟩)	180×10^{-4}	130×10^{-4}	110×10^{-4}
electro-optic coefficient[a] (10^{-12} m/V)			
r_{33}	470	≈550	≈550
r_{51}	80–90	≈200	≈200

[a] Calculated values for SKN.

10^{-4}) [17,18], it may be possible to increase SAW coupling in SKN by altering the Sr:K ratio, although such compositional changes have not yet been explored.

The linear electro-optic effect in SKN is anticipated to be large because of the high dielectric constants found along both polar and non-polar directions. From the phenomenology for tetragonal bronze ferroelectrics [19], the electro-optic coefficients, r_{ij}, are given by

$$r_{33}=2g_{33}P_3\epsilon_0\epsilon_{33}\,,\quad r_{51}=2g_{44}P_3\epsilon_0\epsilon_{11}\,,$$

where ϵ_0 is the permittivity of free space, P_3 is the spontaneous polarization and g is the quadratic electro-optic coefficient. From dielectric measurements on small Czochralski-grown SKN single crystals, $\epsilon_{11}=1000$ and $\epsilon_{33}=1200$ at room temperature. Dielectric measurements on SKN thin films using a close-spaced surface electrode geometry were necessarily influenced by geometric factors and possible substrate contributions, but in general showed semi-quantitative agreement with the bulk crystal values. Using $P_3=0.30$ C/m^2 and $g_{33}=0.09$, $g_{44}=0.04$ m^4/C^2 typical of tetragonal bronze ferroelectrics, the anticipated linear electro-optic coefficients for these films are roughly $r_{33}=550\times10^{-12}$ m/V and $r_{51}=200\times10^{-12}$ m/V, values substantially larger than those encountered in tungsten bronze SBN:60 (470×10^{-12} and $(80–90)\times10^{-12}$ m/V, respectively) and more than an order of magnitude better than r_{33} for $LiNbO_3$ (31×10^{-12} m/V) [20]. Hence, these SKN thin films could prove to be especially important for electro-optic device applications. Although the optical quality of the current films is still not sufficient for detailed electro-optical and optical waveguide characterization, this appears to be largely a consequence of substrate surface preparation (and substrate quality) rather than an inherent problem in the grown films.

4. Conclusions

Tungsten bronze SKN thin films grown by the LPE technique appear to be suitable for SAW device applications upon further evolutionary improvements in thin film quality. Increased SAW electro-mechanical coupling may also be possible through alteration

Volume 6, number 5,6 MATERIALS LETTERS March 1988

of the Sr:K ratio, although such compositional changes should not be so large that the advantages of substrate lattice matching are lost. Perhaps one of the greatest advantages of these films is the high ferroelectric transition temperature (155°C) which permits the application of relatively large applied voltages and usage over a wide temperature range without ferroelectric domain reversal or depoling. With improvements in film quality, these SKN films could also have a significant impact on optical and possibly pyroelectric applications as well.

Acknowledgement

The authors wish to thank W.K. Cory for his insights and discussions on this work, and E.J. Staples for the initial SAW measurements. This research was supported by DARPA (Contract No. N00014-82-C-2466) and by the Office of Naval Research (Contract No. N00014-81-C-0463).

References

[1] E.A. Giess, B.A. Scott, G. Burns, D.F. O'Kane and A. Segmuller, J. Am. Ceram. Soc. 58 (1968) 276.
[2] B.A. Scott, E.A. Giess, D.F. O'Kane and G. Burns, J. Am. Ceram. Soc. 53 (1969) 106.
[3] F.W. Ainger, J.A. Beswick and S.G. Porter, Ferroelectrics 3 (1972) 321.
[4] E.A. Giess, G. Burns, D.F. O'Kane and A.W. Smith, Appl. Phys. Letters 11 (1967) 233.
[5] R. Clarke and F.W. Ainger, Ferroelectrics 7 (1974) 101.
[6] G. Burns, E.A. Giess, D.F. O'Kane, B.A. Scott and A.W. Smith, J. Phys. Soc. Japan 28 Suppl. (1970) 153.
[7] R.R. Neurgaonkar, W.W. Ho, W.K. Cory, W.F. Hall and L.E. Cross, Ferroelectrics 51 (1984) 185.
[8] R.R. Neurgaonkar and E.T. Wu, Mater. Res. Bull. 22 (1987) 1095.
[9] E.J. Staples, R.R. Neurgaonkar and T.C. Lim, Appl. Phys. Letters 32 (1978) 197.
[10] R.R. Neurgaonkar, M.H. Kalisher, E.J. Staples and T.C. Lim, Appl. Phys. Letters 35 (1979) 606.
[11] R.R. Neurgaonkar, T.C. Lim, E.J. Staples and L.E. Cross, Ferroelectrics 27 (1980) 63.
[12] R.R. Neurgaonkar and E.J. Staples, J. Crystal Growth 27 (1981) 352.
[13] R.R. Neurgaonkar, M.H. Kalisher, T.C. Lim, E.J. Staples and K.L. Keester, Mater. Res. Bull. 15 (1980) 1305.
[14] R.R. Neurgaonkar and W.K. Cory, J. Opt. Soc. Am. B3 (1986) 276.
[15] R.R. Neurgaonkar, W.K. Cory, J.R. Oliver, M.D. Ewbank and W.F. Hall, Opt. Eng. 26 (1987) 392.
[16] E.J. Staples, Proc. 28th Ann. Freq. Control Symp. (1974) p. 280.
[17] R.R. Neurgaonkar and L.E. Cross, Mater. Res. Bull. 21 (1986) 893.
[18] P.H. Carr, Proc. IEEE Ultrasonics Symp. (1974) p. 286.
[19] M. DiDomenico and S.H. Wemple, J. Appl. Phys. 40 (1969) 720.
[20] K.-H. Hellwege, ed., Landolt-Bornstein New Series, Group III, Vol. 11 (Springer, Berlin, 1979).